CALIFORNIA INSTITUTE OF TECHNOLOGY

EARTHQUAKE ENGINEERING RESEARCH LABORATORY

UNCERTAINTY PROPAGATION AND FEATURE SELECTION FOR LOSS ESTIMATION IN PERFORMANCE-BASED EARTHQUAKE ENGINEERING

BY

JIANYE CHING, KEITH A. PORTER & JAMES L. BECK

REPORT NO. EERL 2004-02

PASADENA, CALIFORNIA

FEBRUARY 2004

Acknowledgements

The authors gratefully acknowledge the financial support of Caltech's George W. Housner Postdoctoral Fellowship (J. Ching), the George W. Housner Senior Research Fellowship (K. Porter), and the Pacific Earthquake Engineering Research Center under Award Number EEC-9701568 of the Earthquake Engineering Research Centers Program of the National Science Foundation.

ABSTRACT

This report presents a new methodology, called moment matching, of propagating the uncertainties in estimating repair costs of a building due to future earthquake excitation, which is required, for example, when assessing a design in performance-based earthquake engineering. Besides excitation uncertainties, other uncertain model variables are considered, including uncertainties in the structural model parameters and in the capacity and repair costs of structural and non-structural components. Using the first few moments of these uncertain variables, moment matching requires only a few well-chosen point estimates to propagate the uncertainties to estimate the first few moments of the repair costs with high accuracy. Furthermore, the use of moment matching to estimate the exceedance probability of the repair costs is also addressed. These examples illustrate that the moment-matching approach is quite general; for example, it can be applied to any decision variable in performance-based earthquake engineering.

Two buildings are chosen as illustrative examples to demonstrate the use of moment matching, a hypothetical three-story shear building and a real seven-story hotel building. For these two examples, the assembly-based vulnerability approach is employed when calculating repair costs. It is shown that the moment-matching technique is much more accurate than the well-known First-Order-Second-Moment approach when propagating the first two moments, while the resulting computational cost is of the same order. The repair-cost moments and exceedance probability estimated by the moment-matching technique are also compared with those by Monte Carlo simulation. It is concluded that as long as the order of the moment matching is sufficient, the comparison is satisfactory. Furthermore, the amount of computation for moment matching scales only linearly with the number of uncertain input variables.

Last but not least, a procedure for feature selection is presented and illustrated for the second example. The conclusion is that the most important uncertain input variables among the many influencing the uncertainty in future repair costs are, in order of importance, ground-motion spectral acceleration, component capacity, ground-motion details and unit repair costs.

TABLE OF CONTENTS

1 INTRODUCTION

1.1 METHODS TO PROPAGATE UNCERTAINTY IN EARTHQUAKE REPAIR COST MODELS

Implementation of performance-based earthquake engineering (PBEE) often requires the quantification of uncertain future repair costs associated with earthquake damage (e.g. Porter 2003). Furthermore, real-estate investment and business recovery decision-making could also benefit from reliable techniques to estimate future repair costs (Beck et al, 2002, 1999; Porter et al, 2004). These future repair costs are uncertain because they depend on uncertain basic variables such as the occurrence dates and times; shaking intensities, and other aspects of the earthquake ground motions at a site; the dynamic properties of the facility; and the capacities and repair costs of facility components. Each of these uncertainties influence the subsequent ones, as they propagate from earthquake occurrence, to ground motion at a site, to structural response, to damage, and finally to repair cost. A reliable repair-cost estimate based on a model of this entire process must therefore account for this propagation of uncertainties.

Four methods have been used to propagate uncertainties for repair costs: deterministic sensitivity studies; Monte Carlo simulation (MCS); first-order, second-moment (FOSM); and FORM or SORM (first-order or second-order reliability method):

(a) Deterministic sensitivity studies can be used to identify those input variables that most strongly affect uncertainty in an output parameter of interest. Porter et al. (2002a and 2002b) apply this method to examine the contributions of each uncertain input variable to the uncertainty in repair costs by using a graphic depiction called a tornado diagram.

(b) MCS techniques are simple, effective means to propagate uncertainties and to explore the probability distribution of an output parameter. They can be computationally expensive for very large systems or for situations where one wishes to explore low-probability events. Porter

et al. (2002c) and Beck et al. (2002) present two recent examples of Monte Carlo simulation for earthquake loss to individual buildings.

(c) FOSM (Melchers 1999) is a convenient and efficient technique for propagating uncertainty where one is primarily interested in the mean and variance of an output variable rather than the tails of the distribution. Baker and Cornell (2003) summarize such a technique for estimating future earthquake losses. FOSM is less computationally expensive than MCS, but as its name implies, can achieve only first-order accuracy and it is not clear how to improve its accuracy. It cannot handle higher moments and requires quantifications of the correlations of intermediate uncertain variables.

(d) First-order and second-order reliability methods (FORM/SORM) are powerful techniques for estimating the probability of rare events, i.e., for exploring the tails of a loss distribution. Like FOSM, FORM/SORM also requires an estimate of correlation between intermediate variables. Haukaas and Der Kiureghian (2003) summarize a FORM approach to estimating failure probability in a finite-element reliability problem. To our knowledge, FORM and SORM have not yet been used to estimate failure probability for a structural system where the performance function is expressed in terms of repair costs exceeding a prescribed value.

1.2 NEEDED: EFFICIENT UNCERTAINTY PROPAGATION IN A HIGH-ACCURACY LOSS MODEL

Missing from these options is a computationally efficient technique to propagate uncertainty that does not require an estimate of correlation between intermediate variables and that can provide arbitrarily high order moments of repair costs. In this report, we re-cast the uncertainty propagation problem into a general analysis problem. Using a Taylor-series expansion, we propose a moment-matching technique that propagates uncertainties accurately with a few carefully selected sample points in the input-variable space. We show that the new

method possesses all of the afore-mentioned advantages of FOSM and MCS while avoiding many of their limitations. With the moment-matching technique, we study four types of quantitative information regarding repair costs in this report:

1. The central moments (e.g., the mean and variance) of repair costs during the next *T* years.
2. The mean exceedance frequency of single-event repair costs over some threshold during the next *T* years.
3. The central moments of the repair costs due to the extreme event in the next *T* years.
4. The exceedance probability of repair costs due to the extreme event over some threshold in the next *T* years.

Feature selection is also examined, i.e., determining the degree of importance of the uncertainty in each input variable on the repair cost estimate. The benefit of doing this is twofold: first, the input variables with little importance can be considered deterministic to reduce calculation efforts. Second, the input variables that play major roles can be further studied to improve our knowledge of them.

The problem of feature selection has been studied by Porter et al. (2002a b) using a deterministic sensitivity analysis approach, in which an input variable for the loss modeling is considered to be important if and only if repair costs are sensitive to its change. In this report, we reconsider the feature selection problem under a probabilistic approach built on the moment-matching technique. We utilize a measure of information change before and after the removal of the uncertainties of an input variable. An input variable is considered to be important if and only if the corresponding information change is large. This measure can potentially detect any change

in the probability density function (PDF) of repair costs before and after the removal of the uncertainty of an input variable.

1.3 ORGANIZATION OF THE REPORT

The structure of this report is as follows: Section 2 presents an overview of performance-based earthquake engineering (PBEE) as it is currently formulated by the Pacific Earthquake Engineering Research (PEER) Center. Section 2 also defines the problem of uncertainty propagation under this PBEE framework. In Section 3, we briefly discuss the FOSM technique of propagating uncertainty and describe in detail the new moment-matching technique. The performance of the new technique and other techniques is compared using simulations. In Section 4, we derive algorithms for calculating the moments and exceedance probability of repair costs due to a future earthquake. Based on these results, we present procedures for estimating the four types of quantitative information listed in Section 1.2. In Section 5, we present the principle and formulas for feature selection.

We illustrate the moment-matching technique with two examples of uncertainty propagation under the PEER PBEE framework. The first example (Section 4.5) is about estimating the repair cost measures discussed above for a simple three-story shear building. The main focus of this example is to compare the performances of the new moment-matching technique and other techniques.

The second example (Chapter 6) illustrates the estimation of moments and exceedance probability of the single-event repair costs of a non-ductile reinforced concrete moment-frame building (a 1960s-era hotel building in Van Nuys, California) due to the extreme earthquake event in the next 50 years. The main focus of this example is to demonstrate the new moment-matching technique on a real building and to illustrate the feature selection procedure.

2 PERFORMANCE-BASED EARTHQUAKE ENGINEERING

Estimating economic losses of a structure due to future earthquakes is a major part of performance-based earthquake engineering (PBEE). The Pacific Earthquake Engineering Research (PEER) Center has proposed the framework shown in Figure 2-1 (Porter, 2003) for its second-generation PBEE methodology.

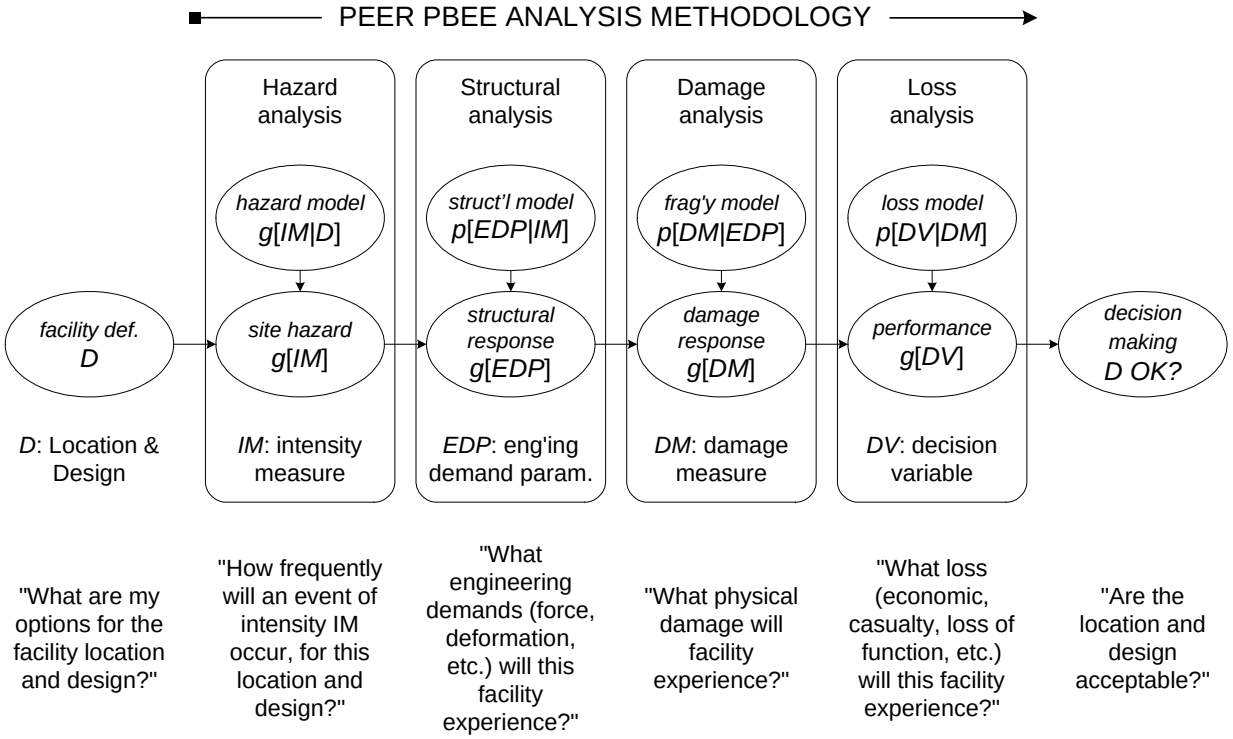

Figure 2-1. PEER's PBEE framework

As discussed in Porter (2003), PEER's PBEE approach begins with a definition of the facility to be analyzed (denoted here by D), and involves four analytical stages: hazard analysis, structural analysis, damage analysis, and loss analysis. In the figure, the expression $p[X|Y]$ refers to the probability density of X conditioned on knowledge Y, and $g[X|Y]$ refers to the mean occurrence frequency of X given Y (equivalent to the absolute value of the first derivative of the frequency with which X is exceeded, given Y). Equation (2.1) frames the PEER methodology

mathematically. Note that Figure 2-1 omits conditioning on D after the hazard analysis for brevity, but it is nonetheless implicit.

$$g[DV] = \iiint p[DV \mid DM, D]\, p[DM \mid EDP, D]\, p[EDP \mid IM, D]\, g[IM \mid D]\, d(IM)\, d(EDP)\, d(DM) \qquad (2.1)$$

Facility definition. To define the facility one must know its location (latitude and longitude) and design, including site soils, substructure, structural and nonstructural components, jointly denoted by D. One creates an inventory of the damageable assemblies and identifies the engineering demand parameter — *EDP*, which might be story drift ratio, member force, etc. — that would cause damage to each assembly.

Hazard analysis. In the hazard analysis, one considers the seismic environment (nearby faults, their magnitude-frequency recurrence rates, mechanism, site distance, site conditions, etc.) and evaluates the seismic hazard at the facility considering D, to produce the seismic hazard, $g[IM|D]$, where *IM* refers to the intensity measure. *IM* can be parameterized in any of a variety of terms, such as peak horizontal ground acceleration, Arias intensity, etc. It is common to use $S_a(T_1)$, the damped elastic spectral acceleration at the small-amplitude fundamental period of the structure, which is readily available by using software such as Frankel and Leyedecker (2001), adjusting to account for site classification such as by using F_a or F_v as appropriate from the 2000 International Building Code (International Code Council, 2000). In the present analysis, we use $S_a(T_1)$ for *IM*.

Structural analysis. In the structural analysis, the engineer creates a structural model of the facility in order to estimate the uncertain structural response, measured in terms of a vector of engineering demand parameters (*EDP*), conditioned on seismic excitation and design ($p[EDP|IM,D]$). *EDP*s can include internal member forces or local or global deformations, including ground failure (a partial list of *EDP*s in use by PEER is provided in Porter, 2002). The

structural analysis typically takes the form of a series of nonlinear time-history structural analyses using a suite of strong-motion records that are scaled to have the specified *IM*. The structural model need not be deterministic — some PEER analyses have included uncertainty in the mass, damping, and force-deformation characteristics of the model. The present study does so, as will be discussed later.

Damage analysis. *EDP* is then input to a set of fragility functions that model the probability of various levels of physical damage (expressed via damage measures, or *DM*), conditioned on structural response and design, $p[DM|EDP,D]$. Physical damage is not described at a detailed level, but instead is defined relative to particular repair efforts required to restore the component to its undamaged state. Fragility functions currently in use give the probability of various levels of damage to individual beams, columns, nonstructural partitions, or pieces of laboratory equipment, as functions of various internal member forces, story drift, etc. These functions are drawn from laboratory or field experience. For example, PEER has compiled a library of destructive tests of reinforced concrete columns (Eberhard et al., 2001). The result of the damage analysis is a probabilistic vector of *DM*. Note that component damage may be correlated with structural characteristics of *D*, even conditioned on *EDP*.

Loss analysis. The last stage in the analysis is the probabilistic estimation of performance (parameterized via various decision variables, *DV*), conditioned on damage and design $p[DV|DM,D]$. Decision variables measure the seismic performance of the facility in terms of greatest interest to stakeholders, whether in dollars, deaths, downtime, or other metrics. Dollar losses can be estimated using standard construction-contracting principles, given the detailed damage state of the facility. Deaths can be estimated using empirical casualty estimates,

as discussed by Seligson and Shoaf (2002). Repair duration can be estimated using construction scheduling principles, as discussed in Porter (2000).

Decision-making. The analysis produces estimates of the frequency with which various levels of *DV* are experienced, given the facility definition *D*. These frequencies can be used to inform a variety of risk-management decisions. For example, a common concern among insurers the need for reinsurance to deal with catastrophically high losses. Consequently, it is of interest to know the frequency with which future repair cost will exceed some ruin threshold, $G[DV|R]$, where $G[X|Y]$ refers to the frequency with which X is exceeded, conditioned on knowledge Y. For an individual facility exposed to seismic risk, one can calculate this ruin frequency as

$$G\left[R \mid D\right] = \int_{DV=R}^{\infty} g\left[DV \mid D\right] dDV \tag{2.2}$$

Defining the problem of uncertainty propagation. Observe that *DV* can be viewed as a deterministic function of a number *n* of uncertain input variables. For example, if we are concerned with uncertain future repair costs, we can consider the hazard model as an uncertain parameter *IM*, the structural model as a as a set of one or more structural variables (*SM*), the fragility model as a set of uncertain capacities *C*, and the loss model as a set of unit repair costs (*URC*), etc, collectively denoted by *X*, i.e.,

$$DV = f(X) \tag{2.3}$$

where $X = \{IM, SM, C, URC, \ldots\} \in R^n$ contains all basic variables. The problem of uncertainty propagation under PEER's PBEE framework can be defined as follows: Given the moments or joint PDF of *X* (we will call it the *X* PDF), the goal is to determine the moments of *DV* or the probability that *DV* will exceed a threshold value (i.e. determine the PDF of *DV*).

3 UNCERTAINTY PROPAGATION

We first briefly discuss the FOSM technique of propagating uncertainties, then present the moment-matching (MM) technique. We show theoretically that the latter is more accurate than the former. The presentation of the two techniques is followed by several simple examples to demonstrate the effectiveness of the MM technique.

3.1 FIRST-ORDER SECOND-MOMENT TECHNIQUE

The FOSM technique assumes the function $f(X)$ in Equation (2.3) for the decision variable DV is roughly linear in $X \in \mathbb{R}^n$ in the support region of the X PDF so that the first two central moments of DV, $E(DV)$ and $Var(DV)$, are simple functions of these moments for X. For the FOSM technique, it is assumed that the Taylor series expansion of $f(X)$ around $X = EX$ exists, then:

$$DV = f(X) = f(EX) + D_x f + D_x^2 f/2! + D_x^3 f/3! + D_x^4 f/4! \ldots, \tag{3.1}$$

where

$$D_x^i f \equiv \left(\sum_{j=1}^{n} (X_j - EX_j) \cdot (\partial/\partial x_j) \right)^i f(x) \Big|_{x=EX}. \tag{3.2}$$

To verify the above multidimensional Taylor series expansion, consider expanding $f(X)$ in the s direction, where $s = (X - EX)/\|X - EX\|$ is the unit vector in the (X-EX)-direction. With the one-dimensional Taylor series expansion, we have

$$f(X) = f(EX) + \sum_{i=1}^{\infty} \frac{\partial^i f(x)}{\partial s^i} \Big|_{x=EX} \cdot \frac{\|X - EX\|^i}{i!}, \tag{3.3}$$

where the term $\partial^i f(x)/\partial s^i \big|_{X=EX}$ is equal to

$$\left.\frac{\partial^i f(x)}{\partial s^i}\right|_{X=EX} = \left.(s\cdot\nabla)^i f(x)\right|_{x=EX}$$
$$= \left.\left(s_1\frac{\partial}{\partial x_1}+\ldots+s_n\frac{\partial}{\partial x_n}\right)^i f(x)\right|_{x=EX} = \left.\left(\sum_{j=1}^{n}\frac{X_j-EX_j}{\|X-EX\|}\cdot(\partial/\partial x_j)\right)^i f(x)\right|_{x=EX} \quad (3.4)$$

Substitute Equation (3.4) into Equation (3.3), then Equation (3.2) follows.

As a result, the first two moments of *DV* are

$$E(DV) = \underbrace{f(EX)}_{0th} + \underbrace{E(D_x f)}_{1st} + \underbrace{E(D_x^2 f/2!)}_{2nd} + \underbrace{E(D_x^3 f/3!)}_{3rd} + \underbrace{E(D_x^4 f/4!)}_{4th}\ldots$$

and (3.5)

$$Var(DV) = E\left([DV-E(DV)]^2\right)$$
$$= \underbrace{E\left((D_x f)^2\right)}_{2nd} + \underbrace{2E\left((D_x f)(D_x^2 f/2!)\right)}_{3rd} + \underbrace{2E\left((D_x f)(D_x^3 f/3!)\right) + E\left((D_x^2 f/2!)(D_x^2 f/2!)\right) - \left[E(D_x^2 f/2!)\right]^2}_{4th} + \ldots$$

Under the assumption that $f(X)$ is linear in the support region of the X PDF, all second or higher derivatives of $f(X)$ with respect to X vanish; therefore, $E(DV)$ and $Var(DV)$ are approximated by:

$$E(DV)_{FOSM} = \underbrace{f(EX)}_{0th} + \underbrace{E(D_x f)}_{1st} = f(EX)$$

and (3.6)

$$Var(DV)_{FOSM} = \underbrace{E\left((D_x f)^2\right)}_{2nd} = (\nabla_x f|_{x=EX})\cdot Var(X)\cdot(\nabla_x f|_{x=EX})^T$$

where $E(DV)_{FOSM}$ and $Var(DV)_{FOSM}$ denote the FOSM estimates for $E(DV)$ and $Var(DV)$, and $\nabla_x f \in R^{1\times n}$ is the Jacobian matrix.

The approximations $E(DV)_{FOSM}$ and $Var(DV)_{FOSM}$ are accurate estimates of $E(DV)$ and $Var(DV)$ if $f(X)$ is almost linear on the support region of the X PDF, and the FOSM approximations become exact when $f(X)$ is indeed linear in X. We say that the accuracy of the FOSM technique is first-order since the technique is exact if $f(X)$ is a first-order polynomial. On

the other hand, the approximations are poor if $f(X)$ is highly nonlinear on the support region of X PDF.

3.2 MOMENT-MATCHING TECHNIQUE

An alternative method for uncertainty propagation is the moment-matching (MM) technique. It is a point-estimate method first proposed by Rosenblueth (1975). Also see Zhao and Ono (2000) and Julier et al. (2000) for recent developments. The MM technique is a procedure where the PDF of X is modeled by an "equivalent" discrete PDF containing several weighted delta functions, where the one-dimensional delta function $\delta(.)$ is a generalized (or symbolic) function that has the properties:

$$\begin{aligned} &\delta(x-a)=0 \qquad x \neq a \\ &\int_{-\infty}^{\infty} \delta(x)\,dx = 1 \end{aligned} \tag{3.7}$$

i.e., it imparts a unit "impulse" to the system at $x = a$, but is zero for all other values of x. The delta functions of the equivalent discrete PDF have specific positions and weights such that the first few moments of this PDF match those of X. Thus, rather than approximating the function $f(x)$ in Equation (2.3) by some simplified functional form, as in the FOSM technique, the MM technique approximates the X PDF with a discrete PDF by matching specified moments of X. Moreover, we show that the MM technique has the potential to propagate uncertainties more accurately than the FOSM technique. As a simple illustration, one could replace a standard Gaussian distribution of Figure 3-1(a) with the PDF of three weighted delta functions whose positions and weights are shown in Figure 3-1(b). The first three moments of the two distributions are equal, although their higher moments are not.

Consider $Y = g(X)$ and we would like to estimate $E(Y)$. According to Equation (3.5), we have

$$E(Y) = \underbrace{g(EX)}_{0th} + \underbrace{E(D_x g)}_{1st} + \underbrace{E(D_x^2 g/2!)}_{2nd} + \underbrace{E(D_x^3 g/3!)}_{3rd} + \underbrace{E(D_x^4 g/4!)}_{4th} \ldots \tag{3.8}$$

Note that if we can estimate $E(Y)$ for general $g(X)$, we can estimate all moments of $DV=f(X)$ by letting $g(X) = f(X)^r$ for the r^{th} moment of DV.

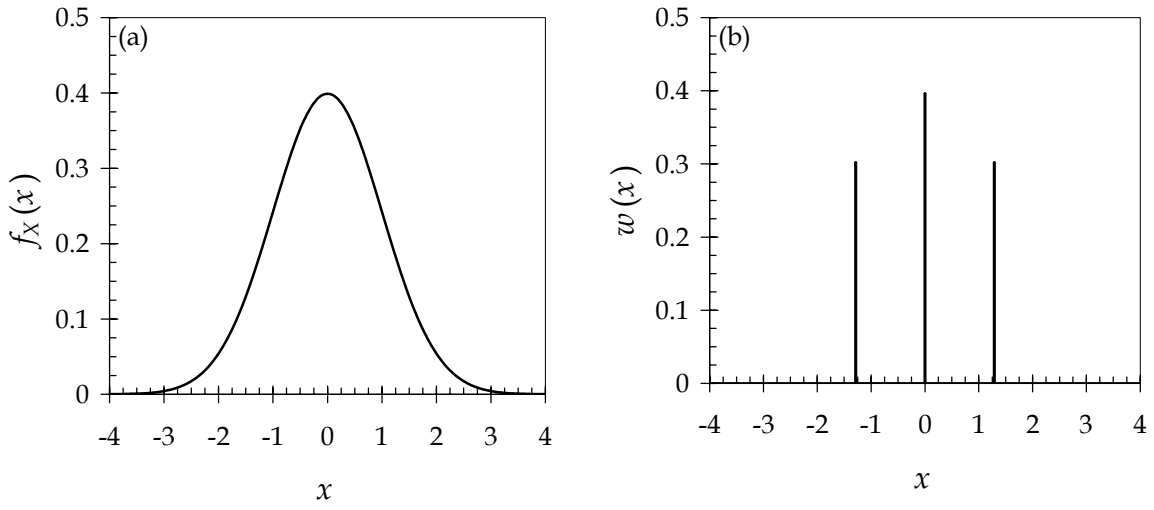

Figure 3-1. Simple illustration of moment-matching approach

The key observation for the MM technique is as follows: the i^{th} order Taylor series term in Equation (3.8), which is

$$E(D_x^i g) \equiv E\left(\sum_{j=1}^{n} (X_j - EX_j) \cdot (\partial / \partial x_j) \right)^i g(x) \Big|_{x=EX}, \tag{3.9}$$

depends on the i^{th} central moments of the X PDF and the i^{th}-order derivatives of $g(X)$. In the MM framework, a pseudo-PDF consisting of weighted delta functions is used to match the first p central moments of the X PDF. (The prefix "pseudo" is used because in some situations we allow the weights of the delta functions to be negative). Since this pseudo-PDF only consists of

weighted delta functions, the propagation of this pseudo-PDF through $g(X)$ can be done analytically, and the corresponding pseudo-PDF of Y also contains weighted delta functions. The mean of this pseudo-PDF of Y, called the MM estimate of $E(Y)$, can be again computed easily and analytically, since the pseudo-PDF contains only weighted delta functions.

In the MM procedure we use the exact functional form for $g(X)$ rather than a linear (or higher order) approximation. Therefore, if we can match up to the p^{th} moment of the X PDF, we are able to characterize up to the p^{th}-order Taylor series term of $E(Y)$. In what follows, we present the procedures of the MM technique for the special case that X is one-dimensional and discuss the idea of the technique. The extension for multi-dimensional X will be described later.

3.2.1 Moment Matching: One-dimensional X

Step 1: Characterize the first p moments of the X PDF: Suppose that we know the first p moments of the X PDF. It is straightforward to find a pseudo PDF that contains q weighted delta functions and has identical first p moments as the X PDF. Let X' denote the uncertain variable associated with the delta-function PDF:

$$p_{X'}(x) = \sum_{i=1}^{q} w_i \delta(x - \chi_i) \qquad \sum_{i=1}^{q} w_i = 1 \tag{3.10}$$

By careful selection of the number q of delta functions, their weights $\{w_i : i = 1,...q\}$ and locations $\{\chi_i : i = 1,...q\}$, we can assure that the delta-function PDF has the first p central moments identical to those of the X PDF. To do this, we need to solve the following nonlinear equations for the weights and locations:

$$\begin{aligned} &\sum_{i=1}^{q} w_i \left(\chi_i - \left(\sum_{j=1}^{q} w_j \chi_j \right) \right)^k = E\left((X - EX)^k \right) \qquad k = 1, 2, ...p \\ &\sum_{i=1}^{q} w_i = 1 \end{aligned} \tag{3.11}$$

The solutions for the weights and locations can be found using standard numerical methods, e.g., Newton methods, descent methods, and direct-search methods. Alternatively, one can solve the following equation to match the non-central moments of the X PDF. The resulting weights and locations will be identical to those obtained by Equation (3.11):

$$\begin{aligned} &\sum_{i=1}^{q} w_i \chi_i^k = E\left(X^k\right) \qquad\qquad k = 1,2,...p \\ &\sum_{i=1}^{q} w_i = 1 \end{aligned} \quad . \tag{3.12}$$

The best that we can do with the q weighted delta functions is to match the first ($2q$-1) moments of X PDF; this is because we have ($2q$-1) adjustable parameters (one degree of freedom is lost since the weights are summed to one). When this is the case and the X PDF is of certain types, the solutions for the weights and locations in Equation (3.11) or (3.12) are related to Gauss-quadrature integration points and weights. For instance, when X is Gaussian, uniform, or exponential, the weights and locations of a q-point Hermite-Gauss, Legendre-Gauss, or Laguerre-Gauss Quadrature rule (Abramowitz and Stegun 1972; Hildebrand 1956), respectively, can be used to match the first ($2q$-1) moments of X. Appendix A describes a general formula for computing the weights and locations of the delta functions when the X PDF is Gaussian, uniform, or exponential.

For other situations (e.g. X PDF is not of the standard types), the weights and locations can be solved using Equation (3.11) or (3.12). An alternative way of obtaining the locations and weights of q delta functions that will match (q-1) moments of a general X PDF is described as follows: First, we choose the locations of the q delta functions a priori, then we solve Equation (3.11) or (3.12) for the q weights that match the first (q-1) moments of X. It is clear that finding the weights is equivalent to solving a linear matrix inversion problem. From our experience, if

the locations of the q delta functions are chosen carefully, this approach usually performs satisfactorily for uncertainty propagation. It is recommended to use the following procedure to choose the locations a priori: First, determine which type of standard PDF (e.g. Gaussian, exponential, uniform, etc.), the X PDF resembles. Next, use Appendix A to determine the locations of the Gauss points of the standard PDF that is determined previously. When doing so, the first one or two moments of the standard PDF are set to be identical to those of the X PDF. Finally, the locations of the calculated Gauss points are used as the locations of the q delta functions.

Step 2: Propagate the delta-function PDF: Now define

$$Y' = g(X') . \tag{3.13}$$

As a consequence, the pseudo-PDF of Y' also contains q weighted delta-functions. In fact, the PDF of Y' has the following analytical form:

$$p_{Y'}(y) = \sum_{i=1}^{q} w_i \delta(y - g(\chi_i)) \tag{3.14}$$

Step 3: Compute the expectation of Y'. Since Y' can only take discrete values, the expected value of Y' are simply the weighted sample mean:

$$E(Y') = \sum_{i=1}^{q} w_i g(\chi_i) . \tag{3.15}$$

Although a pseudo-PDF is not a well-defined PDF, the calculation of the sample mean does not require the weights to be positive. The resulting $E(Y')$ is an estimate of $E(Y)$ that is accurate up to the p^{th}-order Taylor series terms. This can be easily seen from the following equations:

$$E(Y') = \underbrace{g(EX')}_{0th} + \underbrace{E_{X'}(D_x g)}_{1st} + \underbrace{E_{X'}(D_x^2 g/2!)}_{2nd} + \underbrace{E_{X'}(D_x^3 g/3!)}_{3rd} + \underbrace{E_{X'}(D_x^4 g/4!)}_{4th} \ldots , \tag{3.16}$$

where

$$E_{X'}(D_x^i g) \equiv E\left(\sum_{j=1}^{n} (X'_j - EX'_j) \cdot (\partial / \partial x_j) \right)^i g(x) \Bigg|_{x=EX'} . \tag{3.17}$$

The i^{th} Taylor series terms of $E(Y')$ (Equation (3.17)) and $E(Y)$ (Equation (3.9)) would be identical if the i^{th} moments of the pseudo-PDF of X' are identical to those of X PDF. Using the same argument, if X and X' have identical first p moments, the first p^{th}-order Taylor series terms of $E(Y')$ are identical to those of $E(Y)$. We denote $E(Y')$, the MM estimate of $E(Y)$, by $E(Y)_{MM}$.

One can verify that if the first p moments of X PDF are matched and $g(X)$ is a p^{th} or lower-order polynomial, $E(Y)_{MM}$ is identical to $E(Y)$. Therefore, the accuracy of the MM technique is p^{th}-order.

3.2.2 Moment Matching: Multi-dimensional X

Consider now the situation that X is a vector containing n independent uncertain variables. Due to the independence between different components of X, the following equation is true:

$$E\left((X_1 - EX_1)^{\alpha_1} \ldots (X_n - EX_n)^{\alpha_n}\right) = E\left((X_1 - EX_1)^{\alpha_1}\right) \ldots E\left((X_n - EX_n)^{\alpha_n}\right). \tag{3.18}$$

Therefore, the p^{th} central moment of X contains the following terms:

$$\begin{matrix} E\left((X_i - EX_i)^p\right) & E(X_i) \cdot E\left((X_j - EX_j)^{p-1}\right) \\ E\left((X_i - EX_i)^2\right) \cdot E\left((X_j - EX_j)^{p-2}\right) & E(X_i) \cdot E(X_j) \cdot E\left((X_j - EX_j)^{p-2}\right) \ldots \end{matrix} . \tag{3.19}$$

As a result of Equations (3.18) and (3.19), if we can find a one-dimensional delta-function PDF $p_\delta(x_i)$ for each X_i ($i = 1 \ldots n$) that matches the first p central moments of X_i, the joint delta-function PDF of X,

$$p_\delta(x) = \prod_{i=1}^{n} p_\delta(x_i), \tag{3.20}$$

will match the first p central moments of X.

The implementation of the moment-matching technique for multidimensional X is illustrated using the following example: $Y = g(X_1,X_2)$, i.e. $n = 2$, where X_1 is a Gaussian variable with mean 1 and variance 4 (denoted by N(1,4)), X_2 is uniformly distributed over [1 2] (denoted by U[1 2]), and X_1 and X_2 are independent. We consider using a three-delta-function PDF $p_\delta(x_i)$ for both X_1 and X_2, although in general we can assign different number of delta functions for X_1 and X_2. Using the results in Appendix A, the locations and weights of the three delta functions in $p_\delta(x_1)$ are $x_1 = \left[1-2\sqrt{3}, 1,\ 1+2\sqrt{3}\right]$ and $\left[1/6,\ \ 2/3,\ \ 1/6\right]$, respectively; while the locations and weights in $p_\delta(x_2)$ are $x_2 = [1.5-\sqrt{3/20}\ \ 1.5\ \ 1.5+\sqrt{3/20}]$ and $\left[5/18,\ \ 5/19,\ \ 5/18\right]$, respectively. We denote the uncertain variables corresponding to $p_\delta(x_1)$ and $p_\delta(x_2)$ by X'_1 and X'_2. Note that the first five moments of $p_\delta(x_1)$ and $p(x_1)$=N(1,4) are identical:

$$\begin{aligned} E(X'_1) = 1 = E(X_1), \quad & E\left((X'_1 - EX'_1)^2\right) = 4 = E\left((X_1 - EX_1)^2\right), \\ \cdots, \quad & E\left((X'_1 - EX'_1)^5\right) = 0 = E\left((X_1 - EX_1)^5\right) \end{aligned} \tag{3.21}$$

and, similarly, the first five moments of $p_\delta(x_2)$ are identical to those of U[1 2]. We define a p^{th}-order MM technique as one that matches the first p moments of the X PDF.

Consider a delta-function PDF of X, denoted by $p_\delta(x)$, containing five delta functions with the following locations and weights:

$$\begin{aligned} \chi_1 &= [1-2\sqrt{3} \quad 1.5] & w_1 &= 1/6 \\ \chi_2 &= [1+2\sqrt{3} \quad 1.5] & w_2 &= 1/6 \\ \chi_3 &= [1 \quad 1.5-\sqrt{3/20}] & w_3 &= 5/18\,. \\ \chi_4 &= [1 \quad 1.5+\sqrt{3/20}] & w_4 &= 5/18 \\ \chi_0 &= [1 \quad 1.5] & w_0 &= 1/9 \end{aligned} \tag{3.22}$$

Note that χ_0 is the center point located at the mean value of (X_1,X_2); χ_1 and χ_2 are shifted points from the center point in the X_1 direction, and χ_3 and χ_4 are shifted from the center point in the X_2 direction. One can check that these five weighted delta functions give a PDF whose moments match the first five moments of the X PDF.

Note that since the two PDFs are symmetric, the center point χ_0 is shared by $p_\delta(x_1)$ and $p_\delta(x_2)$, so we need five delta functions instead of six. If one of the PDFs is asymmetric, we will need six delta functions. The weight for the center point has been adjusted to ensure that the weights sum to one so that the PDF is properly normalized. Since the central moments of $p_\delta(x)$ do not depend on the center point weight, this adjustment will not affect the moment matching.

For this example, the estimated value of $E(Y)_{MM}$ is $\sum_{i=0}^{4} w_i g(\chi_i)$, which is an estimate of $E(Y)$ that is accurate up to the fifth-order Taylor series term of $E(Y)$. Therefore, the resulting MM technique is a fifth-order MM technique. Moreover, $E(Y)_{MM}$ is identical to $E(Y)$ if $g(X)$ is a fifth-order or lower-order polynomial.

In the case that X is n-dimensional, in which n_{sym} components of X have symmetric PDFs, and the other n_{asym} components have asymmetric PDFs ($n_{sym} + n_{asym} = n$), we need a pseudo PDF of X with at least $(q\text{-}1)n_{sym}+qn_{asym}+1$ delta functions to achieve a $(2q\text{-}1)^{th}$-order accuracy. In practice, the computational costs for a fifth-order (i.e. $q = 3$) MM and FOSM techniques are similar. This is because in order to implement the FOSM technique, we usually have to evaluate the Jacobian matrix of $g(X)$ (see Equation **(3.5)**) numerically, and this requires evaluating $g(X)$ at $2n$ (i.e. $2n_{sym}+2n_{asym}$) points. A fifth-order MM technique requires evaluating $g(X)$ at $2n_{sym}+3n_{asym}+1$ points; nevertheless, the resulting estimate $E(Y)_{MM}$ has a fifth-order accuracy, which is much better than the first-order accuracy of $E(Y)_{FOSM}$. The accuracy for $Var(Y)_{MM}$ with a

fifth-order MM technique is second-order, i.e. if $g(X)$ is a second-order or lower-order polynomial of X, $Var(Y)$ is fourth-order or less, so $Var(Y)_{MM}$ is exact. Compared to the first-order accuracy of $Var(Y)_{FOSM}$, a fifth-order MM technique is more accurate. Furthermore, it is easy to increase the order of accuracy with the MM technique (i.e. just increase the number of delta functions), while it is not clear how to achieve this using the FOSM technique.

To summarize for the general case, a $(2q\text{-}1)^{th}$-order MM technique requires the evaluation of $g(X)$ at $(q\text{-}1)n_{sym} + q \times n_{asym} + 1$ points, and the resulting $E(Y)_{MM}$ has a $(2q\text{-}1)^{th}$-order accuracy, while $Var(Y)_{MM}$ has a $\lfloor (2q-1)/2 \rfloor^{th}$-order accuracy, where $\lfloor \cdot \rfloor$ denotes the integer part of the number.

3.2.3 Moments of X

For the MM technique, we first need to know the moments of the X PDF. In the case that the X PDF is known, but the PDF is not a standard type so that the moments are not known in analytical form, the moments can be estimated using the importance sampling method or numerical integration methods. It can also happen that even the X PDF is not known, and only sampled data of X is available. For this situation, we can use the sample moments as the estimates of the actual moments of the X PDF.

3.3 EXAMPLES WITH COMPARISON TO FOSM

To demonstrate the effectiveness of the MM technique, we present six examples of propagating the first two moments. In these examples, we compare the FOSM and fifth-order (three-point) MM techniques with Monte Carlo simulation (MCS). All of the six examples are $R \rightarrow R$ functions:

1. $g(X) = X^2$
2. $g(X) = X^4$

3. $g(X) = \log(|X|)$

4. $g(X) = e^X$

5. $g(X)$ = a non-differentiable function shown in Figure 3-2

6. $g(X)$ = a discontinuous function shown in Figure 3-3

In each case, we take X as a Gaussian variable with mean and variance equal to two and one, respectively so $p(x) = N(1, 2)$. The goal is to estimate the mean and variance of $g(X)$.

Monte Carlo simulations with sample number equal to 10, 100, 1000 and 10000 are conducted for several trials; in each trial, the sample mean and variance of Y are plotted as circles in Figure 3-4 through Figure 3-9 (MCS with 10, 100, 1000, and 10000 samples is repeated 100, 20, 10 and 5 times, respectively). The delta-function locations and weights for a fifth-order MM technique are $x_1 = \left[2-\sqrt{3},\ \ 2,\ \ 2+\sqrt{3}\right]$ and $\left[1/6,\ \ 2/3,\ \ 1/6\right]$, respectively (determined using the Hermite-Gauss-quadrature rule in Appendix A). The MCS estimates converge to the expected values as the sample number approaches infinity; however, it usually requires more than 1000 sample points to have the MCS moment estimates converge to a reasonable accuracy.

In comparison with the MCS moment estimates, we can see that the MM technique outperforms the FOSM technique significantly in all cases (see Figure 3-4 through Figure 3-9). In particular, $E(Y)_{MM}$ and $Var(Y)_{MM}$ are exact for $g(X) = X^2$ (Figure 3-4), and $E(Y)_{MM}$ is exact for $g(X) = X^4$ (Figure 3-5). Although the MM technique does give inconsistent estimates (compared with the large-sample MCS estimates) for the mean of $\log(|X|)$ and the variances of X^4, e^X, and $\log(|X|)$, the FOSM technique gives inconsistent estimates of the mean and variance for all these cases. The MM technique works quite well even for the non-differentiable function in Figure 3-2, for which the FOSM technique performs poorly. It does not work well for the step function

of Figure 3-3, but neither does the FOSM technique. This is because it is hard to mimic a step function using a fifth-order polynomial so we expect the estimate made by the fifth-order MM technique to be inaccurate.

In order to verify if any improvement can be made, Figure 3-10 through Figure 3-13 show the estimates for X^4, e^X, $\log(|X|)$, and the discontinuous function using a ninth-order (five-point) MM technique. The results indicate that the estimates for the mean of $\log(|X|)$ and variances of X^4 and e^X are significantly improved, while the estimates for the mean of the discontinuous function and the variances of $\log(|X|)$ and the discontinuous function are still inconsistent. These inconsistencies occur because it is still difficult to accurately approximate $\log(|X|)$ and the discontinuous function even with ninth-order polynomials.

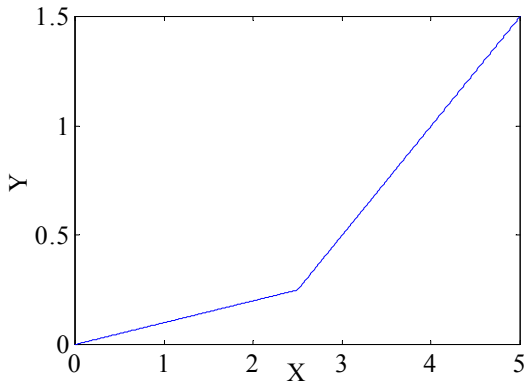

Figure 3-2. A non-analytic function

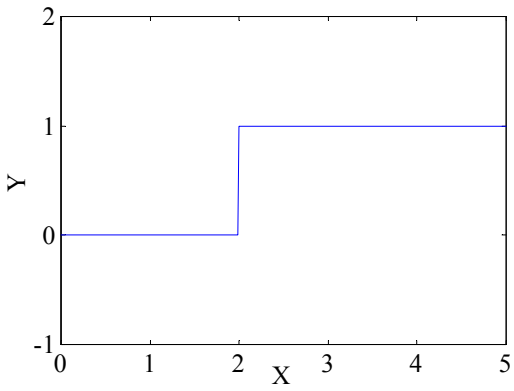

Figure 3-3. A discontinuous function

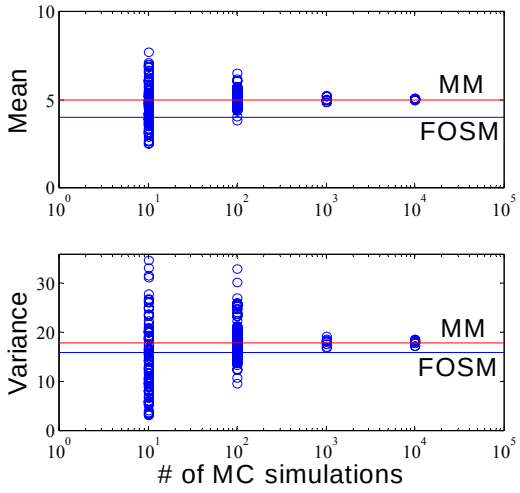

Figure 3-4. Estimation result for $Y=X^2$

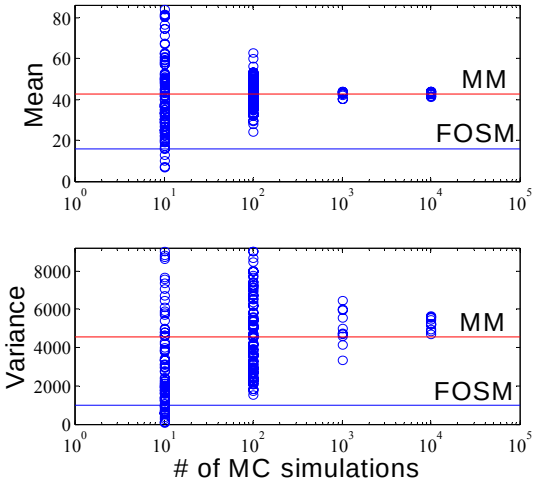

Figure 3-5. Estimation result for $Y=X^4$

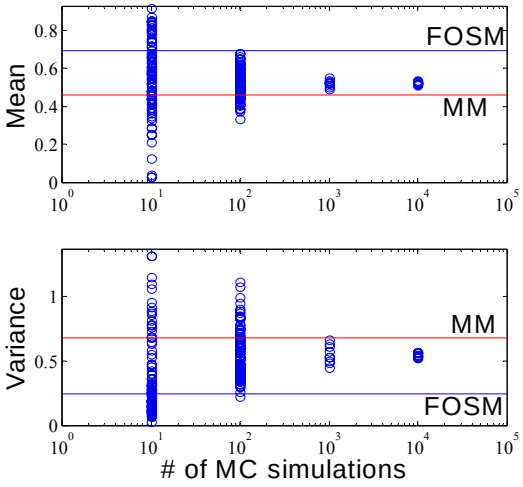

Figure 3-6. Estimation result for $Y=\log|X|$

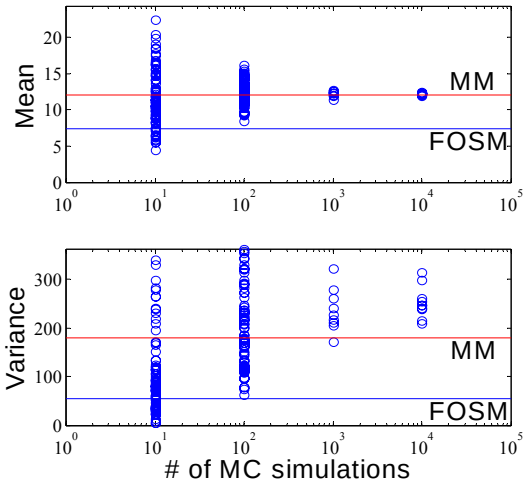

Figure 3-7. Estimation result for $Y=e^X$

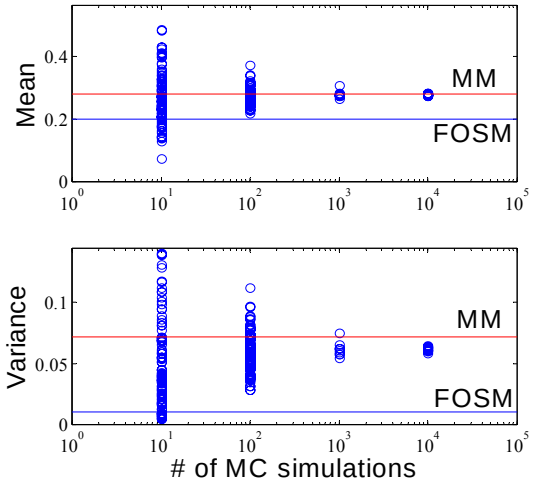

Figure 3-8. Result for the non-analytic function

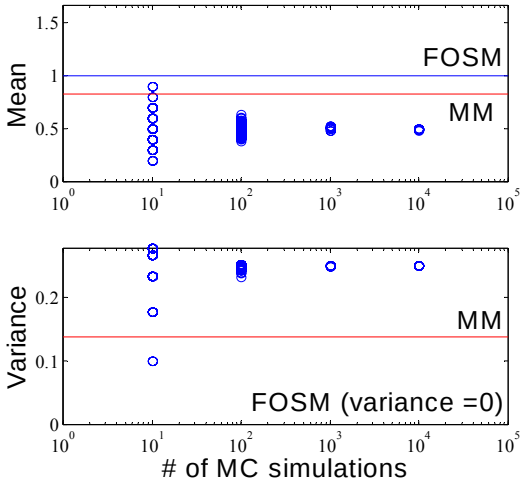

Figure 3-9. Result for the discontinuous function

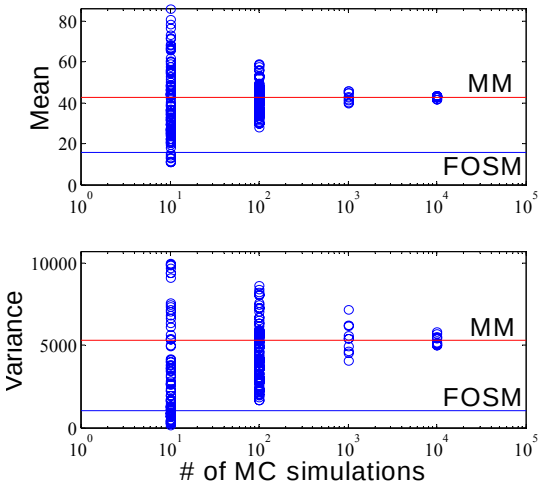

Figure 3-10. Result for $Y=X^4$ (5-point MM)

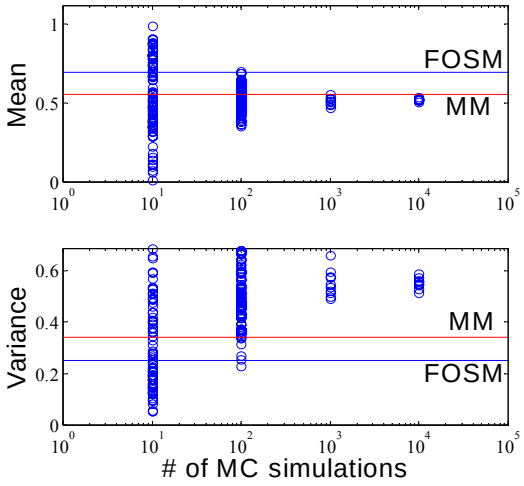

Figure 3-11. Result for $Y=\log|X|$ (5-point MM)

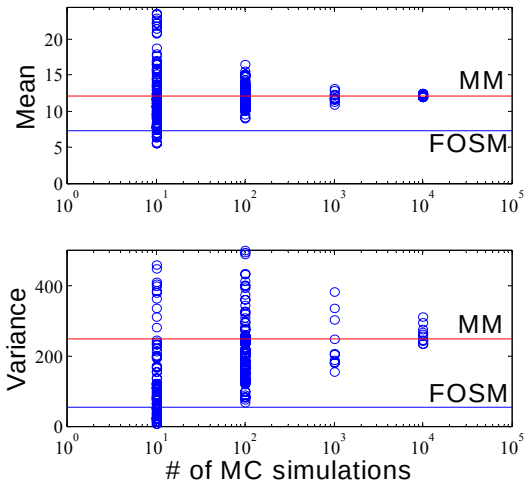

Figure 3-12. Result for $Y=e^X$ (5-point MM)

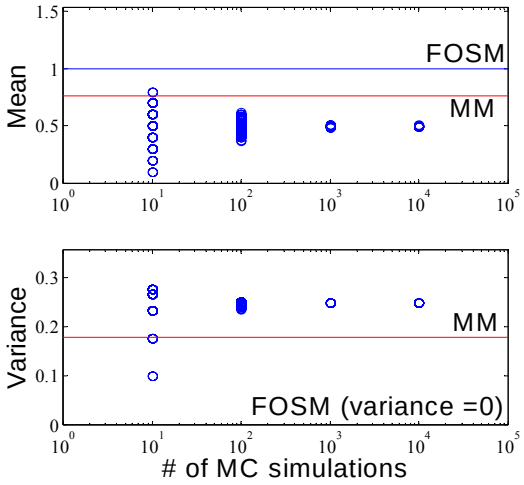

Figure 3-13. Result for discontinuous function (5- point MM)

4 UNCERTAINTY PROPAGATION FOR REPAIR COSTS

We examine here two types of quantitative information about repair costs as a decision variable (*DV*): 1) moments of *DV* and 2) exceedance probability (or mean annual exceedance frequency) of *DV*. In this section, we derive the MM-based algorithms that are used to estimate the moments and exceedance probability of *DV*. In Section 4.1, we summarize aspects of the assembly-based vulnerability (ABV) approach. In Sections 4.2 and 4.3, we derive the moments and exceedance probability of single-event repair costs (denoted by C_R) conditioned on the occurrence of a future earthquake. Several different decision variables (*DV*) will be discussed in Section 4.4, where we show that their moments and exceedance probability (or mean exceedance frequency) can be determined based on the results of Sections 4.2 and 4.3.

4.1 ASSEMBLY-BASED-VULNERABILITY FRAMEWORK

A prerequisite to deriving the moments of an economic-loss *DV,* such as C_R, is knowledge of the basic uncertain variables that contribute to the *DV*. These variables can be categorized as earthquake intensity; ground motion time history; the mass, damping, and force-deformation behavior of the soil, foundation, and structure; component damageability; and repair costs (or other losses) conditioned on physical damage. Using moment-matching to derive the moments of *DV* also requires one to determine the functional relationship between the basic variables and *DV*.

We briefly recap here the assembly-based vulnerability (ABV) approach, which is the PBEE framework that we use for quantifying the uncertain variables and their functional relationship to *DV*. ABV is presented in Beck et al. (1999) and Porter (2000), and is summarized in Porter et al. (2001). Under ABV, a building or other facility is conceived as a collection of structural, architectural, and other components that are classified under a standard taxonomic

system of assembly types, akin to the assembly system of RS Means (e.g., RS Means 1997). An assembly is a collection of building components assembled into a recognizable feature such as a 64-sf segment of gypsum wallboard partition or a reinforced concrete beam-column.

Each damageable assembly type is associated with one or more discrete damage states, defined in terms of the repair efforts required to restore the assembly to its undamaged state. Associated with each repair effort is a unit cost, i.e., the uncertain cost to perform the repairs for a single damaged assembly, such as a single broken window. (Also associated with the repair effort are the trades and grades of craftsmen required to perform the work and the uncertain length of time required to perform the repairs. Herein, we consider only costs.) Unit repair costs vary by geographic location, time, whether union or nonunion labor is used, and possibly other factors.

Damage to each damageable assembly type is treated as a probabilistic function of an engineering demand parameter (*EDP*), i.e., the probability that the assembly type will enter or exceed some damage state *j* is given as a function of *EDP*, called the fragility function of that assembly type. This probability can also be interpreted by supposing that an assembly has an uncertain capacity, denoted by *C*, to resist damage. If $EDP > C$, i.e. demand exceeds capacity, then the assembly is damaged; otherwise it is not. Hence the probability of damage is given by the cumulative distribution of *C* evaluated at *EDP*, and one therefore needs knowledge of the probability distribution of *C* for each damageable assembly type and damage state.

The *EDP* to which a damageable assembly is sensitive could conceivably be a vector of two or more structural-response or other parameters. To date, however, we have defined assembly fragility functions solely as functions of a single, scalar *EDP*. For example, the fragility function for window breakage is given as a function of the peak transient interstory drift

of the story and column line of that window. Other assembly types, such as suspended ceilings, may be sensitive to peak absolute acceleration to which they are subjected, while others, such as beam-column connections, may be sensitive to their peak internal force or deformation.

With this background in mind, one can estimate the single-event building repair costs due to a future earthquake while considering the uncertainties in unit repair costs, assembly damage, and contractor overhead and profit. The building repair cost C_R is given by:

$$C_R = (1 + C_{op}) \sum_{i=1}^{n_a} \sum_{j=1}^{n_D^i} URC_{i,j} \cdot \mathrm{I}(DM_i = j) \tag{4.1}$$

where C_{op} is a factor to account for the uncertain contractor overhead and profit; n_a is the total number of damageable assemblies in the structure; n_D^i is the number of damage states for the i^{th} assembly; $URC_{i,j}$ is the uncertain repair cost for the i^{th} assembly in the j^{th} damage state; DM_i is the damage state for the i^{th} assembly; and $I(.)$ is the indicator function, equal to 1 if the statement in parentheses is true and 0 otherwise.

The indicator function $\mathrm{I}(DM_i = j)$ depends on *EDP* and the capacity *C*. *EDP*, in turn, is determined from structural analysis, given the structural model *SM*, the intensity measure *IM*, and the associated ground-motion time history $a(t)$. If damage states for an assembly type can be ranked in increasing order, i.e., repair from a "higher" damage state necessarily repairs damage associated with each lower state, one can write the transformation from *EDP* and *C* to $\mathrm{I}(DM_i = j)$ as:

$$\begin{aligned}
&\mathrm{I}(DM_i = 0) = 1 \qquad iff \qquad EDP_i < C_{i,1} \\
&\mathrm{I}(DM_i = j) = 1 \qquad iff \qquad C_{i,j-1} \le EDP_i < C_{i,j}, \qquad 0 < j < n_D^i \\
&\mathrm{I}(DM_i = n_D^i) = 1 \qquad iff \qquad C_{i,n_D^i} \le EDP_i
\end{aligned} \tag{4.2}$$

where i is the index of a damageable structural or non-structural assembly; EDP_i is the engineering demand parameter for the i^{th} assembly; and $C_{i,j}$ is the capacity of the i^{th} assembly for the j^{th} damage state. To summarize, C_R is the single-event building repair cost conditioned on the occurrence of a future earthquake. It depends on the following basic uncertain variables: *IM*, $a(t)$, *SM*, *C*, *URC*, and C_{op}. Note that *EDP* and *DM* are intermediate uncertain variables determined by structural analysis.

To begin the derivations of the moments and exceedance probability of C_R, we require the following assumptions:

Assumption 4-1: We assume that all of the basic uncertain variables are stochastically independent, including variables in *IM*, *SM*, *URC*, *C*, C_{op}, etc.

Assumption 4-2: Throughout the derivations, we assume the $URC_{i,j}$ are lognormal variables with median $\hat{U}_{i,j}$ and logarithmic standard deviation $\beta^U_{i,j}$, i.e., $\ln(URC_{i,j}/\hat{U}_{i,j})$ has a Gaussian distribution $N(0, \beta^{U\,2}_{i,j})$. Note that $URC_{i,j}$ is defined for an assembly type and damage state but not for individual instances of an assembly type, so the unit cost to repair two assemblies of the same type and damage state are perfectly correlated. Unit costs for different assembly types or damage states are treated as independent.

Assumption 4-3: We assume that capacities $C_{i,j}$ with different i (assembly index) and j (damage-state index) are independent and are lognormal variables with median $\hat{C}_{i,j}$ and logarithm standard deviations equal to $\beta^C_{i,j}$. Under this assumption, it is true that $I(DM_i = j)$ of different i index are independent conditioned on *EDP*. But it is not true that $I(DM_i = j)$ of different j index are independent conditioned on *EDP*. In fact, the corresponding events are mutually exclusive so only one of them can be equal to one and the others must be zero, corresponding to

the assumption that a particular assembly must be in one and only one damage state (the undamaged state, $j = 0$, included).

It is clear that the transformation in Equation (4.2) is a discontinuous function of *EDP* and *C*; therefore, C_R is also a discontinuous function of *EDP* and *C*. As we have seen in the simulations in Section 3.3, the MM technique works well for most continuous functions but does not work well for discontinuous functions, so the implementation of the MM technique seems at first glance to be inadequate.

Nevertheless, if the coefficients of variation, or lognormal standard deviations, of $C_{i,j}$ are not small, the transformation from *EDP* to $P(DM_i = j \mid EDP)$ is smooth. To be specific,

$$\begin{aligned} &P\left(DM_i = 0 \mid EDP_i = edp_i\right) = 1 - F_{C_{i,1}}(edp_i) \\ &P\left(DM_i = j \mid EDP_i = edp_i\right) = F_{C_{i,j}}(edp_i) - F_{C_{i,j+1}}(edp_i) \qquad 0 < j < n_D^i \\ &P\left(DM_i = n_D^i \mid EDP_i = edp_i\right) = F_{C_{i,n_D^i}}(edp_i) \end{aligned} \tag{4.3}$$

are smooth functions of *EDP* since $F_{Ci,j}$, the cumulative distribution function of $C_{i,j}$, is smooth. We show later that the quantities that we are interested in (i.e. moments and exceedance probability of C_R) depend on *EDP* and *C* through $P(DM_i = j \mid EDP)$, so the implementation of the MM technique is, in fact, appropriate (although when the coefficients of variation of $C_{i,j}$ are small, the use of the MM technique can still be inadequate). For conciseness, we will denote $P(DM_i = j \mid EDP_i = edp_i)$ by $P_{EDP}(DM_i = j)$. Note that for lognormal fragility functions, $F_{Ci,j}$ in Equation (4.3) can be written as

$$F_{C_{i,j}}(edp_i) = \Phi\left(\frac{\log\left(edp_i / \hat{C}_{i,j}\right)}{\beta_{i,j}^C}\right) \tag{4.4}$$

and $\Phi(\cdot)$ is the cumulative distribution function of a standard Gaussian variable.

4.2 MOMENTS OF REPAIR COSTS C_R

We will first derive analytically the first four moments of C_R conditioning on *IM*, $a(t)$, *SM*, *URC*, and C_{op}. Then we show how to use the MM technique to estimate the four moments of C_R conditioning only on *URC* and C_{op}. Finally, we discuss how to compute the four (unconditional) moments of C_R with one more round of the MM technique.

4.2.1 Moments of C_R conditioned on IM, a(t), SM, URC, and C_{op}

Let us denote by

$$RC_i = \sum_{j=1}^{n_D^i} URC_{i,j} \cdot \mathrm{I}(DM_i = j) \tag{4.5}$$

the repair cost for the i^{th} assembly type. Using the fact that

$$\mathrm{I}(DM_i = j_1) \cdot \mathrm{I}(DM_i = j_2) = 0 \qquad for \qquad j_1 \neq j_2 \qquad \forall i\,, \tag{4.6}$$

the first four (non-central) moments of RC_i conditioning on *IM*, $a(t)$, *SM*, and *URC* are simply

$$\begin{aligned}
E(RC_i \mid IM, a(t), SM, URC) &= \sum_{j=1}^{n_D^i} URC_{i,j} \cdot P(DM_i = j \mid IM, a(t), SM) \\
&= \sum_{j=1}^{n_D^i} URC_{i,j} \cdot P_{EDP}(DM_i = j) \\
E(RC_i^2 \mid IM, a(t), SM, URC) &= \sum_{j=1}^{n_D^i} URC_{i,j}^2 \cdot P_{EDP}(DM_i = j) \\
E(RC_i^3 \mid IM, a(t), SM, URC) &= \sum_{j=1}^{n_D^i} URC_{i,j}^3 \cdot P_{EDP}(DM_i = j) \\
E(RC_i^4 \mid IM, a(t), SM, URC) &= \sum_{j=1}^{n_D^i} URC_{i,j}^4 \cdot P_{EDP}(DM_i = j)
\end{aligned} \tag{4.7}$$

For conciseness, we denote $E(\cdot \mid IM, a(t), SM, URC)$ by E_{IASU} so that $E(RC_i^r \mid IM, SM, URC) = E_{IASU}(RC_i^r)$. Note that in Equation (4.7), we have used the fact that $P(DM_i = j \mid IM, a(t), SM) = P(DM_i = j \mid EDP) = P_{EDP}(DM_i = j)$, i.e. conditioning on *IM*, $a(t)$, and *SM* is equivalent to

conditioning on *EDP*. Note that in computing *EDP* for given *IM*, $a(t)$, and *SM*, the ground motion $a(t)$ is scaled to be consistent with the specified *IM* before the structural analysis is done with structural model SM.

Now convert the non-central moments to central moments (no conversion of the first central moment is necessary):

$$\begin{aligned} Var_{IASU}(RC_i) &= E_{IASU}(RC_i^2) - E_{IASU}(RC_i)^2 \\ 3rd_{IASU}(RC_i) &= E_{IASU}(RC_i^3) - 3\cdot E_{IASU}(RC_i^2)\cdot E_{IASU}(RC_i) + 2\cdot E_{IASU}(RC_i)^3 \\ 4th_{IASU}(RC_i) &= E_{IASU}(RC_i^4) - 4\cdot E_{IASU}(RC_i^3)\cdot E_{IASU}(RC_i) + 6\cdot E_{IASU}(RC_i^2)\cdot E_{IASU}(RC_i)^2 - 3\cdot E_{IASU}(RC_i)^4 \end{aligned} \tag{4.8}$$

where *Var*, *3rd*, and *4th* denote the second, third, and fourth central moments, and the *IASU* subscript denotes central moments conditioning on *IM*, $a(t)$, *SM*, and *URC*.

Since $\mathrm{I}(DM_i = j)$ of different i indices are independent conditioned on *EDP* (see Assumption 2), RC_i of different i indices are independent conditioned on *IM*, $a(t)$, *SM*, and *URC*. Because of the following relation for independent *A* and *B*,

$$\begin{aligned} E(A+B) &= E(A) + E(B) \\ Var(A+B) &= Var(A) + Var(B) \\ 3rd(A+B) &= 3rd(A) + 3rd(B) \\ 4th(A+B) &= 4th(A) + 4th(B) + 6\cdot Var(A)\cdot Var(B) \end{aligned} \tag{4.9}$$

and also because

$$C_R = (1 + C_{op}) \sum_{i=1}^{n_a} RC_i \,, \tag{4.10}$$

the four central moments of C_R conditioning on *IM*, $a(t)$, *SM*, *URC*, and C_{op} can be evaluated using the following algorithm (in MATLAB notation):

Algorithm 4-1 – Compute the moments of C_R conditioned on *IM*, $a(t)$, *SM*, *URC* and C_{op}:

Initialize: $Sum(1) = Sum(2) = Sum(3) = Sum(4) = 0$

For $i = 1 : n_a$

Evaluate $E_{IASU}(RC_i)$, $Var_{IASU}(RC_i)$, $3rd_{IASU}(RC_i)$, and $4th_{IASU}(RC_i)$ using Equations (4.7) and (4.8).

Update

$$\begin{aligned} Sum(4) &= Sum(4) + 4th_{IASU}(RC_i) + 6 \cdot Sum(2) \cdot Var_{IASU}(RC_i) \\ Sum(3) &= Sum(3) + 3rd_{IASU}(RC_i) \\ Sum(2) &= Sum(2) + Var_{IASU}(RC_i) \\ Sum(1) &= Sum(1) + E_{IASU}(RC_i) \end{aligned} \quad . \tag{4.11}$$

End;

Finalize:

$$\begin{aligned} E_{IASUC}(C_R) &= Sum(1) \cdot (1 + C_{op}) & Var_{IASUC}(C_R) &= Sum(2) \cdot (1 + C_{op})^2 \\ 3rd_{IASUC}(C_R) &= Sum(3) \cdot (1 + C_{op})^3 & 4th_{IASUC}(C_R) &= Sum(4) \cdot (1 + C_{op})^4 \end{aligned} \tag{4.12}$$

(Subscript *IASUC* denotes central moments conditioning on *IM*, $a(t)$, *SM*, *URC* and C_{op}).

The non-central conditional moments of C_R, which are required in the following derivations, are simply

$$\begin{aligned} E_{IASUC}(C_R^2) &= Var_{IASUC}(C_R) + E_{IASUC}(C_R)^2 \\ E_{IASUC}(C_R^3) &= 3rd_{IASUC}(C_R) + 3 \cdot Var_{IASUC}(C_R) \cdot E_{IASUC}(C_R) + E_{IASUC}(C_R)^3 \\ E_{IASUC}(C_R^4) &= 4th_{IASUC}(C_R) + 4 \cdot 3rd_{IASUC}(C_R) \cdot E_{IASUC}(C_R) + 6 \cdot Var_{IASUC}(C_R) \cdot E_{IASUC}(C_R)^2 + E_{IASUC}(C_R)^4 \end{aligned} \tag{4.13}$$

4.2.2 Evaluation of moments of C_R conditioned on URC and C_{op}

The derivations for the conditional moments of C_R presented in the last few sections are exact. In this section, we show how to estimate the moments of C_R conditioned on *URC and* C_{op} (i.e. the variables that come after the structural analysis) through the MM technique. The following equation is true:

$$\begin{aligned} E(C_R^r \mid URC, C_{op}) &= E\left(E(C_R^r \mid IM, a(t), SM, URC, C_{op}) \mid URC, C_{op}\right) \\ &= E\left(E_{IASUC}(C_R^r) \mid URC, C_{op}\right) \qquad r = 1,2,3,4 \end{aligned} \tag{4.14}$$

where the outer expectation in the last term is with respect to *IM*, $a(t)$, and *SM*, and $E_{IASUC}(C_R^r)$ is a function of *IM*, $a(t)$, *SM*, *URC*, and C_{op}.

Approximation 4-1: $E(C_R^r \mid URC, C_{op})$ in Equation (4.14) can be approximated using the MM technique as follows: It is usually the case that *IM* and *SM* are parameterized by uncertain parameters, e.g. *IM* can be parameterized by spectral acceleration S_a, and *SM* can be parameterized by floor mass, damping ratio, stiffness, etc. Denote all the uncertain variables in *IM* and *SM* by $X_1 \in R^n$. Note that X_1 does not include the uncertain variables in *URC*, C_{op}, and *C* (the expectations with respect to capacity *C* have been solved analytically in Section 4.2.1). Assuming that the PDF for X_1 is known, we use q_1 weighted delta functions in the X_1 domain to match the first p_1 moments of X_1. Since we assume the basic uncertain variables are independent (Assumption 4-1), it suffices to put all the q_1 weighted delta functions on the axes of the basic variables to match all of the moments of X_1. Therefore, q_1 only grows linearly, not exponentially, with the dimension of X_1. Figure 4-1 demonstrates an example of this procedure: the locations of the q_1 delta functions to match the moments of S_a (spectral acceleration, included in *IM*), mass, damping ratio (included in *SM*), etc. are on their axes.

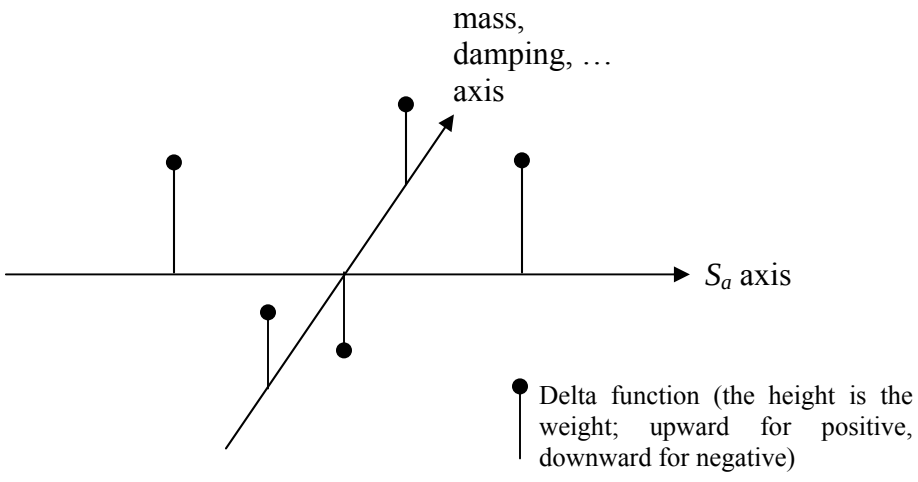

Figure 4-1. An illustration of the placement of the weighted delta functions

Evaluation of $E_{IASUC}(C_R^r)$ at the q_1 points in the X_1 domain (where *URC* and C_{op} are fixed) with a given ground motion history $a(t)$ will give q_1 real numbers, and the weighted sample mean of these q_1 numbers is then the MM estimate of $E(C_R^r \mid a(t), URC, C_{op})$, denoted by $E_{MM}(C_R^r \mid a(t), URC, C_{op})$. Since we match the first p_1 moments of X_1, the resulting accuracy of this MM estimate is p_1th-order.

To remove the conditioning on $a(t)$, we introduce another assumption:

Assumption 4.4: We assume that all ground-motion records in the chosen strong-motion database are equally likely at the site when scaled to have the given *IM*.

The above process is then repeated for N_{EQ} randomly-drawn ground motion time histories $a_m(t), \quad m = 1, \ldots, N_{EQ}$, from the strong-motion database to obtain $E_{MM}(C_R^r \mid a(t), URC, C_{op})$ for each m. The final MM estimate $E_{MM}(C_R^r \mid URC, C_{op})$ is then simply the average of these $E_{MM}(C_R^r \mid am(t), URC, C_{op})$, in view of Assumption 4.4.

The algorithm for estimating moments of C_R conditioned on *URC* and C_{op} is therefore:

Algorithm 4-2 – Compute the first four moments of C_R conditioned on *URC* and C_{op}:

Initialize: Specify the values of *URC* and C_{op}. Given the joint PDF or moments of *IM* and *SM*, find the coordinates $\{IM_k, SM_k\}$ and weights w_k of the q_1 delta functions (k = *1,…*q_1) to match the first p_1 moments of *IM* and *SM*.

For r = 1: 4;
  For m = *1*: N_{EQ};

    Draw a ground motion time history $a_m(t)$ from database.

    For k = *1*: q_1;
      Compute $E(C_R^r \mid IM_k, SM_k, a_m(t), URC, C_{op})$
    End;

$$E_{MM}(C_R^r \mid a_m(t), URC, C_{op}) = \sum_{k=1}^{q_1}\left[w_k \cdot E(C_R^r \mid IM_k, SM_k, a_m(t), URC, C_{op})\right] \tag{4.15}$$

End;

$$E_{MM}(C_R^r \mid, URC, C_{op}) = \frac{1}{N_{EQ}}\sum_{m=1}^{N_{EQ}} E_{MM}(C_R^r \mid a_m(t), URC, C_{op}) \tag{4.16}$$

End;

During the process of estimating the moments of C_R using the MM technique, the most time-consuming step is usually the structural analysis, i.e. computation of *EDP* based on each IM_k, $a_m(t)$, and SM_k. In Algorithm 4-2, structural analysis needs to be carried out $N_{EQ} \times q_1$ times.

4.2.3 Evaluation of moments of C_R

After the moments of C_R conditioned on *URC* and C_{op} are obtained, the (un-conditional) moments of C_R can be evaluated by using the fact that

$$E(C_R^r) = E\left(E(C_R^r \mid URC, C_{op})\right) \qquad r = 1,2,3,4, \tag{4.17}$$

$E(C_R^r)$ can be, in turn, approximated using the MM technique: Use q_2 weighted delta functions in the *URC* and C_{op} domain to match the first p_2 moments of the joint PDF of *URC* and C_{op}; evaluating $E(C_R^r \mid URC, C_{op})$ at the q_2 points in the *URC* and C_{op} domain will give q_2 real numbers, and the weighted sample mean of these q_2 numbers is then the MM estimate of $E(C_R^r)$, denoted by $E_{MM}(C_R^r)$. The resulting algorithm for estimating moments of C_R is as follows:

Algorithm 4-3 – Compute the first four moments of C_R:

Initialize: Given the joint PDF or moments of *URC* and C_{op}, find the coordinates $\{URC_k, C_{op,k}\}$ and weights w_k of the q_2 delta functions ($k = 1,\ldots q_2$) to match the first p_2 moments of *URC* and C_{op}.

For $r = 1: 4$;

For $k = 1: q_2$;

Compute $E_{MM}(C_R^r \mid URC_k, C_{op,k})$ using Algorithm 4-2.

End;

$$E_{MM}(C_R^r) = \sum_{k=1}^{q_2} \left[w_k \cdot E_{MM}(C_R^r \mid URC_k, C_{op,k}) \right] \tag{4.18}$$

End;

In Sections 4.2.2 and 4.2.3, we use the MM technique to approximate the (un-conditional) moments of C_R by progressively eliminating the conditioning variables in Section 4.2.1; in Section 4.2.2 we eliminate *IM*, $a(t)$, and *SM* while in Section 4.2.3 we eliminate *URC* and C_{op}. In principle, we can combine these two MM steps that involve eliminating conditioning variables into a single MM step, i.e. match the moments of the joint PDF of *IM*, $a(t)$, *SM*, *URC*, and C_{op} using some weighted delta functions in the corresponding space, then evaluate $E(C_R^r \mid IM, a(t), SM, URC, C_{op})$ at the locations of the delta functions, and, finally the MM estimate of $E(C_R^r)$ is computed as the weighted sum of these $E(C_R^r \mid IM, a(t), SM, URC, C_{op})$. Although theoretically plausible, this one-step approach is found to be less accurate than the two-step approach when estimating higher moments (higher than the first moment) of C_R.

It seems that Algorithm 4-2 has to be carried out in each loop during Algorithm 4-3, so the entire process of estimating $E(C_R^r)$ using the two-step approach requires $N_{EQ} \times q_1 \times q_2$ structural analyses. It turns out that this is not the case, and we only need $N_{EQ} \times q_1$ structural analyses. This is because when evaluating $E_{MM}(C_R^r \mid URC_k, C_{op,k})$ during Algorithm 4-3, the results of the $N_{EQ} \times q_1$ structural analyses computed during Algorithm 4-2 are re-usable.

If we match the first p_2 moments of *URC* and C_{op} using the MM technique in Algorithm 4-3, and we are only interested in estimating the first m ($\leq p_2$) moments of C_R, Algorithm 4-3 does not introduce any approximation error. This is because C_R is linear in *URC* and C_{op}, so the

m-th moment of C_R depends only on moments of *URC* and C_{op} whose orders are less than or equal to *m*.

4.3 EXCEEDANCE PROBABILITY $P(C_R > THRESH)$

$P(C_R > thresh)$ is the exceedance probability for the building repair cost conditioned on the occurrence of a future earthquake event where the corresponding ground motion at the building site is uncertain. It can be calculated in two steps, as described in the following two sub-sections.

4.3.1 Derivation of $P(C_R > thresh| IM, a(t), SM, C_{op})$

In order to compute $P(C_R > thresh| IM, a(t), SM, C_{op})$, where *thresh* denotes the chosen repair cost threshold, we first construct the PDF of C_R conditioning on *IM, a(t), SM,* and C_{op}. Recall that during the derivations of moments of C_R, we first construct the moments of C_R by conditioning on *IM*, $a(t)$, *SM*, *URC*, and C_{op} (i.e. the contribution of capacity *C* is integrated out analytically). As we have discussed, the conditional moments of C_R are smooth functions of *IM*, $a(t)$, *SM*, *URC*, and C_{op}. However, for the exceedance probability, the situation is different: If we only integrate out the contribution of *C*, the conditional probability $P(C_R > thresh| IM, a(t), SM, URC, C_{op})$ is still a discontinuous function of *URC*. Therefore, it is desirable to also integrate out the contribution of *URC* analytically; the resulting conditional exceedance probability $P(C_R > thresh| IM, a(t), SM, C_{op})$ is a smooth function of *IM*, *SM*, and C_{op}.

Basically, the PDF of C_R conditioning on *IM*, $a(t)$, *SM*, and C_{op}, denoted by $f_{C_R}(thresh \mid IM, a(t), SM, C_{op})$, is the mixture (weighted sum) of $(n_D^1 + 1) \times (n_D^2 + 1) \times \ldots$ PDFs, each of them represents a possible damage configuration in the structure, and the weights of the PDFs indicate the possibility of the occurrence of the configurations:

$$
\begin{aligned}
&f_{C_R}(thresh|\, IM, a(t), SM, C_{op}) \\
&= \sum_{j_1=0}^{n_D^1} \sum_{j_2=0}^{n_D^2} \cdots \sum_{j_{n_a}=0}^{n_D^{na}} P(DM_1 = j_1, ..., DM_{n_a} = j_{n_a} \mid IM, a(t), SM, C_{op}) \\
&\qquad \cdot f_{C_R}(thresh|\, IM, a(t), SM, C_{op}, DM_1 = j_1, ..., DM_{n_a} = j_{n_a})
\end{aligned} \tag{4.19}
$$

where DM_i is the damage state of the i-th assembly; $DM_1 = j_1, ..., DM_{n_a} = j_{n_a}$ denotes a specific damage configuration. The factors $P(DM_1 = j_1, ..., DM_{n_a} = j_{n_a} \mid IM, a(t), SM, C_{op})$ can be evaluated using the fact that DM_i of different i are independent conditioning on IM and SM:

$$
P(DM_1 = j_1, ..., DM_{n_a} = j_{n_a} \mid IM, a(t), SM, C_{op}) = P_{EDP}(DM_1 = j_1) \cdots P_{EDP}(DM_{n_a} = j_{n_a}) \tag{4.20}
$$

Evaluating $f_{C_R}(thresh \mid IM, a(t), SM, C_{op})$ is potentially intractable for large problems since it involves the interactions of $(n_D^1 + 1) \times (n_D^2 + 1) \times \ldots$ PDFs. By slightly sacrificing the accuracy, we can make the evaluation of $f_{C_R}(thresh \mid IM, a(t), SM, C_{op})$ tractable using a procedure described as follows: Let the upper bound of C_R be $C_{R,max}$ (which can be taken as the replacement value of the building), then the axis of C_R is divided into $C_{R,\max} / l_c$ segments of equal length l_c, which is chosen so that there is an integral number of segments. Damage configurations whose mean repair costs are in the same C_R segment are merged into a single new (lumped) damage configuration. The weight (i.e. the probability) of this lumped configuration is the sum of the weights of the configurations that are merged, and the number of the damaged units is the weighted average (i.e. mean) of the numbers of the damaged units for the merged configurations.

For instance, suppose two damage configurations have close mean repair costs so that they are merged. The probabilities of the two configurations are 0.02 and 0.01, and there are 3 and 5 broken windows, as well as 10 and 8 damaged drywalls, in these two damage configurations, respectively. Then the probability of the lumped configuration is 0.03 and the

corresponding damage number is (0.02×3+0.01×5)/(0.02+0.01) = 11/3 broken windows and (0.02×10+0.01×8)/(0.02+0.01) = 28/3 damaged drywalls.

After the merging, the determination of $f_{C_R}(thresh \mid IM, a(t), SM, C_{op})$ becomes tractable since now it only involves up to $C_{R,\max}/l_c$ lumped damage configurations. Let the PDF characterizing the repair costs of the η-th lumped configuration be $f_{C_R}^{\eta}(thresh \mid IM, a(t), SM, C_{op})$ with weight $w_{C_R}^{\eta}$, we have

$$f_{C_R}(thresh \mid IM, a(t), SM, C_{op}) \approx \sum_{\eta=1}^{C_{R,\max}/l_c} w_{C_R}^{\eta} \cdot f_{C_R}^{\eta}(thresh \mid IM, a(t), SM, C_{op}), \tag{4.21}$$

so that

$$P(C_R > thresh \mid IM, a(t), SM, C_{op}) \approx \sum_{\eta=1}^{C_{R,\max}/l_c} w_{C_R}^{\eta} \cdot \left[1 - F_{C_R}^{\eta}(thresh \mid IM, a(t), SM, C_{op})\right], \tag{4.22}$$

where $F_{C_R}^{\eta}(thresh \mid IM, a(t), SM, C_{op})$ is the cumulative distribution function of $f_{C_R}^{\eta}(thresh \mid IM, a(t), SM, C_{op})$.

Due to the assumption that the unit repair costs for units of different types are independent, e.g. the unit repair costs for a broken window and a damaged drywall are independent, $f_{C_R}^{\eta}(thresh \mid IM, a(t), SM, C_{op})$ is equal to the convolution of several lognormal PDFs. Continuing with the previous example, the PDF of the lumped configuration, whose damage number is 11/3 broken windows and 28/3 damaged drywalls, is equal to the convolution of the PDF for the window unit repair cost scaled by 11/3 (i.e. $f_{URC,window}(thresh/(11/3))$) and the PDF for the drywall unit repair cost scaled by 28/3 (i.e. $f_{URC,drywall}(thresh/(28/3))$). The means for $f_{URC,window}(thresh/(11/3))$ and $f_{URC,drywall}(thresh/(28/3))$ are given by $(11/3)\cdot E(URC_{window})$ and $(28/3)\cdot E(URC_{drywall})$, while their variances are given by $(11/3)^2 \cdot Var(URC_{window})$ and

$(28/3)^2 \cdot Var(URC_{drywall})$, respectively. Therefore, the mean and variance of the PDF of the lumped configuration are

$$(11/3) \cdot E(URC_{window}) + (28/3) \cdot E(URC_{drywall}) \tag{4.23}$$

and

$$(11/3)^2 \cdot Var(URC_{window}) + (28/3)^2 \cdot Var(URC_{drywall}). \tag{4.24}$$

Approximation 4-2: We approximate the PDF of a lumped configuration using a lognormal PDF with mean and variance calculated according to its damage number (i.e. similar to Equations (4.23) and (4.24)). Under this assumption, $F_{C_R}^{\eta}(thresh \mid IM, a(t), SM, C_{op})$ in Equation (4.22) is a lognormal cumulative distribution function, which can be easily evaluated.

This approximation uses a lognormal PDF to approximate the convolution of several lognormal PDFs, which is not exactly true. From our experience, however, this is a good approximation when the logarithm standard deviations of the *URCs* are not dramatically non-uniform. As an example, consider repair costs of three different types of units, denoted by RC_1, RC_2, and RC_3 with medians and logarithm standard deviations equal to (200, 600, 800) and (0.4, 0.2, 0.3). The actual PDF of $W=RC_1+RC_2+RC_3$ is the convolution of the three lognormal PDFs and is plotted in Figure 4-2. The mean and variance of W are 1665.6 and 89384, and the lognormal PDF with these mean and variance is also plotted in Figure 4-2. As seen in the figure, the lognormal approximation is satisfactory.

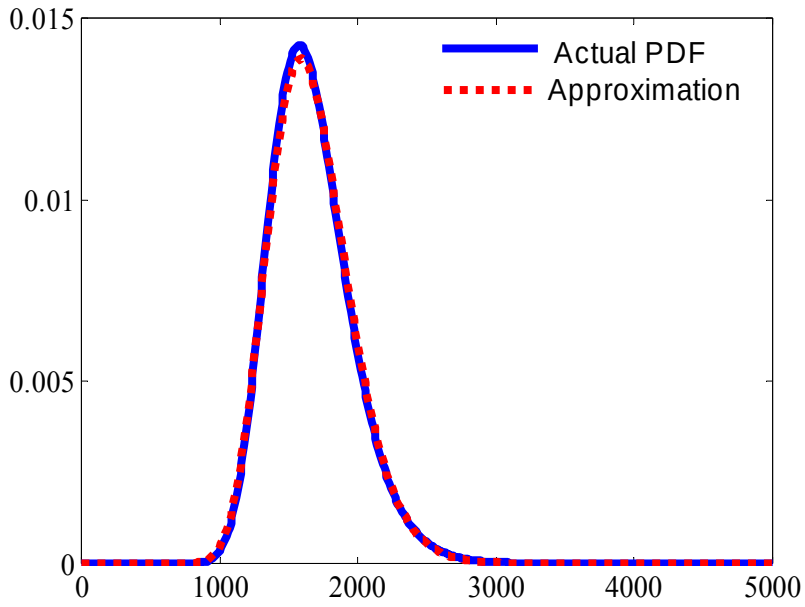

Figure 4-2. The actual and lognormal approximate PDFs of $RC_1+RC_2+RC_3$

4.3.2 Computation of exceedance probability $P(C_R > thresh)$

Approximation 4-3: $E_{IM,a(t),SM,C_{op}}\left(P(C_R > thresh \mid IM, a(t), SM, C_{op})\right) = P(C_R > thresh)$ can be approximated using the MM technique in a manner similar to Approximation 4-1. Denote all the uncertain basic variables for *IM*, *SM*, and C_{op} as $X_3 \in R^n$ (X_3 does not include *C* and *URC*). We use q_3 weighted delta functions in the X_3 domain to match the first p_3 moments of X_3; evaluating $P(C_R > thresh \mid IM, a(t), SM, C_{op})$ at the q_3 points with a given ground motion time history $a(t)$ will give q_3 real numbers, and the weighted sample mean of these q_3 numbers is then the MM estimate of $P(C_R > thresh \mid a_m(t), m = 1\ldots, N_{EQ})$. Since we match the first p_3 moments of X_3, the resulting accuracy of this MM estimate is p_3th-order. Repeat this process for N_{EQ} randomly-drawn ground motion time histories $a_m(t), m = 1,\ldots, N_{EQ}$, from the strong-motion database to obtain several MM estimates $P_{MM}(C_R > thresh \mid a_m(t)), m = 1,\ldots, N_{EQ}$. The final MM estimate

$P_{MM}(C_R > thresh)$ is then simply the average of these MM estimates under Assumption 4-4. The resulting algorithm is as follows:

Algorithm 4-4:

Initialize: Given the joint PDF or moments of *IM*, *SM*, and C_{op}, find the coordinates $\{IM_k, SM_k, C_{op,k}\}$ and weights w_k of the q_3 delta functions ($k = 1,\ldots q_3$) to match the first p_3 moments of *IM*, *SM*, and C_{op}.

For m = 1 : N_{EQ};

Draw a ground motion time history $a_m(t)$ from database.

For k = *1:* q_3;

Compute $P(C_R > thresh \mid IM_k, a_m(t), SM_k, C_{op,k})$ as in Section 4.3.1

End;

$$P_{MM}(C_R > thresh \mid a_m(t)) = \sum_{k=1}^{q} \left[w_k \cdot P(C_R > thresh \mid IM_k, a_m(t), SM_k, C_{op,k}) \right]. \quad (4.25)$$

End;

$$P_{MM}(C_R > thresh) = \frac{1}{N_{EQ}} \sum_{m=1}^{N_{EQ}} P_{MM}(C_R > thresh \mid a_m(t)) \quad (4.26)$$

Notice that for estimating $P(C_R > thresh)$, we have implemented a one-step MM approach, i.e. match the moments of the joint PDF of *IM*, *SM*, and C_{op} at once, instead of the two-step approach adapted in Sections 4.2.2 and 4.2.3. We found that for estimating $P(C_R > thresh)$, the one-step and two-step approaches perform similarly. During the entire process of estimating $P(C_R > thresh)$, we need to carry out $N_{EQ} \times q_{IM,SM}$ structural analyses, where $q_{IM,SM}$ is the total number of weighted delta functions that are used to match the moments in the *IM* and *SM* direction.

4.4 DIFFERENT SCENARIOS AND DECISION VARIABLES *DV*

The single-event repair costs C_R that we have focused on so far are the repair costs conditioned on the occurrence of a future earthquake event whose *IM* has PDF $f_{IM}(im)$. In this report, we consider four different scenarios. We show that different choices of $f_{IM}(im)$ lead to different scenarios. For all scenarios, the hazard function, $\lambda_{IM}(im)$, i.e. the mean annual frequency of having earthquakes with *IM* > *im*, is employed.

4.4.1 Moments of total discounted repair costs during the next T years

We first consider the total discounted repair costs of the structure under study during the next *T* years as the decision variable *DV*. To evaluate the first four moments of this *DV*, we introduce the following assumption:

Assumption 4-5: The intensity measure *IM* for future earthquake events with *IM*>*im* is modeled as a Poisson process with mean annual frequency given by the hazard function $\lambda_{IM}(im)$ for any $im > im_l$, where im_l is the lowest intensity measure of interest.

It then follows from a property of the Poisson process that for all $im > im_l$, $\lambda_{IM}(im) = \lambda_{IM}(im_l).P(IM > im \mid IM > im_1)$, so the PDF of *IM* conditional on an event occurring with $IM > im_l$ is given by:

$$f_{IM}(im) = \frac{-1}{\lambda_{IM}(im_l)} \cdot \frac{d\lambda_{IM}(im)}{d(im)}, \tag{4.27}$$

Moreover, under the additional assumption that the single-event repair costs C_R for each future earthquake event is independent of the repair costs for previous events and independent of the time of occurrence of earthquakes, prior to discounting, then events with $C_R > z$ also form a

Poisson process with mean annual frequency $\lambda_{CR}(z)$ and corresponding PDF $f_{CR}(z)$ for C_R conditioned on an event occurring with $IM > im_l$ given by:

$$\lambda_{CR}(z) = \lambda_{IM}(im_l) \cdot P(C_R > z \mid IM > im_l)$$

and (4.28)

$$f_{CR}(z) = \frac{-1}{\lambda_{IM}(im_l)} \cdot \frac{d\lambda_{CR}(z)}{dz}$$

where $P(C_R > z \mid IM > im_l)$ can be estimated using the procedure described in Section 4.3. When matching the moments of *IM* using weighted delta functions, one matches the moments of $f_{IM}(im)$ described in Equation (4.27).

With Assumption 4-5, the MM estimates of the moments of *DV* are as follows (based on Appendix F of Beck et al. (2002)):

$$\begin{aligned}
E_{MM}(DV) &= \frac{1-e^{-r_d T}}{r_d} \cdot \lambda_{IM}(im_l) \cdot E_{MM}(C_R) \\
Var_{MM}(DV) &= \frac{1-e^{-2r_d T}}{2r_d} \cdot \lambda_{IM}(im_l) \cdot E_{MM}(C_R^2) \\
3rd_{MM}(DV) &= \frac{1-e^{-3r_d T}}{3r_d} \cdot \lambda_{IM}(im_l) \cdot E_{MM}(C_R^3) \\
4th_{MM}(DV) &= \frac{1-e^{-4r_d T}}{4r_d} \cdot \lambda_{IM}(im_l) \cdot E_{MM}(C_R^4) + 3 \cdot \left(\frac{1-e^{-2r_d T}}{2r_d} \cdot \lambda_{IM}(im_l) \cdot E_{MM}(C_R^2) \right)^2
\end{aligned} \quad (4.29)$$

where the expectation E_{MM} is conditional on $IM > im_l$ and r_d is the decision-maker's annual discount rate, taken as the risk free real interest rate.

To evaluate the MM estimates of the moments of C_R in Equation (4.29), the procedures described in Section 4.2 are followed. When matching the moments of *IM* using weighted delta functions, the moments of $f_{IM}(im)$ described in Equation (4.27) are matched (the moments of $f_{IM}(im)$ can be determined using numerical integration techniques).

4.4.2 *Mean exceedance frequency of C_R during the next T years*

Under Assumption 4-5, each C_R due to future earthquakes is independent and identically distributed. The mean exceedance frequency that C_R exceeds z in the next T years is simply $T\lambda_{CR}(z)$ where $\lambda_{CR}(z)$ is given in Equation (4.28).

4.4.3 *Moments of C_R due to a T-year extreme earthquake event*

It is also of interest to know the moments of the single-event repair costs C_R due to the most intense earthquake intensity in the next T years, i.e. the corresponding decision variable *DV* is the C_R due to the extreme *IM* event in the next T years. This special C_R can be also evaluated using the procedure described in Section 4.2; when matching the moments of *IM* using weighted delta functions, one matches the moments of the PDF of the extreme value of *IM* in the next T years, which is derived as follows:

Let $Y_{z,T}$ be the number of the earthquakes in the next T years whose *IM*s are larger than z. Under Algorithm 4-2, $Y_{z,T}$ is a Poisson process with mean arrival rate equal to $T \cdot \lambda_{IM}(z)$. The probability that $Y_{z,T} = 0$ is equal to $e^{-T\cdot\lambda_{IM}(z)}$. In other words, there is a probability $e^{-T\lambda_{IM}(z)}$ that the largest *IM* that occurs during the next T years, denoted by $IM_T^{\max}$, is less than z, i.e. $P(IM_T^{\max} < z) = e^{-T\lambda_{IM}(z)}$, so the PDF of $IM_T^{\max}$ (the extreme event in the next T years) is:

$$f_{IM_T^{\max}}(z) = -T \cdot \frac{d\lambda_{IM}(z)}{dz} \cdot e^{-T\cdot\lambda_{IM}(z)}. \tag{4.30}$$

4.4.4 *Exceedance probability of C_R due to a T-year extreme earthquake event*

On the other hand, it is also of interest to know the probability that C_R due to the extreme seismic intensity event in the next T years will exceed *thresh*. This probability can also be estimated using the procedure described in Section 4.3. When matching the moments of *IM* using weighted delta functions, one matches the moments of $f_{IM_T^{\max}}(z)$ described in Equation (4.30).

4.5 ILLUSTRATIVE EXAMPLE

In this example, we consider an idealized three-story shear building with nine damageable assemblies. The decision variable is the total repair cost during the next 50 years. The goal of the simulation is to estimate the first four central moments of this *DV* and the exceedance frequency of C_R in the next 50 years using the MM technique. The structural model is a linear viscously-damped model, so that the computation of *EDP* is simple and fast, making large-sample Monte Carlo simulations (MCS) feasible. The MCS estimates of the moments of *DV* and exceedance frequency of C_R are used as a comparison standard for this example. Other purposes of this example include:

1. To demonstrate the MM technique in detail as we present the results;
2. To conduct sensitivity analyses on certain variables to better understand the nature of the problem; and
3. To compare the MM estimates with other estimates (e.g. FOSM estimates).

Consider a three-story building located at (34.221°N, 118.471°W) in the Los Angeles area, whose site soil classification is D. A simplified shear-building model for this structure is shown in Figure 4-3, in which each uncertain floor mass (M) has mean value equal to 254,000 kg, each story has lateral stiffness (K) of 496 MN/m, and the story height (h) is 3.94 m. The hazard function is developed using Frankel and Leyendecker (2001) for a structure with a fundamental period T = 0.3s (the fundamental period of the structure in this example) and it is adjusted for the site soil classification. Figure 4-4 shows the resulting mean annual exceedance frequency for spectral acceleration (S_a) (the intensity measure used for this example). We use a recorded acceleration time history of North Palm Springs, 1986, as the earthquake ground motion in this simulation with spectral acceleration scaled to the desired value, i.e. all the results are conditional on a given ground motion time history $a(t)$ in this example.

The damageable assemblies in the building are from the nine assembly groups listed in Table 4-1, in which the corresponding *EDP* types, numbers of units, damage state (*DM*), and the parameters for the PDF of capacities (*C*) and unit repair costs (*URC*) are also specified. The uncertain variables include spectral acceleration (S_a), floor mass (*M*), damping ratio (β), capacities (*C*) and unit repair costs (*URC*) for each assembly type and damage state, and contactor overhead and profit (C_{op}). We assume lognormal PDF for the capacities and unit repair costs. Notice that the *URC* in assembly #1,2,3 are of the same type and have perfect correlation, and similar for the *URC* in assembly #4,5,6 and assembly #7,8,9.

The floor mass *M* is modeled as Gaussian with mean and standard deviation equal to 254,000kg and 25,400kg (the masses of the three floors are assumed to be perfectly correlated); the damping ratio β is Gaussian with mean and standard deviation equal to 0.05 and 0.02 (the damping ratios of different modes are assumed to be perfectly correlated); the contractor overhead and profit factor C_{op} is uniformly distributed over [0.15, 0.2]. The hazard function is differentiated numerically to obtain the PDF of *IM* (see Equation (4.27)), which is plotted in Figure 4-4 (im_l is taken to be 0.01g).

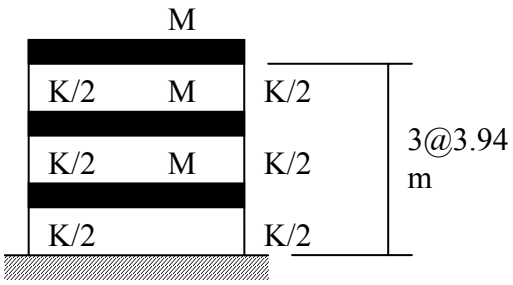

Figure 4-3. The simplified shear building model for the three-story building

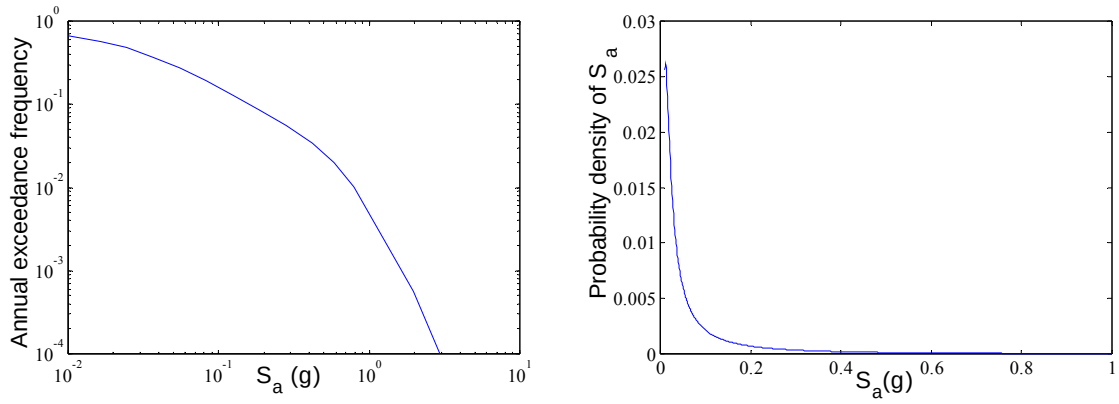

Figure 4-4. The hazard function and the PDF of S_a

Table 4-1. Quantities, capacities, and repair costs of assemblies in simple shear building

	Description	Number of units	EDP	Damage state	Median capacity	Log. std. dev. of capacity	Median unit repair cost ($)	Log. std. dev. of unit repair cost
1.	Windows (1st story)	56	PTD (1st story)	Cracking**	2.30%	0.3	440	0.26
2.	Windows (2nd story)	72	PTD (2nd story)	Cracking**	2.30%	0.3	440	0.26
3.	Windows (3rd story)	72	PTD (3rd story)	Cracking**	2.30%	0.3	440	0.26
4.	Suspended ceiling (1st story)	2	PDA (2nd floor)	Collapse	1.0g	0.8	6700	0.5
5.	Suspended ceiling (2nd story)	2	PDA (3rd floor)	Collapse	1.0g	0.8	6700	0.5
6.	Suspended ceiling (3rd story)	2	PDA (roof)	Collapse	1.0g	0.8	6700	0.5
7.	Drywall (1st story)	58	PTD (1st story)	Visible damage*	0.4%	0.2	90	0.2
				Significant damage**	0.8%	0.2	250	0.2
8.	Drywall (2nd story)	84	PTD (2nd story)	Visible damage*	0.4%	0.2	90	0.2
				Significant damage**	0.8%	0.2	250	0.2
9.	Drywall (3rd story)	84	PTD (3rd story)	Visible damage*	0.4%	0.2	90	0.2
				Significant damage**	0.8%	0.2	250	0.2

PTD: peak transient drift ratio PDA: peak diaphragm acceleration *Repair **Replace

4.5.1 Estimation of the moments of the total repair costs in the next 50 years

The *EDP* of the structure is computed assuming a 1-D (3 DOF) elastic viscously-damped shear-building model. We first use Algorithm 4-2 described in Section 4.2 to estimate the first four moments of C_R conditioning on *URC* and C_{op}. A fifth-order MM technique is used, and the coordinates and weights of the 8 delta functions in the domain of $IM = S_a$ and $SM = (M, \beta)$ are listed in Table 4-2. Since the mass and damping ratio are Gaussian distributed, the fifth-order Hermite-Gauss rule (Appendix A) is used. The locations and weights of the delta functions in the

IM=S_a direction are determined using the following procedure: First, the first five moments of $f_{IM}(im)$ are evaluated using numerical integration technique (listed in Table 4-3). The locations and weights (listed in Table 4-2) are then solved using Equation (3.11) or (3.12) to match the aforementioned five moments. For this specific example, we only need to carry out the structural analysis eight times to compute *EDP* for delta functions #0 through to #7.

Table 4-2. Locations and weights of the delta functions in the *IM* and *SM* space

Delta function number	M (kg)	β	S_a (g)	Weight
0	254,000	0.05	0.1007	-2/3
1	254,000-25,400$\sqrt{3}$	0.05	0.1007	1/6
2	254,000+25,400$\sqrt{3}$	0.05	0.1007	1/6
3	254,000	0.05-0.02$\sqrt{3}$	0.1007	1/6
4	254,000	0.05+0.02$\sqrt{3}$	0.1007	1/6
5	254,000	0.05	0.0557	0.9337
6	254,000	0.05	0.7045	0.0653
7	254,000	0.05	2.8241	0.00095

Table 4-3. The first five central moments of S_a

Mean	Variance	3rd central	4th central	5th central
0.101	3.28×10^{-2}	3.36×10^{-2}	6.12×10^{-2}	1.48×10^{-1}

Table 4-4. The first five central moments of unit repair costs (URC)

	Mean	Variance	3rd central	4th central	5th central
URC_{123}	455.13	1.55×10^{4}	1.42×10^{6}	8.80×10^{8}	2.71×10^{11}
URC_{456}	7592.10	2.10×10^{7}	1.16×10^{11}	2.38×10^{15}	5.31×10^{19}
$URC_{789(1)}$	91.82	3.58×10^{2}	3.92×10^{3}	4.35×10^{5}	1.59×10^{7}
$URC_{789(2)}$	255.05	2.76×10^{3}	8.40×10^{4}	2.59×10^{7}	2.63×10^{9}

Table 4-5. Locations and weights of the delta functions in the *URC* and C_{op} space

Delta function number	C_{op}	URC_{123}	URC_{456}	$URC_{789(1)}$	$URC_{789(2)}$	Weight
0	0.175	455.13	7592.10	91.82	255.05	-32/9
1	$0.175-0.05\sqrt{3/20}$	455.13	7592.10	91.82	255.05	5/18
2	$0.175+0.05\sqrt{3/20}$	455.13	7592.10	91.82	255.05	5/18
3	0.175	330.97	7592.10	91.82	255.05	0.4459
4	0.175	534.76	7592.10	91.82	255.05	0.5161
5	0.175	830.31	7592.10	91.82	255.05	0.03803
6	0.175	455.13	4327.48	91.82	255.05	0.6444
7	0.175	455.13	13273.41	91.82	255.05	0.3515
8	0.175	455.13	33921.52	91.82	255.05	0.00405
9	0.175	455.13	7592.10	70.43	255.05	0.3706
10	0.175	455.13	7592.10	100.59	255.05	0.5703
11	0.175	455.13	7592.10	141.33	255.05	0.05902
12	0.175	455.13	7592.10	91.82	195.64	0.3706
13	0.175	455.13	7592.10	91.82	279.43	0.5703
14	0.175	455.13	7592.10	91.82	392.57	0.05902

After the moments of C_R conditioned on *URC* and C_{op} are obtained, the (un-conditional) moments of C_R are estimated using Algorithm 4-3 described in Section 4.2, and the central moments of the total repair costs during the next 50 years (*DV*) are evaluated using the procedure described in Section 4.4.1 (we take the discount rate r_d in Equation (4.29) to be zero, which is equivalent to assuming that the "risk-free" interest rate equals the inflation rate). When matching moments, C_{op} is uniformly distributed, so the fifth-order Legendre-Gauss rule (Appendix A) is used; for the *URC*, since they are lognormal variables, the first five moments can be computed easily (shown in Table 4-4), which are later matched using Equation (3.11) or (3.12). The resulting locations and weights for the 15 delta functions in the domain of *URC* and C_{op} are listed in Table 4-5, where $URC_{789(1)}$ and $URC_{789(2)}$ are the unit repair costs for the damage states "visible damage" and "significant damage" in Table 4-5.

The solid lines in Figure 4-5 indicate the moment-matching estimates of the first four central moments of *DV*, which is the total repair cost during the next 50 years. We also estimate

the first two central moments of *DV* using the FOSM technique. The FOSM estimates for the first two moments of C_R are simply (see Equation (3.6))

$$\begin{aligned} E(C_R)_{FOSM} &= E(C_R \mid S_a = \bar{s}_a, M = \bar{m}, \beta = \bar{\beta}, URC = \overline{urc}, C_{op} = \bar{c}_{op}) \\ E(C_R^2)_{FOSM} &= E(C_R^2 \mid S_a = \bar{s}_a, M = \bar{m}, \beta = \bar{\beta}, URC = \overline{urc}, C_{op} = \bar{c}_{op}) \end{aligned}, \tag{4.31}$$

where $\bar{s}_a, \bar{m}, \bar{\beta}, \overline{urc}, \bar{c}_{op}$ are the expected values of S_a, M, β, URC, and C_{op}. The FOSM estimates of the first two central moments of *DV* are therefore (see Equation (4.29))

$$E(DV)_{FOSM} = T \cdot \lambda_{IM}(im_l) \cdot E(C_R)_{FOSM} \qquad Var(DV)_{FOSM} = T \cdot \lambda_{IM}(im_l) \cdot E(C_R^2)_{FOSM}. \tag{4.32}$$

The dashed lines in Figure 4-5 indicate the estimates made by the FOSM technique (only the first two central moments).

For comparison, Monte Carlo simulations with sample number equal to 10, 100, 1000 and 10,000 are conducted. For each sample, S_a, M, β, URC, C, and C_{op} are randomly chosen according to their PDFs, and the corresponding *DV* is computed. MCS with 10, 100, 1000 and 10000 samples are repeated 100, 20, 10 and 5 times, respectively. The resulting MCS estimates of the first four central moments of *DV* are equal to the sample central moments, which are plotted as circles in Figure 4-5. The results from MCS with a very large sample size (N = 1,000,000 samples) are also indicated in the figures.

We can see that the MM estimates of the first two central moments of *DV* are satisfactory (close to the large-sample MCS estimates), while the MM estimates of the third and fourth central moments are roughly 25% less than the large-sample MCS estimates. On the other hand, the FOSM technique significantly under-estimates the first two central moments of *DV*. Figure 4-5 shows that it takes many sample points for MCS to converge, although it is guaranteed to asymptotically reach the expected values.

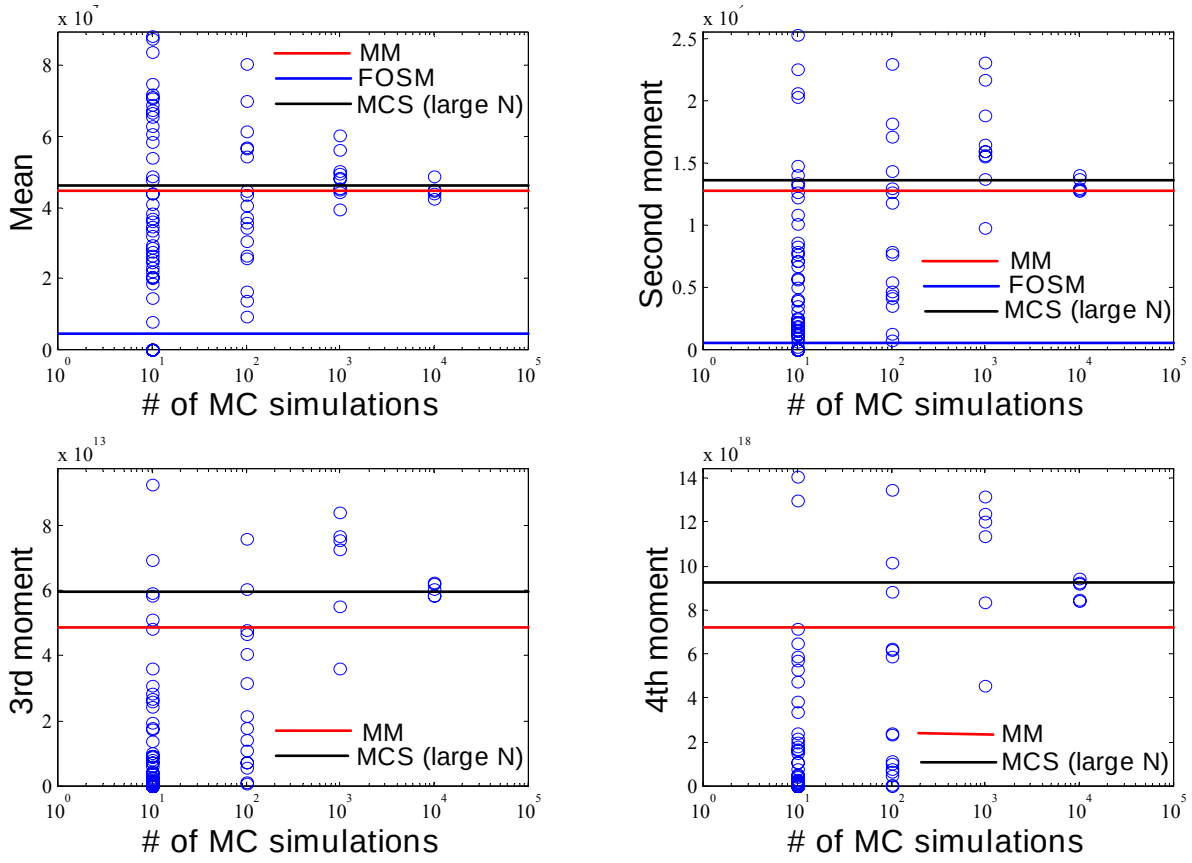

Figure 4-5. Estimated central moments of *DV* using different techniques

The FOSM estimates are inaccurate because $E(C_R \mid S_a, M, \beta, URC, C_{op})$ and $E(C_R^2 \mid S_a, M, \beta, URC, C_{op})$ are highly nonlinear functions of S_a, M, β, URC, and C_{op}. Figure 4-6(a) shows the plot of $E(C_R \mid S_a, M, \beta, URC, C_{op})$ versus S_a and β (while M, URC, and C_{op} are held constant at their mean values since C_R is not highly nonlinear in them). The function is highly nonlinear in the region of small β where the more probable values of the damping ratio lie; therefore, the first-order accuracy of the FOSM technique is not sufficient. Nevertheless, the MM technique, which has fifth-order accuracy, performs satisfactorily in this case. Similar observations apply to $E(C_R^2 \mid S_a, M, \beta, URC, C_{op})$, which is not plotted here.

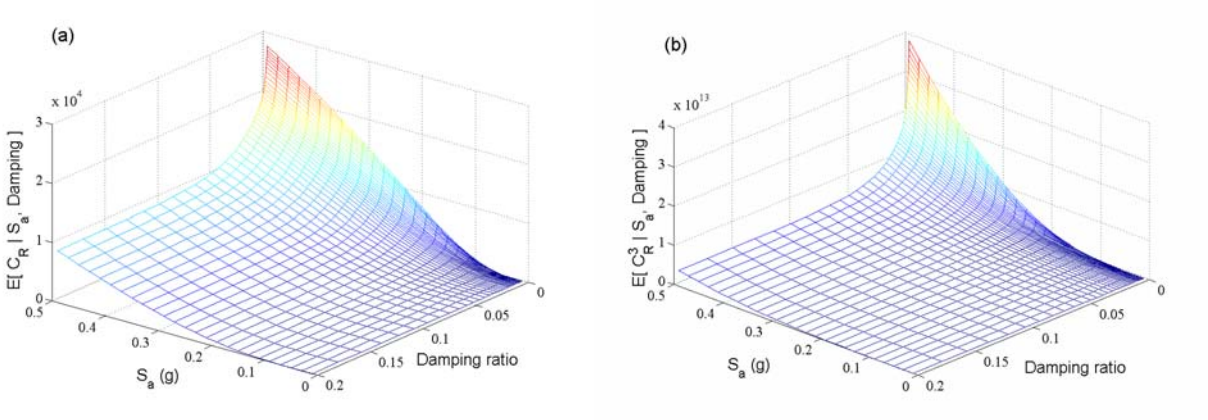

Figure 4-6. $E(C_R \mid S_a, M, \beta, URC, C_{op})$ **and** $E(C_R^3 \mid S_a, M, \beta, URC, C_{op})$ **vs** S_a **and damping ratio** β

The MM estimates for the third and fourth central moments of *DV* are not as accurate as those for the first two central moments. This is due to the highly nonlinear behavior of the functions $E(C_R^3 \mid S_a, M, \beta, URC, C_{op})$ and $E(C_R^4 \mid S_a, M, \beta, URC, C_{op})$ in the region of small damping ratio β (less than 0.02 - see Figure 4-6(b)), where these functions can not be well characterized by a fifth-order polynomial (note that the curvature of the surface in Figure 4-6(b) in the small-damping region is larger than that in Figure 4-6(a)). Recall that the PDF of the damping ratio in this simulation has mean and standard deviation equal to 0.05 and 0.02, respectively. Therefore, there is a significant probability that the damping ratio will be less than 0.02, so the fifth-order MM technique may be inaccurate.

Consider the situation where we have more information about the damping ratio so that we are able to reduce its standard deviation to 0.01 (the mean still remains 0.05). Using this smaller variation in the damping ratio, the MM estimates for the central moments of *DV* are re-calculated and listed in Table 4-6. We see that the MM technique now performs satisfactorily for the third and fourth central moments while the FOSM estimates still remain inaccurate. Of course, the reduction in damping uncertainty makes it less likely to have a damping ratio less

than 0.02, so that the high curvature in the small-damping region has little influence. Another possibility for improving the MM estimates is to implement a higher-order MM technique, at the expense of additional computational effort.

Table 4-6. The estimated central moments of *DV* with less damping uncertainty

Approach	Mean	Variance	3rd central moment	4th central moment	Skewness	Kurtosis
MM	4.37×10^{4}	1.26×10^{9}	4.84×10^{13}	7.12×10^{18}	1.08	4.46
FOSM	0.45×10^{4}	0.05×10^{9}	N/A	N/A	N/A	N/A
MCS (N = 1,000,000)	4.28×10^{4}	1.19×10^{9}	4.79×10^{13}	6.87×10^{18}	1.17	4.88
MM (UMD)	4.41×10^{4}	1.27×10^{9}	4.85×10^{13}	7.15×10^{18}	1.07	4.45

UMD: results for uncorrelated floor masses and damping ratios

When the uncertainties in capacities C are small (e.g. the coefficients of variation of C are small), we expect the performance of the MM technique will degrade because the cumulative distribution function for the capacities is then highly nonlinear, as discussed previously at the end of Section 4.1. Although the uncertainties in capacities are usually not small, it is instructive to consider a hypothetical case where they are small. Table 4-7 shows the results of the fifth-order MM technique and the large-sample MCS technique for the first four central moments of *DV* when all of the logarithm standard deviations of capacities in Table 4-1 are reduced to 0.1 (other parameter values in the table are not changed). The degradation of the fifth-order MM estimates is evident. The degradation can be reduced by taking more weighted delta functions in the S_a direction, but taking more delta functions in the directions of other variables (i.e. M, β, C_{op}) does not significantly improve the accuracy of the MM estimate. This is because the central moments of *DV* are more sensitive to changes in S_a than changes in the other variables. Therefore, we match the first five central moments of S_a using the six weighted delta functions whose locations are chosen a priori using the Gauss points of an exponential PDF whose mean is equal to the mean of S_a (the PDF of S_a shown in Figure 4-4 resembles an exponential PDF). The

resulting locations and weights are listed in Table 4-8; for the other variables, the locations and weights remain the same as before. The resulting MM moment estimates are shown in Table 4-7, and we see that there is a clear improvement in the accuracy of these estimates over the fifth-order MM estimates (compare with MCS results).

Table 4-7. The estimated central moments of *DV* with small capacity uncertainty

	Mean	**Variance**	**3rd central moment**	**4th central moment**	**Skewness**	**Kurtosis**
Fifth-order MM	0.37×10^{4}	1.90×10^{8}	1.35×10^{13}	1.16×10^{18}	5.18	32.14
Improved MM*	1.58×10^{4}	8.78×10^{8}	5.24×10^{13}	5.66×10^{18}	2.01	7.34
FOSM	0.00	0.00	N/A	N/A	N/A	N/A
MCS ($N = 10^{6}$)	1.76×10^{4}	9.07×10^{8}	5.38×10^{13}	6.27×10^{18}	1.97	7.63

* The MM technique with six delta functions in S_a direction

Table 4-8. Delta functions in the *IM* (S_a) space for the improved MM technique

Position (g)	0.047	0.25	0.63	1.22	2.08	3.38
Weight	0.8770	0.06146	0.05588	0.004046	0.001312	0.00026

It is instructive to investigate the influence of the assumption that the masses of the three floors and the damping ratios of different modes are perfectly correlated. Assume instead that the masses of the three floors are independent and similarly for the damping ratios of different modes. Under this assumption, the number of independent basic uncertain variables (excluding capacities) increases from eight (the variables in Table 4-2 and Table 4-5) to twelve (two more mass parameters and two more damping parameters). The resulting estimates of the four central moments of *DV* are listed in Table 4-6 as MM (UMD) (damping standard deviation is equal to 0.01). It can be seen that the assumption that the masses and the damping ratios are perfectly correlated does not significantly influence the estimates.

4.5.2 Estimation of mean exceedance frequency of C_R in the next 50 years

We now consider another decision variable of possible interest, the mean exceedance frequency for C_R in the next 50 years. In this case, the appropriate $f_{IM}(im)$ from Equation (4.27) is identical to the one in Figure 4-4. Using the locations and weights listed in Table 4-9, which is a combination of Table 4-2 and Table 4-5, the fifth-order MM estimate of the mean exceedance frequency can be evaluated following the procedure described in Sections 4.4.2. The solid line in Figure 4-7 indicates the fifth-order MM estimate of the mean exceedance frequency $\lambda_{CR}(thresh)$ in the next 50 years for different values of *thresh* (the resulting $\lambda_{CR}(thresh)$ vs *thresh* plot is called the risk curve for the next 50 years). The segment length l_c mentioned in Section 4.3 is taken to be 100 (dollars), and the resulting total number of segments along the C_R axis is around 2,000.

Table 4-9. Locations and weights of the delta functions in the *IM*, *SM*, and C_{op} space

Delta function number	S_a(g)	M (kg)	β	C_{op}	Weight
0	0.1007	254,000	0.05	0.175	-11/9
1	0.0557	254,000	0.05	0.175	0.9337
2	0.7045	254,000	0.05	0.175	0.0653
3	2.8241	254,000	0.05	0.175	0.00095
4	0.1007	$254{,}000-25{,}400\sqrt{3}$	0.05	0.175	1/6
5	0.1007	$254{,}000+25{,}400\sqrt{3}$	0.05	0.175	1/6
6	0.1007	254,000	$0.05-0.02\sqrt{3}$	0.175	1/6
7	0.1007	254,000	$0.05+0.02\sqrt{3}$	0.175	1/6
8	0.1007	254,000	0.05	$0.175-0.05\sqrt{3/20}$	5/18
9	0.1007	254,000	0.05	$0.175+0.05\sqrt{3/20}$	5/18

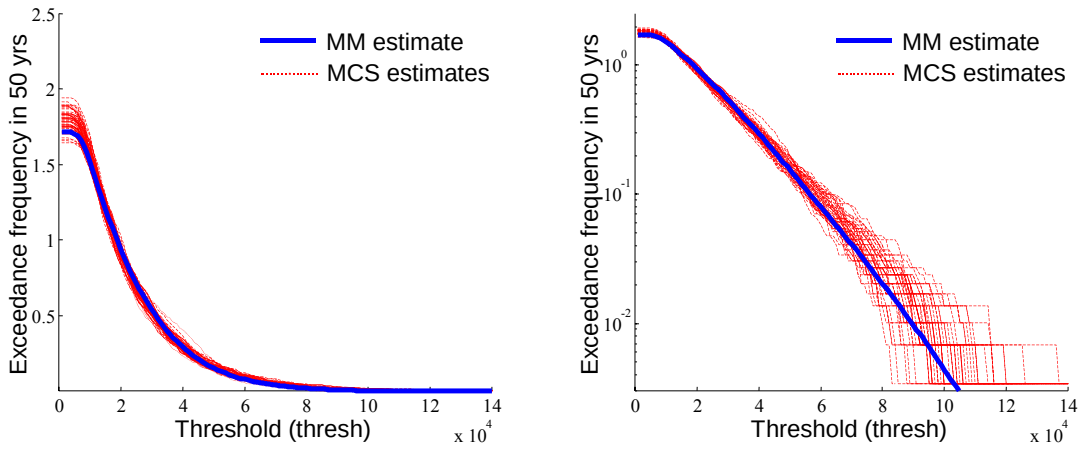

Figure 4-7. The MM and MCS estimates of the risk curves

Monte Carlo simulations with 10,000 samples are also conducted to estimate the risk curve: for each MCS sample, one draws S_a, C, URC, M, β, C_{op} randomly according to their PDF and then computes the single-event repair costs C_R for this MCS sample. The MCS estimate of the mean exceedance frequency is simply the relative frequency that the sampled C_R are greater than *thresh* (i.e. the number of C_R that are greater than *thresh* divided by 10,000), which gives an estimate of the probability that *thresh* is exceeded, multiplied by $T \cdot \lambda_{IM}(im_l)$. We conduct this 10,000-sample MCS for 50 times, resulting in 50 MCS-estimated risk curves, which are plotted as dashed lines in Figure 4-7 for both linear and logarithm scales on the vertical axis.

From Figure 4-7, we see that the MM estimate of the risk curve is satisfactory in the low repair-cost region (*thresh* < 40,000) compared to the MCS estimates. In the high repair-cost region (*thresh* > 40,000), slight under-estimation of the risk curve is found; compared to the mean of the 50 MCS estimates, the MM estimate of the risk curve is roughly $(5\text{-}10)\times10^{-3}$ less than the MCS mean.

The slight inaccuracy of the MM estimate in the high repair-cost region is probably due to the fact that the exceedance probability $P(C_R > thresh \mid S_a, M, \beta, C_{op})$ is highly nonlinear

when the damping ratio is small and *thresh* is large. Figure 4-8 shows the plot of $P(C_R > 80{,}000 \mid S_a, M, \beta, C_{op})$ with respect to S_a and β (M and C_{op} are held constant since the probability is not a highly nonlinear function of them), in which we see the high nonlinearity in the region of small damping ratio; as a result, the function $P(C_R > 80{,}000 \mid S_a, M, \beta, C_{op})$ is not well characterized by a fifth-order polynomial. Recall that the PDF of the damping ratio in this example has mean and standard deviation equal to 0.05 and 0.02, respectively. Therefore, there is a significant probability that the damping ratio will be small.

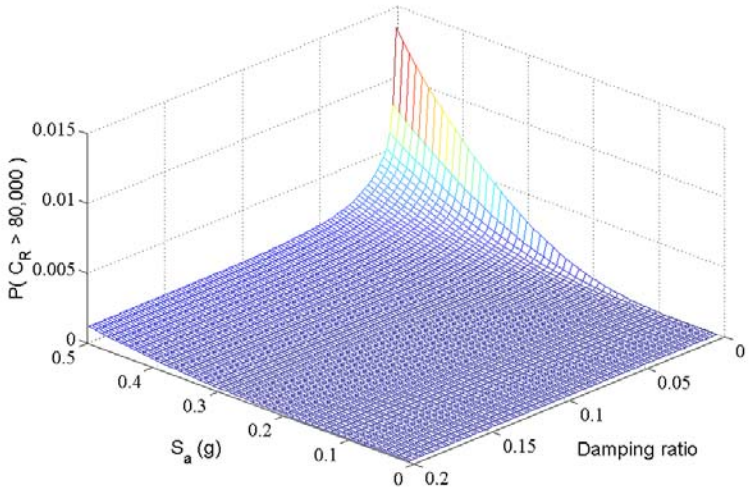

Figure 4-8. The plot of $P(C_R > 80{,}000 \mid S_a, M, \beta, C_{op})$ vs S_a and β

Consider the situation where we have more information about the damping ratio so that we are able to reduce its standard deviation to 0.01 (the mean still remains 0.05). Using this smaller variation in the damping ratio, the MM estimate of the risk curve is re-calculated and plotted in Figure 4-9; now the MM technique performs better. The reduction in the damping uncertainty makes it less likely that the damping ratio is small, so the high curvature in the small-

damping region has little influence. Another possibility for improving the MM estimate is to match more central moments of β, at the expense of additional computational effort.

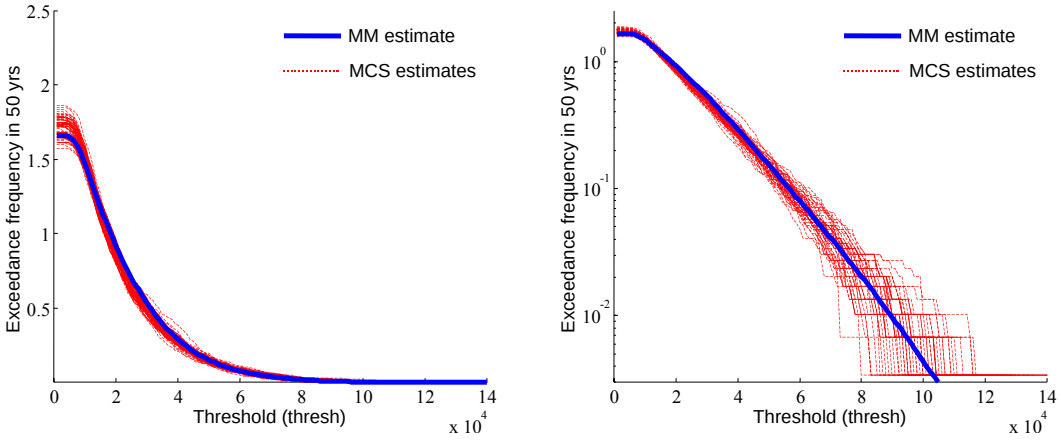

Figure 4-9. The MM and MCS estimates of the risk curve for smaller damping uncertainty

To better understand the behavior of the MM estimate, we further consider the cases where the uncertainties in *C* and *URC* are small. When the uncertainties in *C* are small (e.g. the logarithm standard deviations of *C* are small), we expect that the performance of the MM technique will degrade, as discussed previously. As an example, the solid lines in Figure 4-10 indicate the fifth-order MM estimates and 10 MCS estimates (thin dashed lines) of the risk curve with 10,000 samples when all of the logarithmic standard deviations of capacities in Table 4-9 are set to values ranging from 0.1 to 0.6 (other parameter values in the table are not changed). The degradation of the fifth-order MM estimate is evident when the logarithm standard deviation is less than 0.6.

The degradation can be reduced by taking more delta functions in the S_a direction, but taking more delta functions in the directions of the other variables (i.e. M, β, C_{op}) does not significantly improve the accuracy of the MM estimate. This is because the exceedance probability $P(C_R > thresh \mid S_a, M, \beta, C_{op})$ is most sensitive to the changes in S_a. Therefore, we

match the first five central moments of S_a using the six weighted delta functions listed in Table 4-8; for other variables, the locations and weights of the delta functions remain the same. The improved MM estimates are shown in Figure 4-10 as the thick dashed lines, and we can see that there is a clear improvement compared to the fifth-order MM estimates when the logarithm standard deviations of the capacities are less than 0.6.

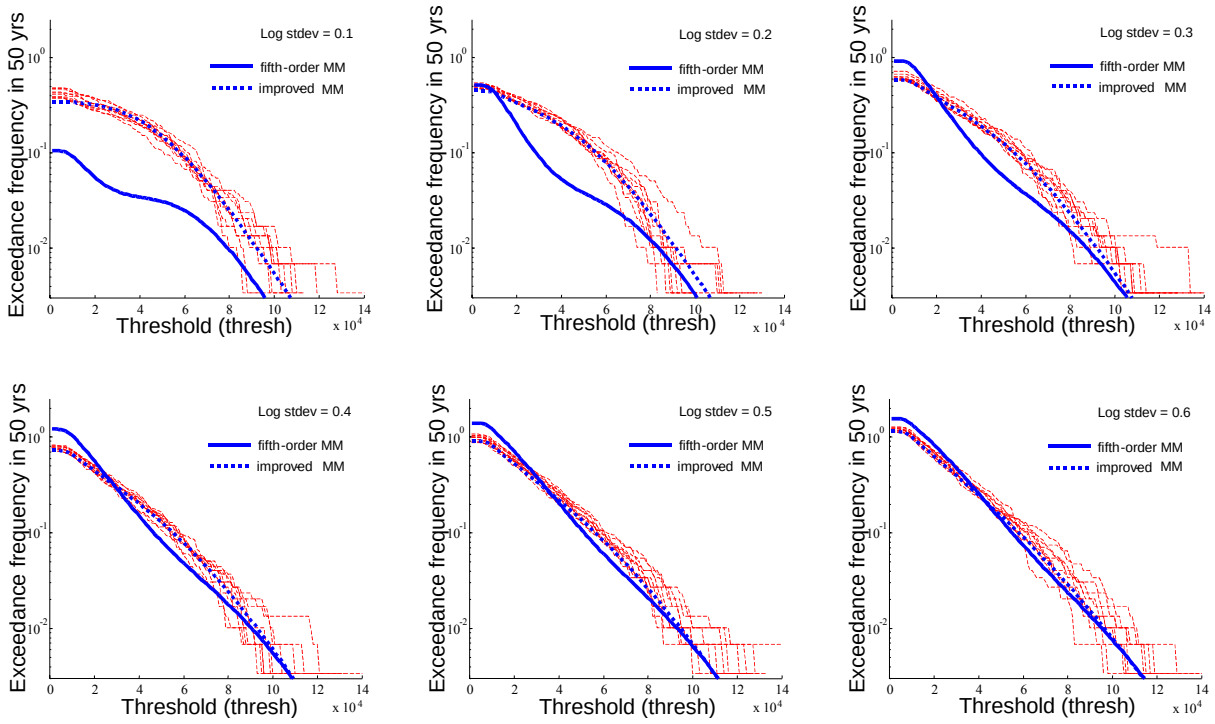

Figure 4-10. MM and MCS estimates (the ten dashed lines in each plot) of the risk curve for various logarithm standard deviations of capacity

Unlike capacities, when the logarithm standard deviations of the unit repair costs *URC* are small, the performance of the MM technique does not significantly degrade. Figure 4-11 shows the fifth-order MM estimates (solid lines) and 10 MCS estimates (thin dashed lines) of the risk curve when all of the logarithm standard deviations of *URC* in Table 4-9 are set to values ranging from 0.1 to 0.6 (other values in the table are not changed). The improved MM estimates

when taking more delta functions in the S_a direction are also shown in Figure 4-11 as the thick dashed lines for comparison.

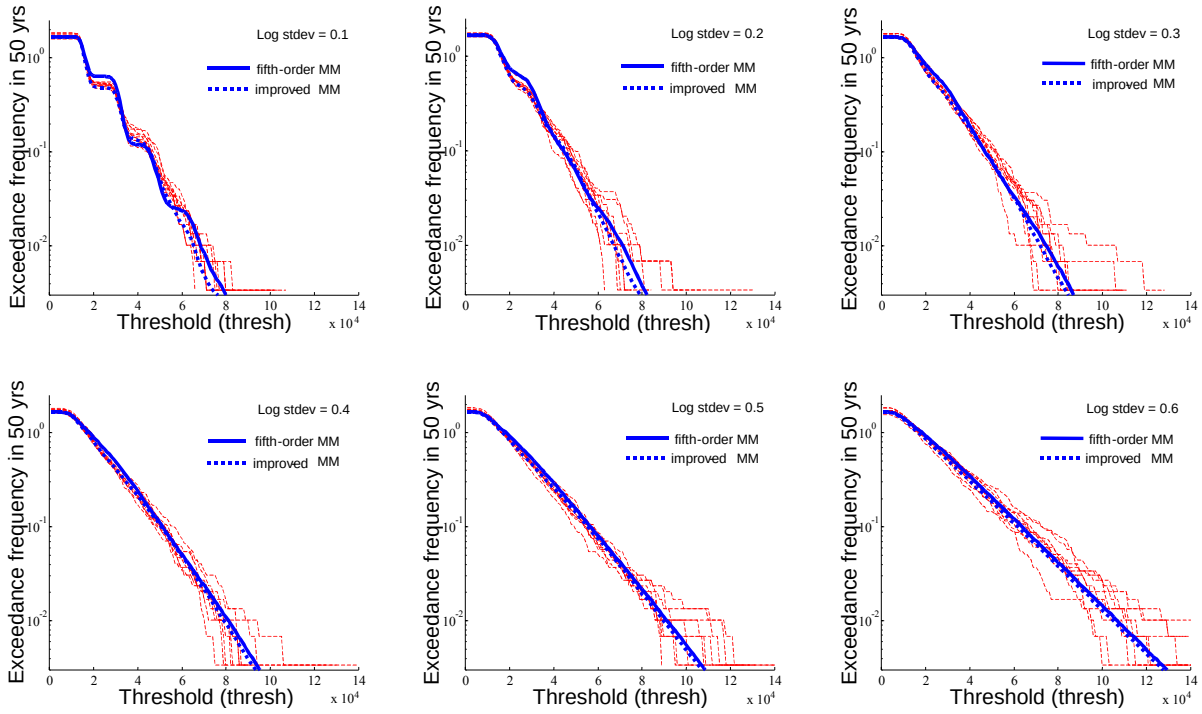

Figure 4-11. MM and MCS estimates (the ten dashed lines in each plot) of the risk curve for various logarithm standard deviations of URC

It is instructive to investigate the influence of the assumption that the masses of the three floors and the damping ratios of different modes are perfectly correlated. Consider a more realistic situation: assume that the masses of the three floors are uncorrelated and similarly for the damping ratios of different modes. Under this assumption, the number of basic uncertain variables other than capacities and unit repair costs increases from four (the variables in Table 4-9) to eight (two more mass parameters and two more damping parameters). As seen in Figure 4-12, the MM estimates under the perfectly correlated and uncorrelated assumptions are very close.

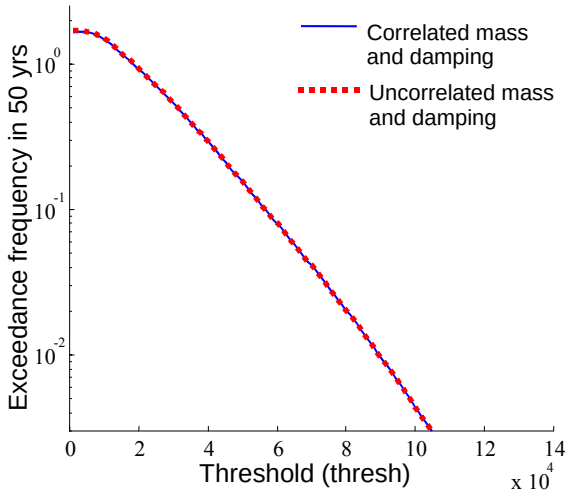

Figure 4-12. The MM estimates of the risk curves under the correlated and uncorrelated mass and damping assumptions

5 FEATURE SELECTION

When evaluating the decision variable *DV*, we usually have to consider several uncertain basic variables, e.g. uncertainties in the structural model (*SM*), ground motion (*IM* and $a(t)$), unit capacity (*C*), repair costs (*URC*), etc. It is always helpful to eliminate unimportant basic variables to reduce the computational burden for evaluating *DV*, which otherwise may become too large for practical applications.

In this section, we consider a rational way of measuring the importance of any basic variable as follows: a basic variable is important if and only if the removal of the uncertainty of that variable by setting it equal to its mean value also significantly affects the uncertainty of *DV* (e.g. the first few moments or exceedance probability of *DV*). To make this statement move quantitative, the following question needs to be answered: How do we measure the change in uncertainty of *DV* from before to after the removal of the basic variable? The answer to this question is the main topic of the following discussion.

Basically, the uncertainty parameters of interest (e.g. moments, exceedance probability, etc.) of *DV* reflect different aspects of the PDF of *DV*. Therefore, if we can find a plausible measure for the change of the PDF of *DV* from before to after the removal of the uncertainty of a basic variable, it should be suitable as a measure of the change in uncertainty of *DV*. In this report, we consider the relative entropy (Cover and Thomas 1991) (also known as the cross entropy, Kullback-Leibler distance and information divergence) as a measure of the change of the PDF of *DV*:

$$D(f\|\tilde{f}) = \int \log(f(dv)/\tilde{f}(dv))\, f(dv)\cdot d(dv) = E_f \log(f(DV)/\tilde{f}(DV)), \tag{5.1}$$

where f and $\tilde{f}$ are the PDFs of *DV* before and after removal of the uncertainty of a basic variable, respectively; E_f denotes expectation with respect to the PDF of f, and $D(f\|\tilde{f})$

denotes the relative entropy, which, technically, measures the uncertainty reduction (or information gain) when the PDF $\tilde{f}$ is used in place of the true PDF f (Cover and Thomas 1991). One can show that $D(f\|\tilde{f})$ is always non-negative and is equal to zero if and only if $f = \tilde{f}$, so it has some aspects of a distance measure.

Based on the relative entropy as a measure of the change in uncertainty of *DV*, we discuss two scenarios: when the uncertainty parameters under study are moments of *DV* and when they are the mean exceedance frequencies (or exceedance probabilities) of *DV*.

5.1 MOMENTS OF *DV* AS UNCERTAINTY PARAMETERS

Given the first *m* moments of *DV* before and after the removal of the uncertainty of a basic variable, denoted by $\{E(DV^r), r = 1,2,...m\}$ and $\{\tilde{E}(DV^r), r = 1,2,...m\}$, respectively, the goal is to find a scalar measure of the change from $\{E(DV^r), r = 1,2,...m\}$ to $\{\tilde{E}(DV^r), r = 1,2,...m\}$.

Notice that the given moments are not sufficient to determine the relative entropy defined in Equation (5.1). This is due to the fact a finite set of moments does not uniquely define a PDF. Nevertheless, one can construct a least-informative PDF of *DV* constrained on the given moments using the maximum-entropy principle (Jaynes, 1957). The procedure for calculating the change in information content of *DV* is as follows:

1. Given $\{E(DV^r), r = 1,2,...m\}$ and $\{\tilde{E}(DV^r), r = 1,2,...m\}$, compute the corresponding least-informative PDFs, denoted by f_{LI} and $\tilde{f}_{LI}$, respectively, by solving the appropriate constrained maximum entropy problem.

2. Compute the relative entropy $D(f_{LI} \| \tilde{f}_{LI})$, which quantifies the change in the uncertainty parameters of *DV* before and after the removal of the uncertainty of a basic variable.

When the uncertainty parameters only contain the first two moments of *DV*, the least-informative PDF is Gaussian, and the relative entropy can be evaluated in closed form:

$$\begin{aligned} D(f \| \tilde{f}) &= E_f \log(f(DV) / \tilde{f}(DV)) \\ &= E_f \left[-\log(\sigma_f) + \log(\tilde{\sigma}_f) - \frac{1}{2\sigma_f^2}(DV - \mu_f)^2 + \frac{1}{2\tilde{\sigma}_f^2}(DV - \tilde{\mu}_f)^2 \right] \\ &= -\log(\sigma_f / \tilde{\sigma}_f) - \frac{1}{2} + \frac{1}{2}\left[\sigma_f^2 / \tilde{\sigma}_f^2 + (\mu_f - \tilde{\mu}_f)^2 / \tilde{\sigma}_f^2\right] \end{aligned} \tag{5.2}$$

where μ_f, σ_f^2 and $\tilde{\mu}_f, \tilde{\sigma}_f^2$ are means and variances of the two PDF f and $\tilde{f}$, respectively.

5.2 MEAN EXCEEDANCE FREQUENCIES AS DECISION VARIABLES

Mean exceedance frequencies of *DV* are closely related to the PDF of *DV*. The absolute value of the derivative of $\lambda_{DV}(thresh)$ (the exceedance frequency of *DV* over *thresh*) is proportional to the PDF of *DV* (e.g. See Equation (4.28)). Therefore, given the risk curves before and after the removal of the uncertainty of an basic variable, denoted by $\lambda_{DV}(thresh)$ and $\tilde{\lambda}_{DV}(thresh)$, respectively, the following measure is also proportional to $D(f \| \tilde{f})$:

$$\int \log\left[\left| \frac{d[\lambda_{DV}(z)]}{dz} \right| \Big/ \left| \frac{d[\tilde{\lambda}_{DV}(z)]}{dz} \right| \right] \cdot \left| \frac{d[\lambda_{DV}(z)]}{dz} \right| \cdot dz \tag{5.3}$$

After $\lambda_{DV}(thresh)$ and $\tilde{\lambda}_{DV}(thresh)$ are obtained, the integral in Equation (5.3) can be evaluated numerically.

5.3 PROCEDURE FOR FEATURE SELECTION

The procedure for conducting feature selection is as follows:

1. For all basic variables (i.e. S_a, mass, damping, *F-d* multiplier, etc.) that are active (treated as uncertain), compute the first two moments and the exceedance probability of *DV* and treat these as reference moments and reference exceedance probability.
2. Make one of the basic variables inactive (i.e. hold it fixed at its mean value) and compute the first two moments and exceedance probability of *DV*. Do this for each basic variable.
3. Compute the measure of uncertainty reduction (relative entropy) using Equation (5.2) for the moments and Equation (5.3) for the exceedance probability. Do this for each basic variable. If the uncertainty reduction is large, the corresponding basic variable that is set to its mean value (i.e., is inactivated) is important, and so its uncertainty should be explicitly treated.

In Chapter 6 we will discuss an acceptance threshold for the relative entropy. If the relative entropy corresponding to setting a basic variable to its mean value is below the threshold, the basic variable is considered unimportant and can be set to its mean value without significantly affecting the moment and exceedance probability estimates.

6 CASE STUDY: VAN NUYS HOTEL BUILDING

6.1 DESCRIPTION OF CASE-STUDY BUILDING

6.1.1 Summary description

In this chapter we apply the analysis procedure described in the preceding chapters to a actual building: a 66,000 sf (6,200 m^2), seven-story hotel building located in Van Nuys, California, as it existed just prior to the 1994 Northridge Earthquake. (It has since been seismically strengthened and a modified lateral-force-resisting system installed.) The building is located at 34.221°N, 118.471°W, in the San Fernando Valley, just northwest of downtown Los Angeles, as shown in Figure 6-1.

Figure 6-1. Location of the case-study building: the "+" symbol above the "405" shield

The building has been affected by a number of earthquakes, most notably by the M6.6 1971 San Fernando earthquake, approximately 20 km to the northeast, which caused primarily nonstructural damage, and by the M6.7 1994 Northridge earthquake, whose epicenter was

approximately 4.5 km to the southwest and which resulted in extensive structural damage. The building location relative to these events is shown in Figure 6-2.

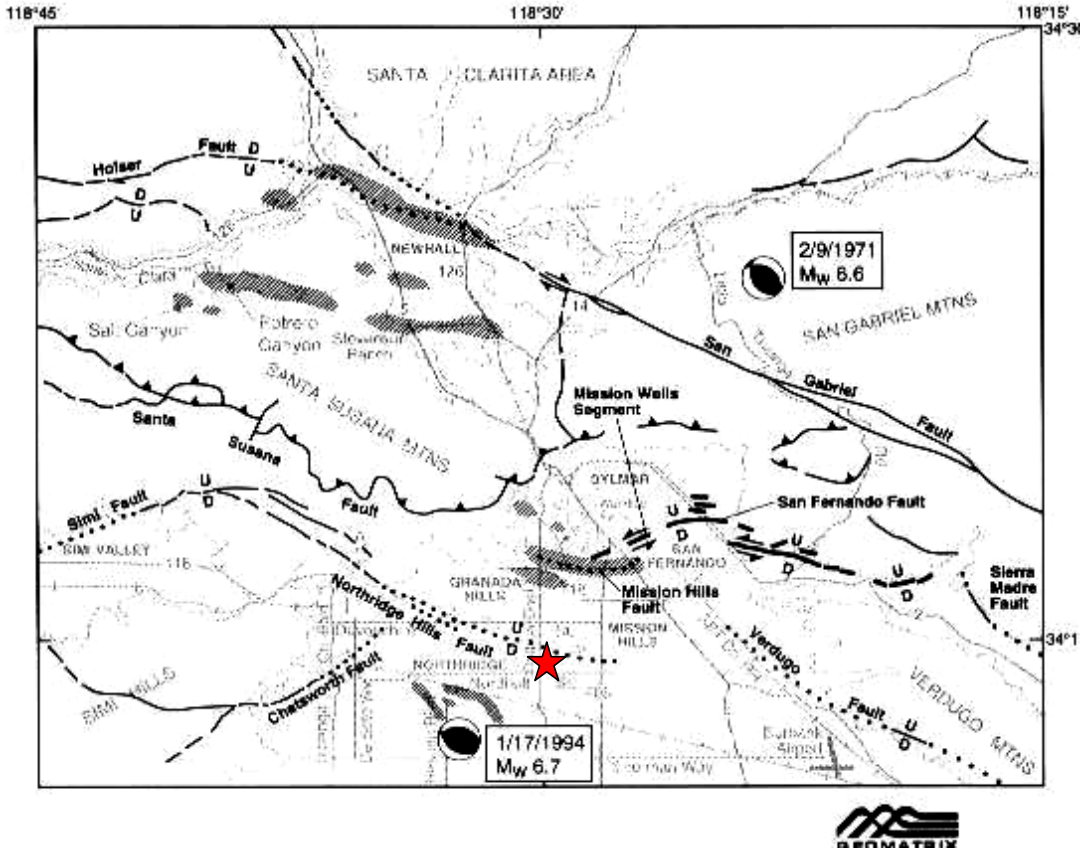

Figure 6-2. Case-study building (star) relative to earthquakes (EERI, 1994b)

6.1.2 Prior studies

The case-study building has been studied by a number of authors. Notable examples include Jennings (1971), Scholl et al. (1982), Islam (1996a, 1996b), Islam et al. (1998), Li and Jirsa (1998), and Trifunac et al. (1999); the last of these provides a thorough description of the damage suffered by the building in the 1994 Northridge Earthquake. It has also been used as a testbed for studies of performance-based earthquake engineering by researchers funded by the PEER Center (see www.peer.berkeley.edu).

We also examined the building in Beck et al. (2002) to estimate future repair costs using assembly-based vulnerability and in Porter et al. (2002a,b) to explore the effect of basic uncertain variables using a simple deterministic sensitivity study.

6.1.3 Building Design

The building was designed in 1965 according to the 1964 Los Angeles City Building Code, and built in 1966. The architect was Rissman and Rissman Associates (1965), then of Pacific Palisades, CA, and until October 2001 of Las Vegas, NV. The structural engineer was Harold Epstein, a licensed Civil Engineer of Los Angeles, CA (1965).

In plan, the building is 63 ft by 150 ft, and it has 3 bays by 8 bays that are 7 stories tall. The long direction is oriented east-west. The building is approximately 65 ft tall: the first story is 13 ft, 6 in; stories 2 through 6 are 8 ft, 6-½ in; the 7th story is 8 ft. The ground floor contains a lobby, dining room, tavern, banquet room, and various hotel support services. Upper floors are arranged with 22 hotel suites accessed via a central corridor running along the longitudinal axis of the building.

Soil conditions at the site are found in Tinsley and Fumal (1985), who map surficial soil deposits in the Los Angeles region using a variety of sources. They describe the site soil as Holocene fine-gained sediment (silt and clay) with a mean shear-wave velocity of 200 m/sec (and a standard deviation of 20 m/sec), corresponding to site class D, stiff soil, as defined by the International Code Council (2000), and soil profile type S_D according to the Structural Engineers Association of California (1999). In his study of the same building, Islam (1996b) reaches the same conclusion, that site soils are "primarily fine sandy silts and silty fine sands. This suggests a site coefficient factor of S2 or greater."

The structural system is a cast-in-place reinforced-concrete moment-frame building with non-ductile column detailing. Perimeter moment frames provide the primary lateral force resistance, although the interior columns and slabs also contribute to lateral stiffness. The gravity system comprises 2-way reinforced-concrete flat slabs supported by square columns at the interior and by the rectangular columns of the perimeter frame. Slabs are 10-in deep at the 2nd floor, 8½ in at the 3rd through 7th floors, and 8 in at the roof. The roof also has lightweight concrete topping varying in thickness between 3-1/4 in and 8 in. The column plan (with the designer's column numbers) is shown in Figure 6-3. As shown in the figure, the building is founded on 24-in diameter drilled piers in groups of two, three, and four piers per pile cap. Pier lengths vary between 31.5 ft and 37 ft.

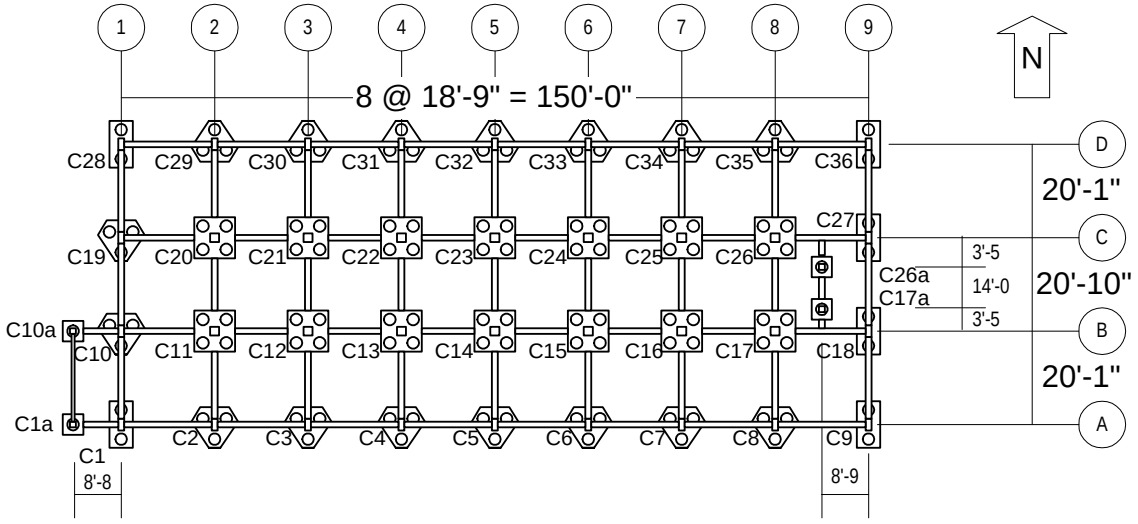

Figure 6-3. Foundation and column plan. "C1" through "C36" are the designer's column numbers

Frames are regular in elevation; the south frame elevation is shown in Figure 6-4. Floor and roof beams and spandrel marks are shown in Figure 6-5. These figures also show the designer's notation for beam and column numbering. Perimeter columns are 14 in. by 20 in., oriented to bend in their strong direction about the east-west axis. Interior columns are 18 in square. Spandrel beams are generally 16 in. wide by 30 in. deep at the 2nd floor, 16 in. wide by

22-½ in. deep at the 3rd to 7th floors, and 16 in. wide by 22 in. deep at the roof. The tops of the spandrel beams are flush with the top of the floor slab.

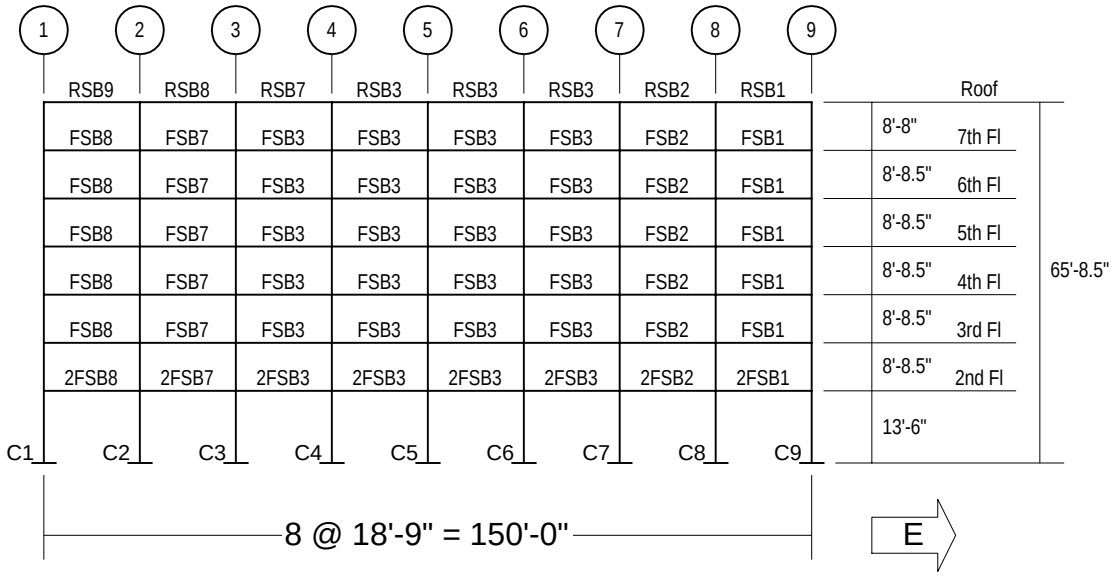

Figure 6-4. South frame elevation, omitting stair tower at west end

Column concrete has nominal strength of f'_c = 5 ksi for the first story, 4 ksi for the second story, and 3 ksi from the third story to the seventh. Beam and slab concrete strength is nominally f'_c = 4 ksi at the second floor and 3 ksi from the third floor to the roof. Table 6-1 provides the column reinforcement schedule. The reinforcement of floor spandrel beams for floors 3 through 7 is shown in Table 6-2. Reinforcement of floor spandrel beams for the 2nd floor and roof is shown in Table 6-3. Column reinforcement steel is A432-62T (Grade 60) for billet bars. Beam and slab reinforcement is ASTM A15-62T and A305-56T (Grade 40) for intermediate grade, deformed billet bars. Column reinforcement is arranged as shown in Figure 6-6. Drilled piers are reinforced with 4-#6 longitudinal bars, #2 ties at 12-in centers, 3-in cover. Pile caps are 10'-0" square by 38-in deep (4-pier pile cap), 4'-0" by 10'-0" by 38-in deep (2-pier pile cap), or 2'-6" square by 38-in deep (1-pier pile cap). Triangular pile caps have edges 2'-0" from pier centers. All piers are spaced at 6'-0" centers. Pier tips are 34.5 to 40 ft below grade.

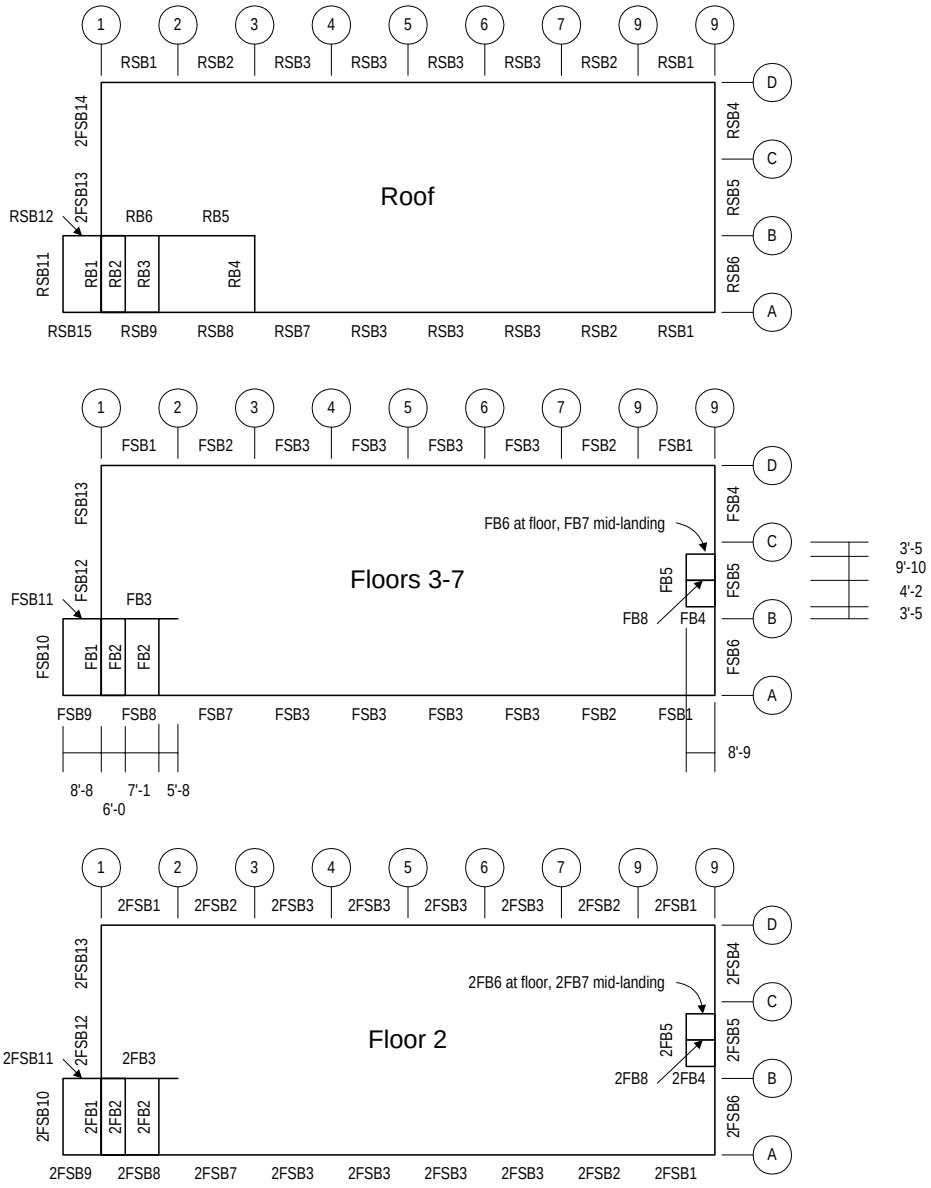

Figure 6-5. Floor beam and floor spandrel beam plans

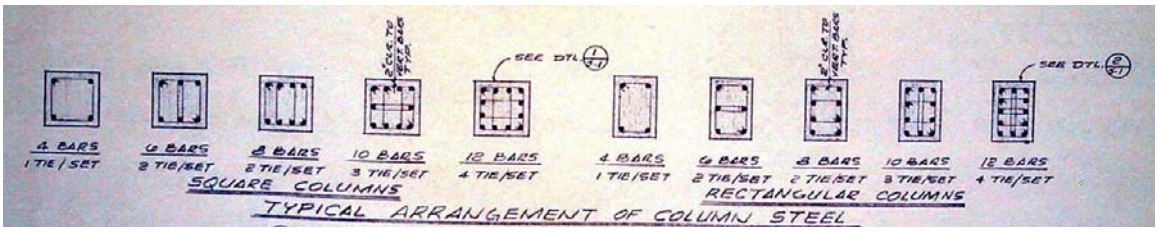

Figure 6-6. Arrangement of column steel (Rissman and Rissman Associates, 1965)

Table 6-1. Column reinforcement schedule

		Column mark							
		C13 to C17, C21 to C26	C11, C12, C20	C30 to C34	C10, C18, C19, C27	C2, C3, C8, C29, C35	C1, C9, C28, C36	C1A, C10A	C17A, C26A
Level	Col size	18"x18"	18"x18"	14"x20"	14"x20"	14"x20"	14"x20"	10"x12"	10"x12"
7th floor	Vert. bars	6-#7	6-#7	6-#7	6-#7	6-#7	6-#7	4-#5	
	Ties	#2@12"	#2@12"	#2@12"	#2@12"	#2@12"	#2@12"	#2@10"	
6th floor	Vert. bars	6-#7	6-#7	6-#7	6-#7	6-#7	6-#7	4-#5	4-#5
	Ties	#2@12"	#2@12"	#2@12"	#2@12"	#2@12"	#2@12"	#2@10"	#2@10"
5th floor	Vert. bars	6-#7	6-#8	6-#7	6-#7	6-#7	6-#7	4-#5	4-#5
	Ties	#2@12"	#3@12"	#2@12"	#2@12"	#2@12"	#2@12"	#2@10"	#2@10"
4th floor	Vert. bars	6-#8	8-#9	6-#7	6-#9	6-#7	6-#7	4-#5	4-#5
	Ties	#3@12"	#3@12"	#2@12"	#3@12"	#2@12"	#2@12"	#2@10"	#2@10"
3rd floor	Vert. bars	8-#9	12-#9	6-#9	8-#9	8-#9	6-#7	4-#6	4-#5
	Ties	#3@12"	#3@12"	#3@12"	#3@12"	#3@12"	#2@12"	#2@10"	#2@10"
2nd floor	Vert. bars	10-#9	12-#9	6-#9	8-#9	8-#9	6-#7	4-#6	4-#5
	Ties	#3@12"	#3@12"	#3@12"	#3@12"	#3@12"	#2@12"	#2@10"	#2@10"
1st floor	Col size	20"x20"	20"x20"						
	Vert. bars	10-#9	12-#9	10-#9	12-#9	10-#9	8-#9	4-#8	4-#6
	Ties	#3@12"	#3@12"	#3@12"	#3@12"	#3@12"	#3@12"	#3@10"	#2@10"

Table 6-2. Spandrel beam reinforcement schedule, floors 3 through 7

Beam mark	Width	Height	Top bars					Bottom bars	#3 ties
			7F	6F	5F	4F	3F		
FSB1	16”	22-½”	①⑨ 2#7	2#9	2#9	3#8	3#8	2#7 (2#8 @ 3F, 4F)	①⑨ 3@5”, 5@6”, rest @10”, 3F- 5F
			②⑧ FSB2 top bars						②⑧ 6@4”, 5@6”, 3F-5F
FSB2	16”	22-½”	②⑧ 2#9	3#8	3#8	3#8	3#9	2#6	8@5”, 5@6” ea end
			③⑦ FSB3 top bars						Rest @ 10” 3F-5F
FSB3	16”	22-½”	2#8	2#9	3#8	3#8	3#9	2#6	3@5”, 5@6” ea end
									Rest @ 10” 3F-5F
FSB7	16”	22-½”	③ FSB3 top bars					2#7	3@5”, 5@6” ea end
			② FSB8 top bars						Rest @ 10” 3F-5F
FSB8	16”	22-½”	② 2#8	2#9	2#9	3#8	3#8	2#7 (2#8 @ 5F, 2#9 @ 3F, 4F)	① 3@5”, 5@6”, rest@10” 3F-5F
			① 2#7	2#8	2#9	2#9	3#8		② 6@4”, 5@6” 3F-5F

①, ②, etc.: column lines; 3F, 4F, etc: floor levels

The ground floor has full-height masonry infill walls in the north frame between column lines 5 and 9, and partial-height masonry walls between column lines 1 and 5. Above the 2nd floor there are no other stiff elements between the columns that might produce a short-column effect. The building is clad on the north and south facades with aluminum window wall, comprising 3/16-in heavy sheet glass in sliding frames, and ¼-in cement asbestos board panels with an ornamental sight-obscuring mesh of baked enamel or colored vinyl. The east and west endwalls are finished on the inside with gypsum wallboard and on the outside with stucco.

Table 6-3. Roof and second-floor spandrel beam reinforcement schedule

Beam mark	Width	Height	Top bars	Bottom bars	#3 ties
RSB1	16”	22”	①⑨ 2#6 ②⑧ 2#8	2#7	#3@10”
RSB2	16”	22”	②⑧ RSB1 top bars ③⑦ RSB3 top bars	2#6	Same
RSB3	16”	22”	2#8	2#6	Same
RSB7	16”	22”	④ RSB3 top bars ③ 2#9	2#6	Same
RSB8	16”	22”	③ 2#9 ② 3#9	2#9	Same
2FSB1	16”	30”	①⑨ 2#9 ②⑧ 2FSB2 top bars	2#8	4 @ 6”, 2 @ 8”, ea end, rest @ 13”
2FSB2	16”	30”	②⑧ 3#8 ③⑦ 2FSB3 top bars	2#6	Same
2FSB3	16”	30”	2#9	2#6	Same
2FSB7	16”	30”	③ 2FSB3 top bars ② 2FSB8 top bars	2#7	Same
2FSB8	16”	30”	② 2#9 ① 2#9	2#8	Same

Interior partitions are constructed of 5/8-in gypsum wallboard on 3-5/8 in metal studs at 16-in centers. Ceilings in the suites in the 2nd through 7th stories are a textured coating applied to the soffit of the concrete slab above. At the first floor, ceilings are suspended wallboard or acoustical ceiling tiles (2-ft grid). Upper-story hallway ceilings are suspended ceiling on 2-ft-by-4-ft T-bar grid, just deep enough to accommodate fluorescent fixtures (approximately 2 in).

6.1.4 Site hazard

The site hazard is calculated as follows. Frankel and Leyendecker (2001) provide the seismic hazard—defined in terms of the annual expected frequency of exceedance versus spectral acceleration response—for any latitude and longitude in the United States. The site hazard is available for soil at the boundary between NEHRP soil classes B and C, and for the fundamental periods of 1.0 and 2.0 sec. As discussed in Beck et al. (2002), the fundamental period for the case-study building is estimated to be approximately 1.5 sec.

The site of interest stands on soil class D, so it is first necessary to adjust shaking severity to account for soil class. Figure 6-7(a) shows the soil adjustment factor used here, which is the ratio of the site coefficient F_V for soil class D to that of the average of soil classes B and C, according to International Code Council (2000). Dots in the figure give tabulated values. They are plotted as a function of the spectral acceleration response on B-C soil for a fundamental period of 1 sec. The solid curve between the upper and lower plateaus is a polynomial fit to the data. Figure 6-7(b) shows the resulting site hazard, after adjusting for site soil and interpolating for the fundamental period of 1.5 sec.

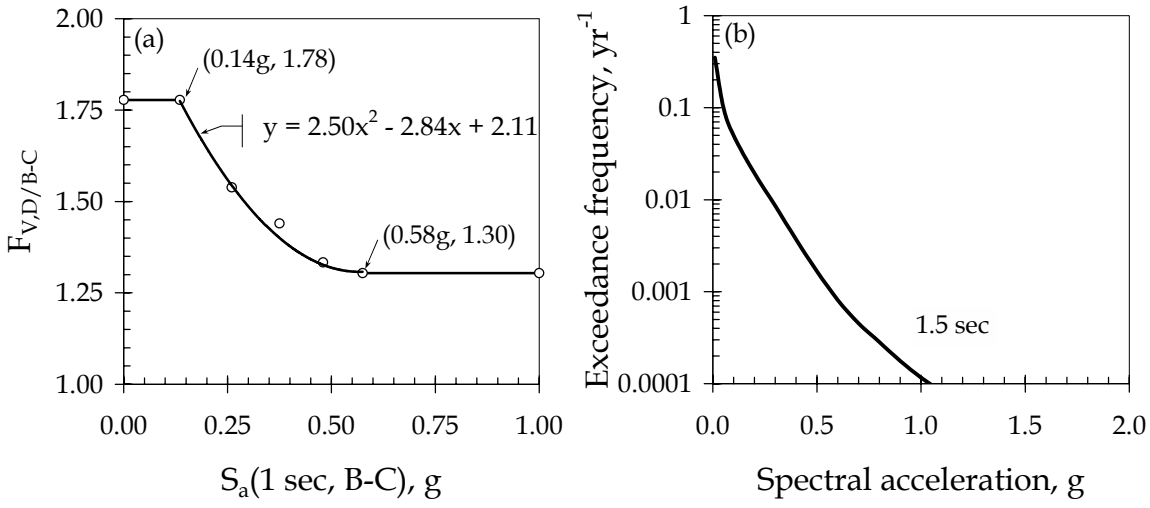

Figure 6-7. Adjusting site hazard to account for site soil conditions

6.2 STRUCTURAL MODEL

6.2.1 Structural elements

During the 1994 Northridge Earthquake, the south frame of the case-study building suffered severe damage. For the present study, this frame was chosen for performing a 2-dimensional nonlinear time-history structural analysis using a finite-element model. We employ the same structural model as in Beck et al. (2002) and the finite-element software Ruaumoko

(Carr, 2001) was used for performing the structural analyses. A model representing the south frame of the building uses two generic types of elements: nonlinear inelastic flexural members and nonlinear inelastic shear springs. The flexural behavior of the beams and columns is represented by a one-component Giberson beam with plastic hinges at the ends (Sharpe, 1974). Shear deformation for the beams is assumed to be elastic and is incorporated in the flexural elements. Shear deformation of the columns is modeled by using inelastic nonlinear springs attached to the ends of the flexural elements. Figure 6-8 shows a fragment of the structural model. In the figure, beams and columns are marked according to the original structural drawings: 1C-1 refers to column number 1, first floor; 1C-2 refers to column number 2, first floor; and 2FSB-8 refers to spandrel beam 8 on the second floor.

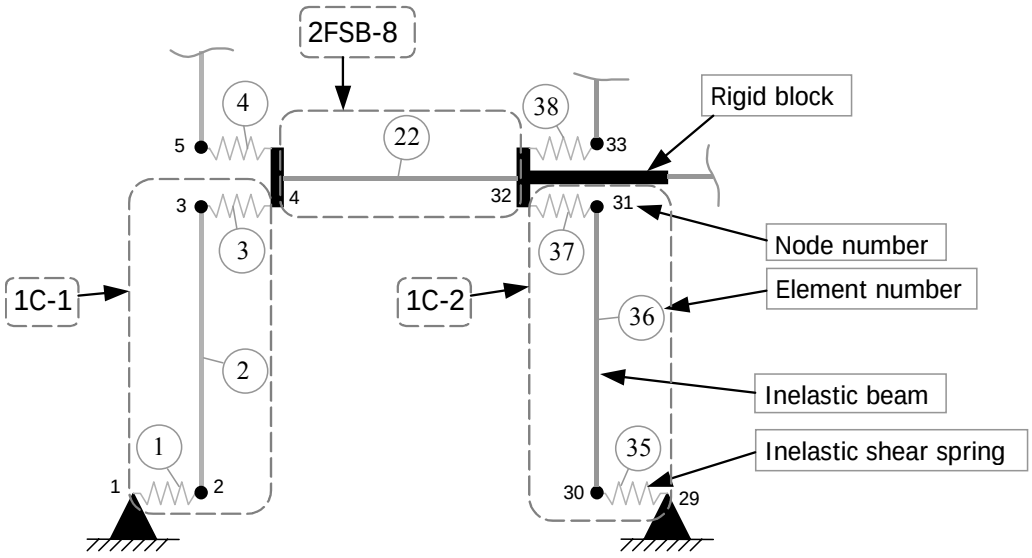

Figure 6-8. Fragment of the finite element model

Two types of inelastic hysteretic rules are used to model the nonlinear behavior of the reinforced reinforced-concrete members. The SINA tri-linear hysteresis rule (Saiidi and Sozen, 1979) is used to model the stiffness degradation of the reinforced concrete members in flexure. The Q-HYST bi-linear hysteresis (Saiidi and Sozen, 1979) is used to model the stiffness

degradation of the reinforced concrete members in shear. A strength-degradation introduced by Pincheira *et al.* (1999) is applied to both hysteretic rules. The models are depicted in Figure 6-9 and Figure 6-10. Parameters for the beam-column models, including their moment-axial yield surface, are calculated using UCFyber (ZEvent, 2000).

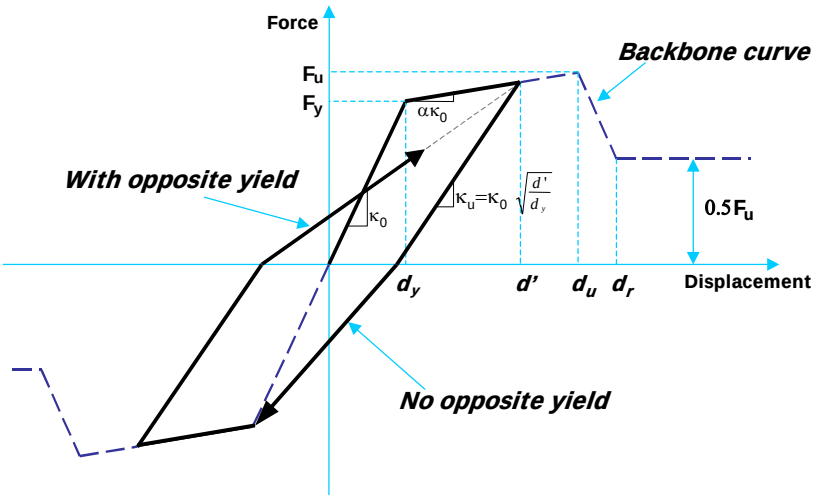

Figure 6-9. Shear-spring hysteresis rule: Q-HYST with strength degradation

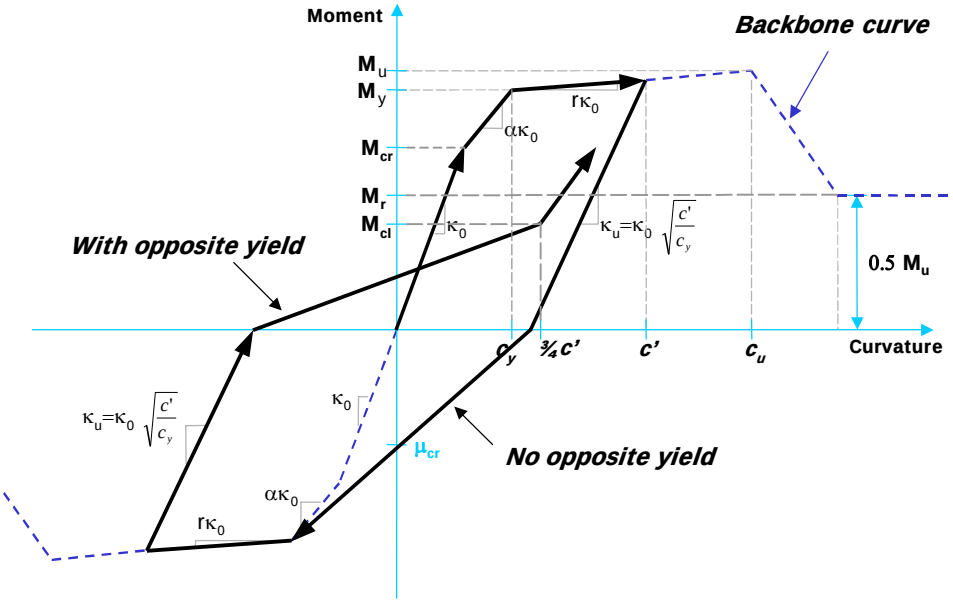

Figure 6-10. Flexure hysteresis rule: SINA with strength degradation

Shear-spring parameters are estimated by conventional analytical models. The spring stiffness is found as:

$$K = \frac{GA_s}{L/2} \tag{6-1}$$

where G = concrete shear modulus; L = member length; A_s = effective shear area, computed as $A_s = k_i A_g / k_s$; A_g is the gross section area; k_s =1.2 is the shape coefficient for a rectangular cross section, and k_i reflects the increased shear deformation in a flexurally-cracked reinforced-concrete column. It is usually assumed that the reduction in shear stiffness is proportional to the reduction in flexural stiffness (Priestley et al., 1996), leading to $k_i = I_e/I_g$, where I_e is the effective moment of inertia and I_g is the gross moment of inertia of the cross section for the uncracked member. Equivalently, k_i can be found as K_e/K_0, the ratio of the effective stiffness to the initial stiffness of the member. The effective stiffness is determined from the moment-curvature relationship as αK_0 = stiffness demonstrated by the member within the range of pre-yield loads. This makes $k_i = \alpha$. The yield force for shear springs is obtained from the ACI-recommended expression (MacGregor, 1998):

$$F_y = 2(1 + \frac{N_u}{2000 A_g})\sqrt{f'_c} b_w d \tag{6-2}$$

where N_u = axial compression; A_g = gross cross sectional area; f'_c = 28-day concrete cylinder strength; b_w = web width; and d = distance from the extreme compression fiber to centroid of longitudinal tension reinforcement.

6.3 UNCERTAIN BASIC VARIABLES

6.3.1 Uncertainties recognized in the case study

In this study, we recognize uncertainties in the values of maximum spectral acceleration that the building will experience; the details of the ground motion time history with that

associated S_a; the mass, damping, and force-deformation behavior of the structure; the capacities of damageable structural and architectural building elements; the unit costs to repair damage; and the contractors overhead and profit factor.

This list excludes some potentially important uncertain parameters, most notably, site soil characteristics, site hazard parameters, choice of repair procedure for a given assembly damage state, union vs. nonunion labor, and demand surge (the potential for greater costs because of labor or material shortages after catastrophic events).

6.3.2 Model for the uncertainties

The following is a summary of how we have modeled uncertainties for the case-study building. These uncertainties are discussed in detail in Porter et al. (2002b); the interested reader is referred to that study for justification.

Ground motion. To model uncertainty in S_a, we use the hazard model discussed above and calculate the probability distribution of the largest S_a that the building will experience in the next 50 years, assuming a Poisson model for earthquake occurrence. To model uncertainty in the details of the ground motion $a(t)$ in any structural analysis, we draw at random from a bin of 100 ground-motion time histories and scale the selected record to the desired level of S_a, and for each desired S_a level, 20 randomly sampled ground motion records are used. The ground-motion records are those provided by Somerville et al. (1997) for the SAC steel project, with the exception that all amplitudes are set to their original (recorded) values before scaling for present purposes. A preference rule is employed in sampling from these records as follows:

1. To minimize errors associated with soil nonlinearity, uniformly scale acceleration amplitudes at most by a factor of 2 (i.e., x2 or ÷2).

2. Prefer real recordings to simulated recordings.

3. Prefer recordings made near the site of interest, so in this case from California.

Structural characteristics. Building masses are modeled as perfectly correlated with a Gaussian distribution that has a coefficient of variation of 0.10. Viscous damping is modeled with a Gaussian distribution that has a mean value of 5%, a coefficient of variation of 0.40 (as detailed in Porter et al., 2002b), and a minimum value of 0.1%. Force-deformation behavior is modeled by assuming a fixed stiffness, and by assuming the force and deformation control points (e.g., yield strength, ultimate strength, etc.) of all structural elements are uncertain but perfectly correlated, with a Gaussian scaling factor that has unit mean and standard deviation of 0.1.

Assembly capacity and unit repair cost. Recall that by "capacity" we mean the value of the *EDP* that causes an assembly to reach a given damage state. A single *EDP* is associated with each assembly. Capacities are assumed to be lognormally distributed, with logarithmic means and logarithmic standard deviations estimated from the results of laboratory testing. Table 6-4 summarizes the assembly capacities used in the present study, and Table 6-5 details unit cost distributions which are all lognormal and are specified by their median and logarithmic standard deviations. For derivation of stucco-wall and window capacities and costs, see Porter et al. (2002a). For drywall, see Porter (2000). For concrete beams and columns, see Beck et al. (2002).

Contractor overhead and profit. Contractors add between 15% and 20% to their total direct cost (labor, materials, equipment, and supplies). We therefore treat overhead and profit as uniformly distributed between 0.15 and 0.20.

Table 6-4. Assembly capacities used in case study

Assembly type	Description	d	Limit State	EDP	x_m	β
6.1.510.1202.02	Stucco finish, 7/8", on 3-5/8" mtl stud, 16"OC	1	Cracking	PTD	0.012	0.5
6.1.500.0002.01	Drywall finish, 5/8-in., 1 side, on metal stud, screws	1	Visible dmg	PTD	0.0039	0.17
6.1.500.0002.01	Drywall finish, 5/8-in., 1 side, on metal stud, screws	2	Signif dmg	PTD	0.0085	0.23
6.1.500.0001.01	Drywall partition, 5/8-in., 1 side, on metal stud, screws	1	Visible dmg	PTD	0.0039	0.17
6.1.500.0001.01	Drywall partition, 5/8-in., 1 side, on metal stud, screws	2	Signif dmg	PTD	0.0085	0.23
3.5.180.1101.01	Nonductile CIP RC column	1	Light	PADI	0.080	1.36
3.5.180.1101.01	Nonductile CIP RC column	2	Moderate	PADI	0.31	0.89
3.5.180.1101.01	Nonductile CIP RC column	3	Severe	PADI	0.71	0.8
3.5.180.1101.01	Nonductile CIP RC column	4	Collapse	PADI	1.28	0.74
3.5.190.1102.01	Nonductile CIP RC beam	1	Light	PADI	0.080	1.36
3.5.190.1102.01	Nonductile CIP RC beam	2	Moderate	PADI	0.32	0.89
3.5.190.1102.01	Nonductile CIP RC beam	3	Severe	PADI	0.71	0.8
3.5.190.1102.01	Nonductile CIP RC beam	4	Collapse	PADI	1.28	0.74
4.7.110.6700.02	Window, Al frm, sliding, hvy sheet glass, 4'x2'-6"x3/16"	1	Cracking	PTD	0.023	0.28

EDP = type of engineering demand parameter used as excitation in the fragility function

PTD = peak transient drift ratio

PADI = Modified Park-Ang damage index (displacement portion): $(\phi_m - \phi_y)/(\phi_u - \phi_y)$, where ϕ_m = maximum curvature, ϕ_y = yield curvature, ϕ_u = curvature at maximum moment for the element in question, considering the element's own material and geometric properties

x_m = median capacity; β = logarithmic standard deviation of capacity

Table 6-5. Assembly unit costs used in case study

Assembly Type	Description	*d*	Repair	Unit	x_m	β
6.1.510.1202.02	Stucco finish, 7/8", on 3-5/8" mtl stud, 16"OC	1	Patch	64 sf	125	0.2
6.1.500.0002.01	Drywall finish, 5/8-in., 1 side, on metal stud, screws	1	Patch	64 sf	88	0.2
6.1.500.0002.01	Drywall finish, 5/8-in., 1 side, on metal stud, screws	2	Replace	64 sf	253	0.2
6.1.500.0001.01	Drywall partition, 5/8-in., 1 side, on metal stud, screws	1	Patch	64 sf	88	0.2
6.1.500.0001.01	Drywall partition, 5/8-in., 1 side, on metal stud, screws	2	Replace	64 sf	525	0.2
3.5.180.1101.01	Nonductile CIP R/C column	1	Epoxy	ea	8000	0.42
3.5.180.1101.01	Nonductile CIP R/C column	2	Jacket	ea	20500	0.4
3.5.180.1101.01	Nonductile CIP R/C column	3,4	Replace	ea	34300	0.37
3.5.190.1102.01	Nonductile CIP R/C beam	1	Epoxy	ea	8000	0.42
3.5.190.1102.01	Nonductile CIP R/C beam	2	Jacket	ea	20500	0.4
3.5.190.1102.01	Nonductile CIP R/C beam	3,4	Replace	ea	34300	0.37
4.7.110.6700.02	Window, Al frame, sliding, hvy sheet glass, 4'-0x2'-6"x3/16"	1	Replace	ea	180	0.2
09910.700.1400	Paint on exterior stucco or concrete	1	Paint	sf	1.45	0.2
09910.920.0840	Paint on interior concrete, drywall, or plaster	1	Paint	sf	1.52	0.2

x_m = median unit cost, dollars, in Van Nuys in 2002

β = logarithmic standard deviation of cost

6.4 LOSS ANALYSIS RESULTS

In this case study, our interest is to estimate the moments of the building repair costs C_R due to the largest *IM* event in the next 50 years (Section 4.4.3) as well as the exceedance probability of the 50-year repair costs over some loss threshold (Section 4.4.4). The PDF of the largest S_a in 50 years, which is plotted in Figure 6-11, is obtained using the hazard curve (Figure 6-7) and Equation (4.30). The first five central moments of this PDF are listed in Table 6-6.

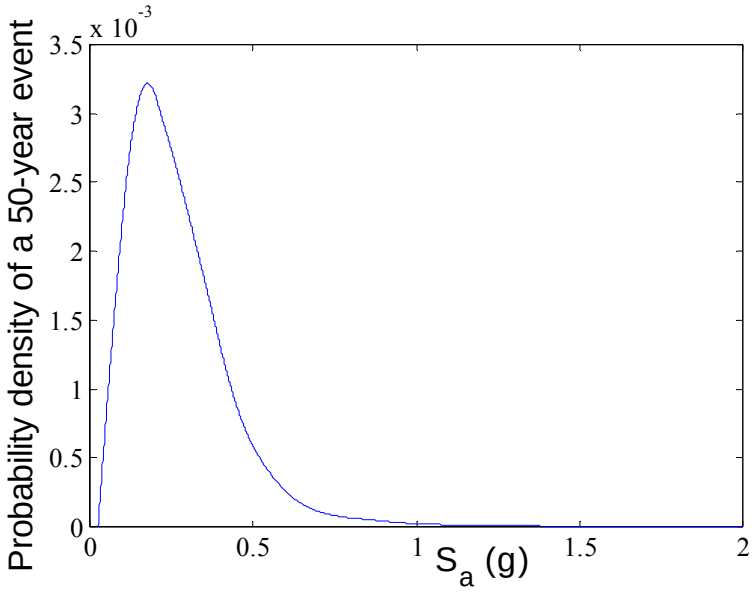

Figure 6-11. Probability density of largest S_a in 50 years

Table 6-6. The first five moments of S_a

Mean	Variance	3rd central	4th central	5th central
0.2743	2.77×10^{-2}	9.77×10^{-3}	9.38×10^{-3}	9.55×10^{-3}

6.4.1 *Estimating moments of C_R for extreme 50-year event*

We first compute $E(C_R^r \mid S_a, a(t), mass, damping, F_d, URC, C_{op})$ (r = 1…4) where $a(t)$ denotes ground motion details, and F_d denotes the *F-d* multiplier; this is done analytically using the derivations in Section 4.2.1. Following Algorithm 4-2, we estimate the first four moments of C_R conditioned on *URC* and C_{op} by averaging the outcomes of the 20 random samples for each S_a level. A fifth-order MM technique is used, and the coordinates and weights of the delta functions in the domain of *IM* (S_a) and *SM* (mass, damping, and *F-d* multiplier) are listed in Table 6-7. Since the mass and damping ratio are Gaussian variables, the fifth-order Hermite-Gauss rule (Appendix A) is used. In Table 6-7, the S_a locations and weights for delta functions #7-#12 match the first five moments of S_a in Table 6-6.

Table 6-7. The locations and weights of the delta functions in the mass, damping, *F-d* multiplier, and S_a space

Delta function number	M/M_0	β	*F-d multiplier*	S_a (g)	Weight
0	1	0.05	1	0.2743	-1
1	$1-0.1\sqrt{3}$	0.05	1	0.2743	1/6
2	$1+0.1\sqrt{3}$	0.05	1	0.2743	1/6
3	1	$0.05-0.02\sqrt{3}$	1	0.2743	1/6
4	1	$0.05+0.02\sqrt{3}$	1	0.2743	1/6
5	1	0.05	$1-0.1\sqrt{3}$	0.2743	1/6
6	1	0.05	$1+0.1\sqrt{3}$	0.2743	1/6
7	1	0.05	1	0.01873	0.01628
8	1	0.05	1	0.05042	0.02463
9	1	0.05	1	0.1201	0.2371
10	1	0.05	1	0.6267	0.1199
11	1	0.05	1	1.4925	0.003284
12	1	0.05	1	4.0178	1.905×10^{-7}

After the $E(C_R^r \mid URC, C_{op})$ are obtained, the (unconditional) moments of C_R are estimated using Algorithm 4-3 described in Section 4.2.3. When matching moments, C_{op} is

uniformly distributed, so the fifth-order Legendre-Gauss rule (Appendix A) is used; for the *URC*, since they are lognormal variables, the first five moments can be computed easily (shown in Table 6-8), which are matched using Equation (3.11) or (3.12). The total number of the weighted delta functions in the *URC* and C_{op} domain is 45. Table 6-9 shows the resulting estimates of the first four moments of C_R corresponding to the largest intensity event in the next 50 years (Section 4.4.3).

Table 6-8. The first five moments of the unit repair costs

Assembly Type	*d*	$\hat{U}$	β^U	Mean	Variance	3rd central	4th central	5th central
6.1.510.1202.02	1	125	0.2	127.53	6.64×10^{2}	1.05×10^{4}	1.62×10^{6}	8.23×10^{7}
6.1.500.0002.01	1	88	0.2	89.78	3.29×10^{2}	3.66×10^{3}	3.98×10^{5}	1.42×10^{7}
6.1.500.0002.01	2	253	0.2	258.11	2.72×10^{3}	8.71×10^{4}	2.72×10^{7}	2.79×10^{9}
6.1.500.0001.01	1	88	0.2	89.78	3.29×10^{2}	3.66×10^{3}	3.98×10^{5}	1.42×10^{7}
6.1.500.0001.01	2	525	0.2	535.61	1.17×10^{4}	7.78×10^{5}	5.04×10^{8}	1.08×10^{11}
3.5.180.1101.01	1	8000	0.42	8737.65	1.47×10^{7}	7.93×10^{10}	1.45×10^{15}	2.41×10^{19}
3.5.180.1101.01	2	20500	0.4	22207.38	8.56×10^{7}	1.05×10^{12}	4.58×10^{16}	1.73×10^{21}
3.5.180.1101.01	3,4	34300	0.37	36730.05	1.98×10^{8}	3.36×10^{12}	2.23×10^{17}	1.17×10^{22}
3.5.190.1102.01	1	8000	0.42	8737.65	1.47×10^{7}	7.93×10^{10}	1.45×10^{15}	2.41×10^{19}
3.5.190.1102.01	2	20500	0.4	22207.38	8.56×10^{7}	1.05×10^{12}	4.58×10^{16}	1.73×10^{21}
3.5.190.1102.01	3,4	34300	0.37	36730.05	1.98×10^{8}	3.36×10^{12}	2.23×10^{17}	1.17×10^{22}
4.7.110.6700.02	1	180	0.2	183.64	1.38×10^{3}	3.14×10^{4}	6.97×10^{6}	5.09×10^{8}
09910.700.1400	1	1.45	0.2	1.48	8.93×10^{-2}	1.64×10^{-2}	2.93×10^{-2}	1.73×10^{-2}
09910.920.0840	1	1.52	0.2	1.55	9.81×10^{-2}	1.89×10^{-2}	3.54×10^{-2}	2.19×10^{-2}

Table 6-9. Moments of repair cost for extreme 50-year intensity event

Mean	Variance	3rd central moment	4th central moment	Standard deviation	Skewness	Kurtosis
5.06×10^{5}	2.88×10^{11}	3.07×10^{17}	7.11×10^{23}	5.37×10^{5}	1.99	8.59

6.4.2 Estimating exceedance probability for C_R for extreme 50-year event

Using the locations and weights listed in Table 6-10, the fifth-order MM estimate of the exceedance probability for C_R for the largest intensity event in the next 50 years can be evaluated following the procedure described in Sections 4.3 and 4.4.4. Figure 6-12 shows the fifth-order

MM estimate of this exceedance probability for different values of *thresh*. The segment length l_c mentioned in Section 4.3 is taken to be 100 (dollars).

Table 6-10. The locations and weights of delta functions in mass, damping, *F-d* multiplier, C_{op}, and S_a space

Delta function number	M/M_0	β	*F-d multiplier*	C_{op}	S_a (g)	Weight
0	1	0.05	1	0.175	0.2743	-14/9
1	$1-0.1\sqrt{3}$	0.05	1	0.175	0.2743	1/6
2	$1+0.1\sqrt{3}$	0.05	1	0.175	0.2743	1/6
3	1	$0.05-0.02\sqrt{3}$	1	0.175	0.2743	1/6
4	1	$0.05+0.02\sqrt{3}$	1	0.175	0.2743	1/6
5	1	0.05	$1-0.113\sqrt{3}$	0.175	0.2743	1/6
6	1	0.05	$1+0.113\sqrt{3}$	0.175	0.2743	1/6
7	1	0.05	1	$0.175-0.05\sqrt{3/20}$	0.2743	5/18
8	1	0.05	1	$0.175+0.05\sqrt{3/20}$	0.2743	5/18
9	1	0.05	1	0.175	0.01873	0.01628
10	1	0.05	1	0.175	0.05042	0.02463
11	1	0.05	1	0.175	0.1201	0.2371
12	1	0.05	1	0.175	0.6267	0.1199
13	1	0.05	1	0.175	1.4925	0.003284
14	1	0.05	1	0.175	4.0178	1.905×10^{-7}

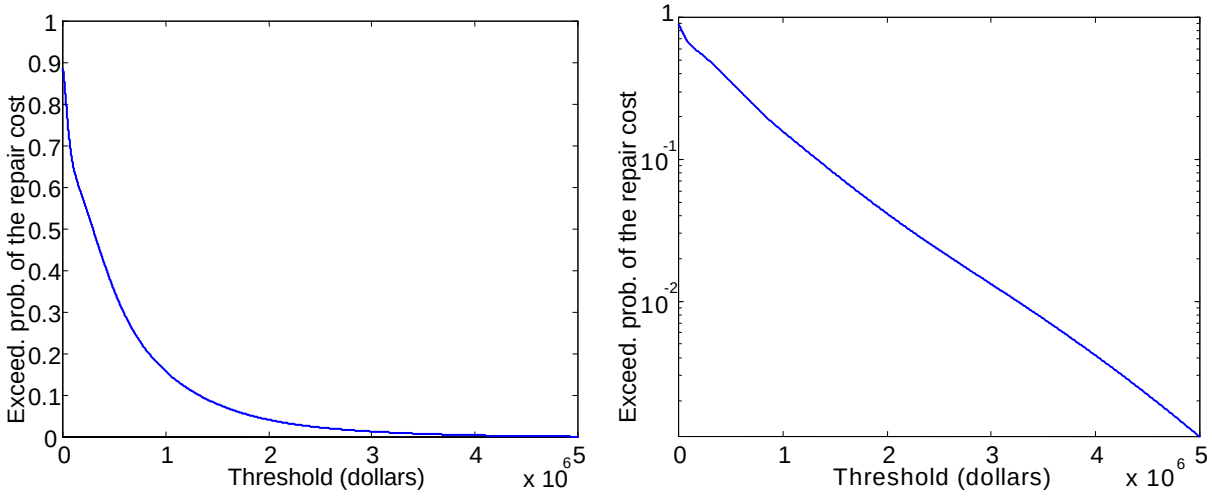

Figure 6-12. Probability of exceeding various levels of repair cost for 50-year intensity event

6.5 FEATURE SELECTION

Our procedure for conducting feature selection for a *DV* equal to the repair cost for the extreme 50-year intensity event is described in Section 5.3. Table 6-11 shows the relative entropy for each basic variable type when we are concerned with the first two moments of C_R for the extreme 50-year intensity event (i.e. the relative entropy is computed using Equation (5.2)). In the table, we rank the importance of the basic variable type from top to bottom. In the case that we are concerned with the exceedance probability for C_R for the extreme 50-year intensity event, Figure 6-13 shows the probability density functions of the C_R where each basic variable type in turn is set to be inactive. For convenience of comparison, the probability density function for the reference case is also plotted in each sub-figure. Table 6-12 shows the relative entropy for each basic variable type computed using the mean exceedance frequency of C_R over 50 years (see Section 4.4.2) in Equation (5.3).

Table 6-11. Moments of repair cost for 50-year intensity event when one variable is fixed at its mean value

Variable that is set to mean value (decreasing importance)	Mean	Variance	3rd central moment	4th central moment	Relative entropy to the original moments
None	5.06×10^{5}	2.88×10^{11}	3.07×10^{17}	7.11×10^{23}	0
S_a	4.97×10^{5}	6.23×10^{10}	1.83×10^{16}	1.84×10^{22}	1.0463
Capacities	2.35×10^{5}	1.47×10^{11}	2.37×10^{17}	5.52×10^{23}	0.393
Ground motion	4.93×10^{5}	1.97×10^{11}	1.22×10^{17}	2.56×10^{23}	0.04088
URC	5.06×10^{5}	2.65×10^{11}	2.44×10^{17}	4.98×10^{23}	0.0017
Damping	4.92×10^{5}	2.75×10^{11}	3.13×10^{17}	7.23×10^{23}	0.000926
F-d multiplier	4.96×10^{5}	2.81×10^{11}	3.10×10^{17}	7.19×10^{23}	0.000325
Mass	5.01×10^{5}	2.79×10^{11}	3.06×10^{17}	7.12×10^{23}	0.000307
C_{op}	5.06×10^{5}	2.88×10^{11}	3.07×10^{17}	7.11×10^{23}	4.33×10^{-9}

From Table 6-11, we see that *URC*, mass, damping, *F-d* multiplier and C_{op} are less important compared to the other variables because the estimated first two moments of C_R for the

50-year intensity event do not significantly change after making these basic variables inactive. This is reflected in the corresponding very small relative entropy changes in Table 6-11. On the other hand, from Figure 6-13, we see that mass, damping, *F-d* multiplier and C_{op} are less important in the sense that the estimated PDF for the 50-year intensity event C_R does not significantly change after making them inactive. Also from Figure 6-13, we can see that setting the ground motion inactive creates a noticeable (but small) difference in the PDF of C_R for the 50-year event. From the above observations, we conclude that it is reasonable to treat 0.01 as an acceptance threshold for the relative entropy, that is, a basic variable is considered to be unimportant if and only if the relative entropy from setting the basic variable inactive is less than 0.01. Under this criterion, *URC*, mass, damping, *F-d* multiplier, and C_{op} are unimportant when estimating the first two moments of the C_R for the 50-year event, while mass, damping, *F-d* multiplier, and C_{op} are unimportant when estimating the exceedance probability for C_R for the 50-year event.

Notice from Table 6-11 and Figure 6-13 that mass, damping, *F-d* multiplier, and C_{op} are unimportant for both cases (the first two moments and exceedance probability for C_R for the 50-year event). If we set mass, damping, *F-d* multiplier, and C_{op} to be simultaneously inactive, Table 6-13 and Figure 6-14 show the resulting moments and exceedance probability of C_R for the 50-year event. It can be seen that the resulting first two moments and exceedance probability do not deviate from the reference ones significantly. This result implies that for this case study, an analysis with deterministic mass, damping, *F-d* multiplier, and C_{op} should not significantly degrade the results. This conclusion is consistent with the tornado-diagram analysis of Porter et al. (2002a) for the same building, which shows that the same variables are important as in the present study, although the order of importance is different.

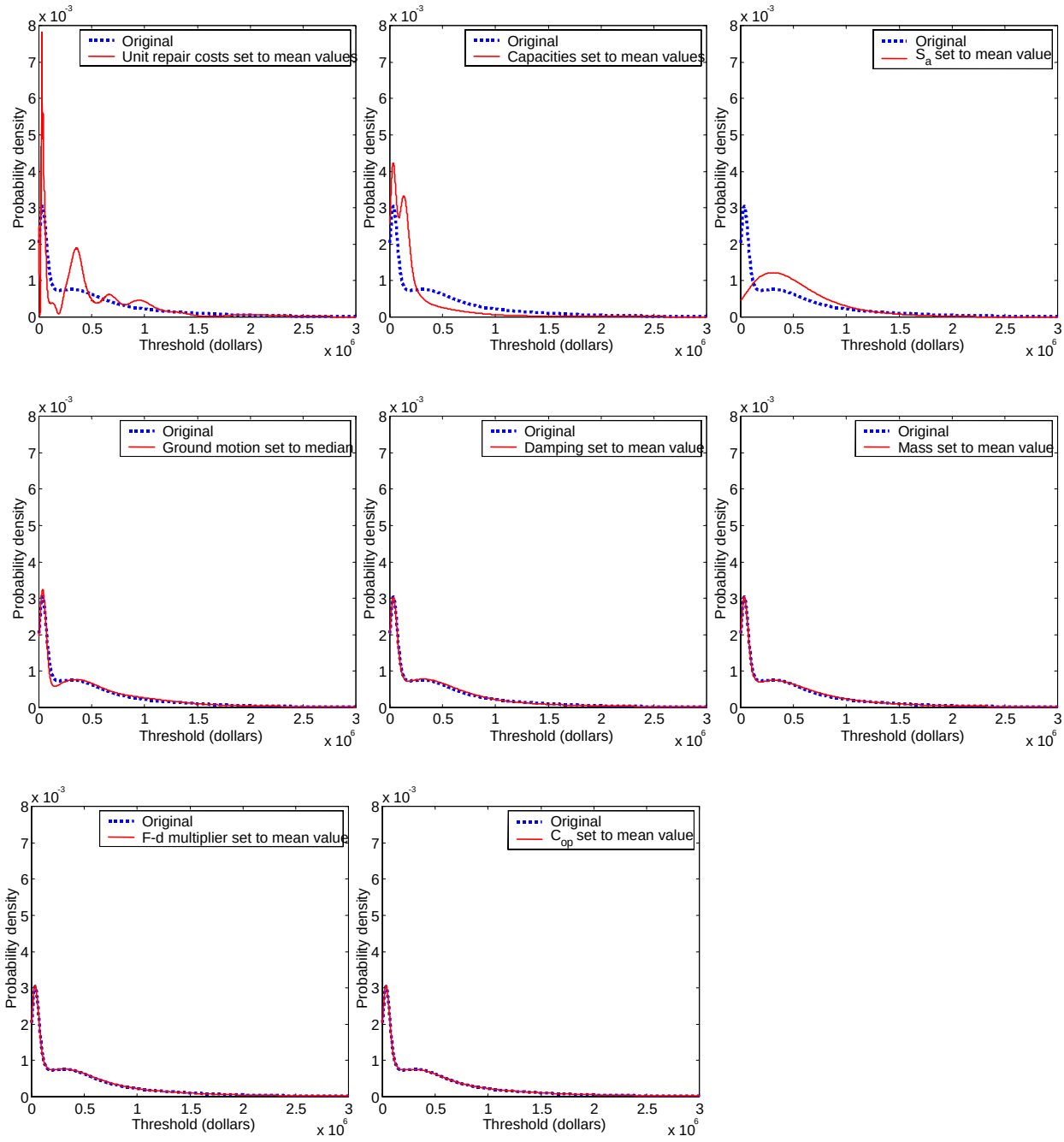

Figure 6-13. Effect on PDF of repair cost for 50-year intensity event when fixing one basic uncertain variable

Table 6-12. Relative entropy based on mean exceedance frequencies for C_R over 50 years

Variable that is set to mean value	Relative entropy to the original PDF
Unit repair cost	0.3319
Capacity	0.3148
S_a	0.3020
Ground motion	0.01163
Damping	0.00235
Mass	0.00111
F-d multiplier	0.000477
C_{op}	0.0000094

Table 6-13. Effect on repair cost for 50-year event of fixing least-important variables at their mean values

Variables that are set to mean values	Mean	Variance	3rd central moment	4th central moment	Relative entropy to the original moments
Damping, F-d multiplier, Mass, C_{op}	5.11×10^{5}	2.73×10^{11}	3.58×10^{17}	8.44×10^{23}	0.00081

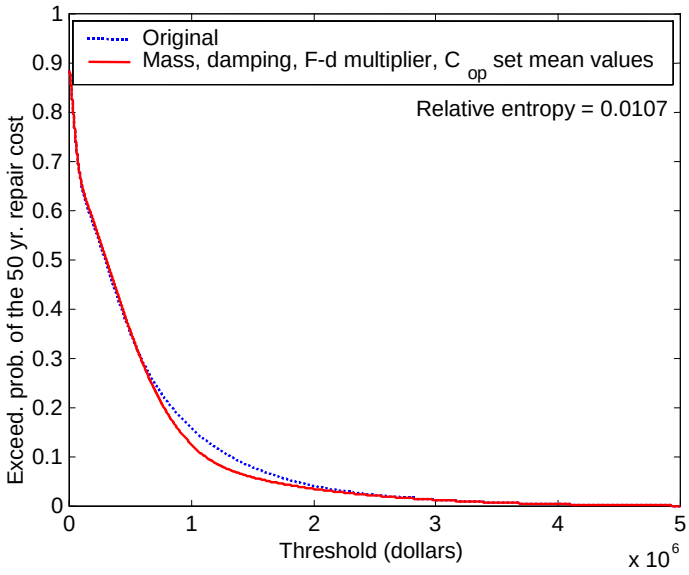

Figure 6-14. Effect on repair cost for 50-year event of fixing least-important variables at their mean values

7 CONCLUDING REMARKS

We have introduced a method called the moment-matching (MM) technique for uncertainty propagation for loss estimation in performance-based earthquake engineering (PBEE). It is a new technique that generalizes Gauss-quadrature numerical methods. With the MM technique, the basic idea is to match the moments of the probability density function (PDF) of the basic uncertain variables in the PBEE framework instead of approximating the nonlinear function that maps the uncertain basic variables to the decision variable (*DV*) by using a simplified functional form (e.g. by linearizing the nonlinear function, as done in the FOSM method).

We have shown that the MM technique is more accurate than the FOSM (First-Order Second-Moment) method, while requiring similar computational resources. This is because with the same computational cost as in the FOSM method, we are able to match up to the fifth moment of the basic variables, so that the order of accuracy is fifth-order for E(*DV*) and second-order for Var(*DV*); in contrast, the FOSM method only provides first-order accuracy for both E(*DV*) and Var(*DV*). The MM technique enjoys some of the advantages of Monte Carlo simulation (MCS) in that it does not require the correlation between the state variables to be estimated and it can achieve any order of accuracy by increasing the sample size (number of moments matched). Also, MM converges faster than does MCS. However, one does not have a priori bounds on the accuracy of the estimates, in contrast to MCS.

The MM technique is used to simplify the evaluation of a function $Y = g(X)$ of basic uncertain variables X. In the case of PBEE, Y might reflect a *DV* such as future repair cost, while X reflects parameters of the ground motion, structural model, damageability, and repair costs. MM works by replacing the PDF for each basic uncertain variable X with a small number of

weighted delta functions that together form a pseudo-probability density function of a variable *X*'. (*X*' is said to have a pseudo-PDF because, although its weights sum to unity, they can be negative.) The number, weights, and positions of the delta functions in the basic variable space are chosen such that *X*' has the same first *p* moments as the variable *X* it replaces, hence the term *moment matching*. The output function evaluated at the *X*' points, i.e., *Y*' = g(*X*'), then also becomes a set of delta functions that, when weighted, has the same first few moments as does the continuous distribution of $Y = g(X)$. The number of *X*' points at which *Y*' is evaluated is small, and scales linearly—not exponentially—with the number of basic uncertain variables in *X*.

An attractive feature of the MM technique is that the order of accuracy grows linearly with the number of the delta functions used. Suppose that for each basic uncertain variable, *r* delta functions are used to match the moments (so that there are in total $r \times \dim(X)$ delta functions used), then the order of accuracy of the MM technique is $(2r\text{-}1)^{\text{th}}$-order for $E(Y)$ and $\lfloor (2r-1)/2 \rfloor^{\text{th}}$-order for $Var(Y)$, where $\lfloor \cdot \rfloor$ denotes the integer part of the number.

A case study using a simple three-story shear building shows that the MM technique is able to estimate the moments, exceedance probability and mean exceedance frequency accurately compared to the results from Monte Carlo simulation, while the FOSM technique performs poorly. The *DV* was the total repair cost over fifty years. The MM analysis used 23 samples in the *X*-space and produced estimates of the first four moments of *DV* that agree within 5% of the same moments calculated using 1 million Monte Carlo simulations. By comparison, estimates of the mean and variance of this *DV* by the FOSM approach were one to two orders of magnitude too low, and FOSM is incapable of estimating higher moments. It is also found in this simulated case study that sometimes it is necessary to adopt more delta functions in the MM technique for the intensity measure (i.e. spectral acceleration in the case study) to achieve the desired accuracy.

We also apply the MM technique with feature selection to a demonstration building, a seven-story hotel located in Van Nuys, California, to estimate the moments and exceedance probability of the repair costs for an extreme 50-year intensity event. Using relative entropy as a measure of sensitivity of the results to uncertainty in the basic variables, we show that capacities, unit repair costs, spectral acceleration, and earthquake ground motion details are among the most important basic variables, and should be treated probabilistically in order to capture uncertainty in repair cost; on the other hand, uncertainty in mass, viscous damping, force-deformation multiplier, and contractor overhead and profit contribute little uncertainty to future repair cost. We show that an analysis with deterministic mass, damping, force-deformation multiplier, and contractor overhead and profit produces a PDF of repair cost nearly identical to that produced with all of these features treated probabilistically. One implication is that a stochastic structural model is not required to treat uncertainty in repair cost. These results are consistent with a tornado-diagram analysis of this building examined in an earlier study. We also establish an empirical threshold for the relative entropy: if the relative entropy with respect to a basic variable is less than 0.01, this variable is considered to be unimportant and can be fixed at its mean value without significantly affecting the results.

One limitation of all of the approaches examined here: MCS, FOSM, and MM, is that in each case, we do not know the features of ground motion (beyond the *IM* such as S_a) that contribute most strongly to uncertainty in *DV*. Consequently, we must perform structural analyses with many ground motions in the hope that by using a large number of them (20 or more), we capture the effect of variability in ground motion beyond that due to the uncertain intensity measure. It would be desirable to identify one or two key features of ground motion that govern its effect on *DV*, quantify the PDFs of these features, and treat them as basic

uncertain variables in the MM technique. This would require the ability to select or generate ground-motion time histories with the desired values of these features.

8 REFERENCES

Abramowitz, M. and I.A. Stegun (Eds.), 1972, *Handbook of Mathematical Functions with Formulas, Graphs, and Mathematical Tables,* 9th printing, Dover, New York, NY.

Baker, J.W. and C.A. Cornell, 2003, "Uncertainty specification and propagation for loss estimation using FOSM methods," *Proceedings of the Ninth International Conference on Applications of Statistics and Probability in Civil Engineering*, San Francisco, July.

Beck, J.L., K.A. Porter, R.V. Shaikhutdinov, S.K. Au, K. Mizukoshi, M. Miyamura, H. Ishida, T. Moroi, Y. Tsukada, and M. Masuda, 2002, *Impact of Seismic Risk on Lifetime Property Values*, Report EERL 2002-04, Earthquake Engineering Research Laboratory, Pasadena, CA: http://resolver.caltech.edu/CaltechEERL:2002.EERL-2002-04

Beck, J.L., A. Kiremidjian, S. Wilkie, A. Mason, T. Salmon, J. Goltz, R. Olson, J. Workman, A. Irfanoglu, and K. Porter, 1999, *Decision Support Tools for Earthquake Recovery of Businesses,* Final Report of CUREE-Kajima Joint Research Program Phase III, Consortium of Universities for Earthquake Engineering Research, Richmond, CA.

Carr, A.J., 2001, *Ruaumoko,* University of Canterbury, Christchurch, New Zealand.

Cover, T.M. and J.A. Thomas, 1991, *Elements of Information Theory*, John Wiley and Sons, New York, NY.

Eberhard, M.O., A. Mookerjee, and M. Parrish, 2001, *Uncertainties in Performance Estimates for RC Columns,* Report, Pacific Earthquake Engineering Research Center, Richmond, CA: http://ce.washington.edu/~peera1

Frankel, A. and E.V. Leyendecker, 2001, *Uniform Hazard Response Spectra and Seismic Hazard Curves for the United States*, Open-File Report, US Geological Survey, Menlo Park, CA.

Haukaas, T. and A. Der Kiureghian, 2003, "Developments in finite element reliability and sensitivity analysis of nonlinear structures," *Proceedings of the Ninth International Conference on Applications of Statistics and Probability in Civil Engineering*, San Francisco, July.

Hildebrand, F.B., 1956, *Introduction to Numerical Analysis,* McGraw-Hill, New York, NY.

International Code Council, 2000, *International Building Code 2000,* International Conference of Building Officials, Whittier, CA.

Islam, M.S., 1996a, "Analysis of the response of an instrumented 7-story non-ductile concrete frame building damaged during the Northridge Earthquake," *Proceedings of 1996 Annual Meeting of Los Angeles Tall Buildings Structural Council,* Los Angeles, CA, May.

Islam, M.S., 1996b, "Holiday Inn," *1994 Northridge Earthquake Buildings Case Study Project, Proposition 122: Product 3.2,* Seismic Safety Commission, Sacramento CA, 189-233.

Jaynes, E.T., 1957, "Information theory and statistical mechanics," *Physical Review*, **106**, 620-630. Also in Rosenkrantz, R. D. (Ed), 1982, *E. T. Jaynes: Papers on Probability, Statistics and Statistical Physics*, D. Reidel Publishing Co, Dordrecht, Holland.

Jennings, P.C., 1971, *Engineering Features of the San Fernando Earthquake of February 9, 1971,* Report EERL 71–02, California Institute of Technology, Pasadena, CA.

Julier, S., J. Uhlmann, and H.F. Durrant-Whyte, 2000, "A new method for the nonlinear transformation of means and covariances in filters and estimators," *IEEE Transactions on Automatic Control*, **45**(3), 477-482.

Li, Y.R., and J.O. Jirsa, 1998, "Nonlinear analyses of an instrumented structure damaged in the 1994 Northridge Earthquake," *Earthquake Spectra*, **14** (2), 245-264.

MacGregor, J.G., 1988, *Reinforced Concrete. Mechanics and Desig*n, Prentice Hall, Englewood Cliffs, New Jersey.

Melchers, R.E., 1999, *Structural Reliability Analysis and Prediction*, John Wiley and Sons, New York, NY.

PEER Testbed Website. URL: http://www.peertestbeds.net/

Pincheira, J.A., F.S. Dotiwala, and J.T. D'Souza, 1999, "Seismic analysis of older reinforced concrete columns," *Earthquake Spectra*, **15** (2), 245-272.

Porter, K.A., 2000, *Assembly-Based Vulnerability of Buildings and Its Uses in Seismic Performance Evaluation and Risk-Management Decision-Making,* Doctoral Dissertation, Stanford University, Stanford, CA.

Porter, K.A., 2002, Preliminary EDP List, Pacific Earthquake Engineering Research Center, Richmond, CA: www.peertestbeds.net/Crosscutting.htm

Porter, K.A., 2003, "An overview of PEER's Performance-Based Earthquake Engineering methodology," *Proceedings of the Ninth International Conference on Applications of Statistics and Probability in Civil Engineering*, San Francisco, July.

Porter, K.A., A.S. Kiremidjian, and J.S. LeGrue, 2001, "Assembly-based Vulnerability of Buildings and Its Use in Performance Evaluation," *Earthquake Spectra,* **17** (2), 291-312.

Porter, K.A., J.L. Beck, and R.V. Shaikhutdinov, 2002a, "Sensitivity of building loss estimates to major uncertain variables," *Earthquake Spectra*, **18**(4), 719-744.

Porter, K.A., J.L. Beck, and R.V. Shaikhutdinov, 2002b, *Investigation of Sensitivity of Building Loss Estimates to Major Uncertain Variables for the Van Nuys Testbed*, Report to Pacific Earthquake Engineering Research Center, Richmond, CA.

Porter, K.A., J.L. Beck, H.A. Seligson, C.R. Scawthorn, L.T. Tobin, R. Young, and T. Boyd, 2002c, *Improving Loss Estimation for Woodframe Buildings,* Report EERL 2002-01, Earthquake Engineering Research Laboratory, Pasadena, CA: http://resolver.caltech.edu/caltechEERL:2002.EERL-2002-01.

Priestley, M.J.N., F. Seible, and G.M. Calvi, 1996, *Seismic Design and Retrofit of Bridge*s, John Wiley & Sons, Inc., New York, NY.

Rissman and Rissman Associates, 1965, *Holiday Inn Van Nuys Structural Drawings,* Pacific Palisades, CA.

Rosenblueth, E., 1975, "Point estimates for probability moments," *Proc. Nat. Acad. of Science*, **72**(10), 3812-3814.

Rosenblueth, E., 1981, "Two-point estimates in probabilities," *Applied Math. Modeling*, **5**, 329-335.

RS Means Corp., 1997, *Means Assemblies Cost Data,* RS Means Co, Kingston, MA.

Saiidi, M., and Sozen, M.A., 1979, *Simple and Complex Models for Nonlinear Seismic Response of Reinforced Concrete Structures,* Report UILU-ENG-79-2031, Department of Civil Engineering, University of Illinois, Urbana, IL.

Scholl, R.E., Kustu, O., Perry, C.L., and Zanetti, J.M., 1982, *Seismic Damage Assessment for High-Rise Buildings,* Report URS/JAB 8020, URS/John A. Blume & Associates, Engineers, San Francisco, CA.

Seligson, H.A. and K.I. Shoaf, 2002, "Human impacts of earthquakes," Chapter 28 in W.F. Chen and C.R. Scawthorn, eds., *Earthquake Engineering Handbook,* CRC Press, New York, NY.

Sharpe, R.D., 1974, *The Nonlinear Response of Inelastic Structures,* Ph.D. Thesis, Department of Civil Engineering, University of Canterbury, Christchurch, New Zealand.

Somerville, P., Smith, N., Punyamurthula, S., and Sun, S., 1997, *Development of Ground Motion Time Histories for Phase 2 of the FEMA/SAC Steel Projec*t, Report No. SAC/BD-97/04, SAC Joint Venture, Richmond, CA.

Structural Engineers Association of California, 1999, *Recommended Lateral Force Requirements and Commentary,* 7th Edition, Sacramento, CA.

Tinsley, J.C., and Fumal, T.E., 1985, "Mapping quaternary sedimentary deposits for areal variations in shaking response," *Evaluating Earthquake Hazards in the Los Angeles Region—An Earth-Science Perspective, U.*S. Geological Survey Professional Paper 1360, U.S. Government Printing Office, Washington DC, pp. 101-126.

Trifunac, M.D., S.S. Ivanovic, and M.I. Todorovska, 1999, *Instrumented 7-Story Reinforced Concrete Building in Van Nuys, California: Description of the Damage from the 1994 Northridge Earthquake and Strong Motion Data,* Report CE 99-02, Department of Civil Engineering, University of Southern California, Los Angeles, CA.

ZEvent, 2000, *UCFyber Version 2.4.1,* Berkeley, CA

Zhao, Y. and T. Ono, 2000, "Now point estimates for probability moments," *Journal of Engineering Mechanics*, **126**(4), 433-436.

9 APPENDIX A. LOCATIONS AND WEIGHTS OF DELTA FUNCTIONS FOR SPECIAL PDFs

This appendix describes general formulas for computing the weights and locations of the delta functions for the MM technique when a scalar X is Gaussian, uniform, or exponential. The resulting pseudo-PDF can match the first ($2q$-1) central moments of X with q weighted delta functions.

When X is Gaussian with zero mean and standard deviation equal to $\sqrt{2}$, the locations of the delta functions for a q-point MM technique are the roots $\{r_i : i = 1,...q\}$ of the Hermite polynomial $H_q(x)$:

$$H_q(x) = \sum_{m=0}^{\lfloor q/2 \rfloor} \frac{(-1)^m \cdot q!}{(q-2m)!\cdot m!} \cdot x^{q-2m}, \tag{A.1}$$

where $\lfloor \cdot \rfloor$ denotes the integer part of the number, and the weights are:

$$w_i = \frac{2^{q-1} \cdot q!}{q^2 [H_{q-1}(r_i)]^2}. \tag{A.2}$$

If X is Gaussian with mean μ and standard deviation σ, the locations of the q delta functions are shifted by μ and scaled by σ, i.e.

$$\chi_i = \mu + \sigma \cdot r_i / \sqrt{2} \qquad i = 1,...q, \tag{A.3}$$

while the weights remain the same.

When X is uniform over [-1, 1], the locations of the delta functions for a q-point MM technique are the roots $\{r_i : i = 1,...q\}$ of the Legendre polynomial $P_q(x)$:

$$P_q(x) = \sum_{m=0}^{\lfloor q/2 \rfloor} \frac{(-1)^m \cdot (2q-2m)!}{2^q (q-m)!\cdot (q-2m)!} \cdot x^{q-2m}, \tag{A.4}$$

and the weights are:

$$w_i = \frac{(1-r_i^2)}{(q+1)^2[P_{q+1}(r_i)]^2}. \tag{A.5}$$

If X is uniform over $[a, b]$, the locations of the q delta functions are

$$\chi_i = (a+b)/2 + (b-a)r_i/2 \qquad i = 1,...q, \tag{A.6}$$

while the weights remain the same.

When X is exponential with PDF e^{-x}, the locations of the delta functions for a q-point MM technique are the roots $\{r_i : i = 1,...q\}$ of the Laguerre polynomial $L_q(x)$:

$$L_q(x) = \sum_{m=0}^{q} \frac{(-1)^m \cdot q!}{(q-m)!\cdot(q!)^2} \cdot x^m, \tag{A.7}$$

and the weights are:

$$w_i = \frac{r_i^2}{(q+1)^2[L_{q+1}(r_i)]^2}. \tag{A.8}$$

If X is exponential with PDF $\lambda e^{-\lambda x}$, the locations of the q delta functions are

$$\chi_i = r_i/\lambda \qquad i = 1,...q, \tag{A.9}$$

while the weights remain the same.